

Università degli Studi di Pavia
Facoltà di Ingegneria
Corso di Laurea Specialistica in Ingegneria Biomedica

**AORTIC VALVE MECHANICAL BEHAVIOR
THROUGH FINITE ELEMENT ANALYSIS**

Relatore: Chiar.mo Prof. Ferdinando Auricchio

Correlatori: Dr. Stefanos Demertzis
Ing. Davide Fugazza

**Tesi di Laurea di:
Sara Pugliese**

Anno Accademico 2007/2008

A Giuseppe.

Contents

Introduction	1
1 Aortic valve: anatomy and biomechanical properties	3
1.1 Heart and heart valves	3
1.2 Aortic valve anatomy	5
1.2.1 Dimensions and relationships among the components	8
1.3 Biomechanical properties	9
1.3.1 Valve anatomy influence on biomechanical properties	9
1.3.2 Mechanics of movement	12
2 Diseases of the aortic valve and aortic valve sparing operations	17
2.1 Stenosis	17
2.2 Insufficiency	19
2.2.1 Annuloaortic ectasia and Marfan syndrome	21
2.2.2 Aortic dissection	22
2.2.3 Ascending aortic aneurysm	23
2.3 Aortic valve sparing operations	23
2.3.1 Screening and contraindications of Aortic Valve Sparing Operations	24
2.3.2 Aortic remodeling surgery	25
2.3.3 Aortic reimplantation surgery: procedure description	26
2.3.4 Limitations and problems concerning the aortic reimplantation surgery	32
3 Analysis preliminary remarks	35
3.1 Material property: Isotropy and orthotropy	35
3.1.1 Linear elastic behavior for isotropic material	36

3.1.2	Linear elastic behavior for orthotropic material	38
3.2	Finite Element Method	39
3.3	Previous works in literature	40
3.3.1	Finite-Element Analysis of Aortic Valve-Sparing: Influence of Graft Shape and Stiffness	40
3.3.2	Functional analysis of bioprosthetic heart valves	42
3.3.3	Geometric modeling of functional trileaflet aortic valves: De- velopment and clinical applications	45
4	Study of aortic valve mechanical behavior through Finite Element Analysis	47
4.1	Introduction	47
4.2	Geometric model design and construction	48
4.3	Mesh generation	53
4.4	Constraints and Loading conditions	55
4.4.1	Definition of constraints	55
4.4.2	Loading phases: <i>diastole</i> and <i>systole</i>	57
4.5	Material properties and Analysis	59
4.5.1	Material isotropic analysis and Results	59
4.5.2	Material orthotropic analysis and Results	66
4.6	Pathological model Analysis	73
4.6.1	Model design and construction	73
4.6.2	Analysis and results	76
5	The parametric aortic valve model: an alternative approach	80
5.1	Pyformex	80
5.2	Parametric model generation	81
5.3	Study of parametric model through F.E.A.	85
	Conclusions	89
A	Early geometrical models	92
A.1	First model	92
A.2	Second model	93
A.3	Third model	94

B Definition of orthotropic properties for aortic valve elements	95
B.1 Orthotropy for a cylinder	95
B.2 Orthotropy for a sphere	100
Bibliography	102
Ringraziamenti	106

Introduction

Surgery of the aortic valve continues to evolve. Intraoperative transesophageal Doppler echocardiography and better methods of myocardial preservation have opened opportunities to develop new surgical approaches to treat aortic valve disease and to re-evaluate old ones. The traditional surgical approach for patients with aortic root disease, whether it associated with aortic stenosis or regurgitation, is to replace the diseased aorta with a synthetic valved-conduit, using either a mechanical or a biological valve prosthesis. But, in patients with aortic root disease associated with aortic regurgitation, the aortic valve may be structurally normal and valve incompetence is the result of leaflets being stretched open by a dilated aortic root.

The presence of a structurally normal valve offers the possibility of saving the native aortic valve while at the same time removing the diseased aortic root tissue. From this, the *aortic valve sparing* surgery is born.

Interest in these aortic valve sparing operations has increased considerably over the last decade since they have the clear advantage of avoiding all of the problems associated with artificial valves.

As for all surgeries, also for the valve sparing there are some problems concerning the procedure success. The coaptation area (the contact area among the aortic leaflets) is the crucial parameter for durability of the surgery: if it is not perfect, there will be an aortic valve prolapse towards the left ventricle.

So, the valve sparing operation is technically high demanding and we can use computational tools to simulate physiological behavior of aortic valve and to understand if the coaptation level influenced the valve functionality, making it competent or not. First of all, we will describe the anatomical and physiological properties of the aortic valve and its pathological conditions, to know in details the object on which we will work.

In particular we will provide a detailed description of diseases related to the valve incompetence, because they are classical pathologies in which an aortic valve sparing

operation is needed. Then we will describe the steps of the surgical procedure.

To investigate the role of the coaptation level in the valve competence, at first, we have created a three-dimensional model of the healthy aortic valve. This to simulate the aortic valve behavior during cardiac cycle. In fact, before dealing with the pathological case, it is fundamental to study and understand which is the healthy valve behavior. We will explain the steps for the model generation and the working hypothesis made. These are necessary, because the aortic valve is a complex biological structure both from anatomical and physiological point of view. So, it is necessary to introduce some simplifications about valve geometry, materials and loading conditions.

We will perform our analysis defining two loading conditions (i.e. systole and diastole), consisting in a pressure in the valve leaflets in order to simulate respectively valve opening and closing.

The soft tissue material has been firstly assumed linear elastic isotropic and subsequently linear elastic orthotropic.

All simulations will be performed on one third of the valve for our symmetry hypothesis and some appropriate constraints will be applied to mimic the remaining structure behavior.

After healthy valve simulation, we will perform the same analysis on the pathological model.

As reference values to validate our results we will use literature, not having experimental data because of the particular exam object.

Finally we will describe briefly an alternative way to generate a pathological model. It is still a developing approach, but it allows to perform a parametrical analysis without, every time, creating a new model.

Chapter 1

Aortic valve: anatomy and biomechanical properties

In this chapter anatomical and physiological properties of the aortic valve will be described. First of all its position and its role in the circulatory system is explained. Then aortic anatomy and histology are detailed. Finally its mechanics of movement is described.

1.1 Heart and heart valves

The heart has four chambers (right and left atria, right and left ventricles) and four valves (Fig.1.1)[1]:

1. *Tricuspid* valve, located between the right atrium and the right ventricle
2. *Pulmonary* valve, located between the right ventricle and the pulmonary artery
3. *Mitral* valve, located between the left atrium and the left ventricle
4. *Aortic* valve, located between the left ventricle and the aorta.

The tricuspid and mitral valves are called atrioventricular valves since they are between the atrium and the ventricle, while the pulmonary and aortic valves are called arterioventricular valves since they are between the artery and the ventricle. The essential function of the heart is to pump blood to various parts of the body. Heart valves allow blood flow in one direction to prevent the back flow. Deoxygenated blood returns from the body via venae cavae to the right atrium

and through the tricuspid valve to the right ventricle. Then it goes through the pulmonary valve to the pulmonary artery, and to the lungs. Oxygenated blood from the lungs returns via pulmonary veins to the left atrium and through the mitral valve to the left ventricle. It then goes through the aortic valve to the aorta, and finally to the whole body. The cycle of pumping starts with the simultaneous contraction of the two atria. This contraction gives an added push to get the blood into the ventricles at the end of the slow-filling portion of the pumping cycle called *diastole*. Successively, the ventricles contract, defining the beginning of *sistole*. During this phase the aortic and pulmonary valves open and blood is ejected from the ventricles, while the mitral and tricuspid valves close to prevent back flow. At the same time, the atria start to fill with blood again. During the last part of systole, ventricles relax, aortic and pulmonary valves close, and mitral and tricuspid valves open. The blood refills the ventricles, marking the end of systole and the beginning of diastole.

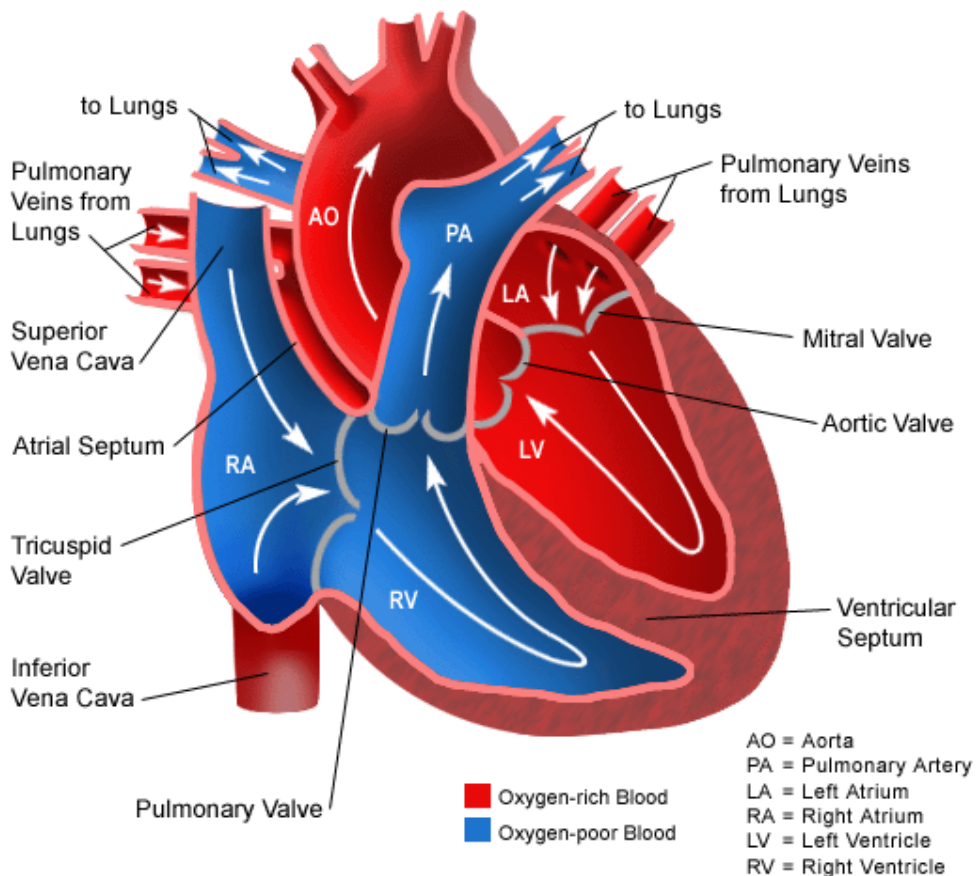


Figure 1.1: Heart with its chambers, the heart valves and the blood flow inside of it. The path of the oxygenated blood (in red), and the path of the deoxygenated blood (in blue) [2].

1.2 Aortic valve anatomy

The aortic valve (Fig.1.2) is a biological structure made of three moving flaps (leaflets) attached to the aorta at one edge (base), and free to move at the other edge (free edges) (Fig. 1.5).



Figure 1.2: Anatomical photograph of opened aortic valve [3].

The morphologic characteristics and function of the aortic valve are related to the *aortic root* and are optimally described as a single functional unit (Fig.1.4). The aortic root connects the left ventricle with the ascending aorta. The aortic root has four anatomic components:

1. *aortoventricular junction or aortic annulus*
2. *leaflets*
3. *aortic sinuses or sinuses of Valsalva*
4. *sinotubular junction*

The *aortic annulus* attaches the aortic root to the left ventricle. The aortic root is attached to the left ventricular myocardium in approximately 45% of its circumference and to fibrous structures (mitral valve and membranous septum) in the remaining 55%. The aortic annulus has a scalloped shape. Histologic examination of the aortic annulus shows that the aortic root has a fibrous continuity with the

anterior leaflet of the mitral valve and membranous septum, and it is attached to the muscular interventricular septum through fibrous strands. The fibrous tissue separating the aortic valve from the mitral valve is called the intervalvular fibrous body.

The aortic *leaflets* have a semilunar shape. The base of each leaflet is attached to the aortic annulus increasingly, whereas the free edge coapts against the other two free edges of the leaflets. The contact area of leaflets is called the *coaptation surface*. At the center of the free edge there is a nodule called *Nodule of Arantius* that permits valve closing. The triangular space underneath two leaflets is part of the left ventricle. The highest point of this triangle where two leaflets are attached is called the *commissure* and represents the point where the free margin of a cusp joins its base. Immediately above the commissures there is the *sinotubular junction*. It represents the end of the aortic root and it is an important structure because it changes the diameter of the sinotubular junction affecting the motion and coaptation of the aortic leaflets. The segment of arterial wall of the aortic root delineated by a leaflet proximally and by the sinotubular junction distally is called the aortic sinus or *sinus of Valsalva*.

Aortic leaflets and sinuses are named according to their relationship to the coronary arteries:

1. the *left coronary* leaflet and sinus
2. the *right coronary* leaflet and sinus
3. the *noncoronary* leaflet and sinus.

The left main coronary artery arises from the left aortic sinus and the right coronary artery arises from the right aortic sinus. The left main coronary artery orifice (*coronary ostium*) is closer to the aortic annulus than is the right coronary artery orifice.

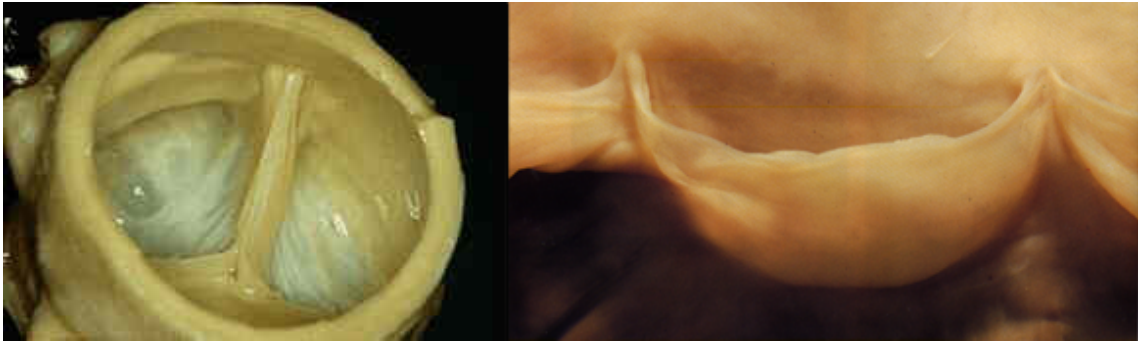


Figure 1.3: Real images of the aortic root. Left: the whole structure. Right: A single opened leaflet [4].

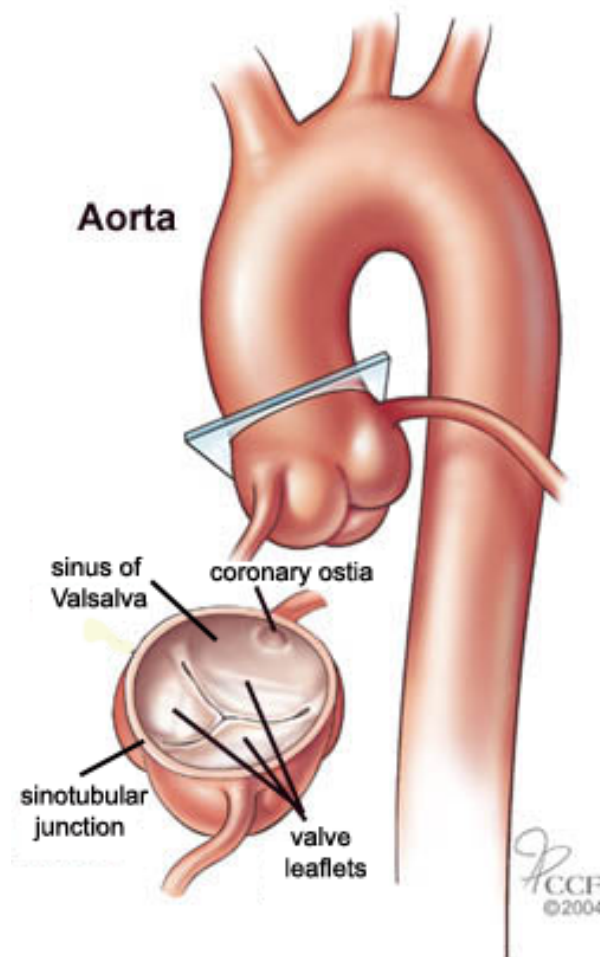


Figure 1.4: Aortic root

1.2.1 Dimensions and relationships among the components

The anatomy of the aortic root varies somewhat from individual to individual, but the geometric relationships among the various components are fairly constant. Thus, the sizes of the aortic leaflets determine the diameters of the aortic annulus and the sinotubular junction, as well as the sizes of the sinuses of Valsalva. Each aortic leaflet has a crescent shape, and the length of its base is approximately 1.5 times longer than the length of its free margin. The lengths of the free margins vary from leaflet to leaflet in an individual; the noncoronary leaflet is often the largest of the three, followed by the right leaflet. The lengths of the leaflet free margins and the diameter of the aortic annulus are related: the diameter of the aortic annulus cannot exceed the average lengths of the free margins of the leaflets, because the free margin of a leaflet extends from one commissure to another (Fig 1.5).

The diameter of the aortic annulus is 15% to 20% larger than the diameter of the sinotubular junction [5]. The average of a normal aortic root diameter is 2-3 cm [6].

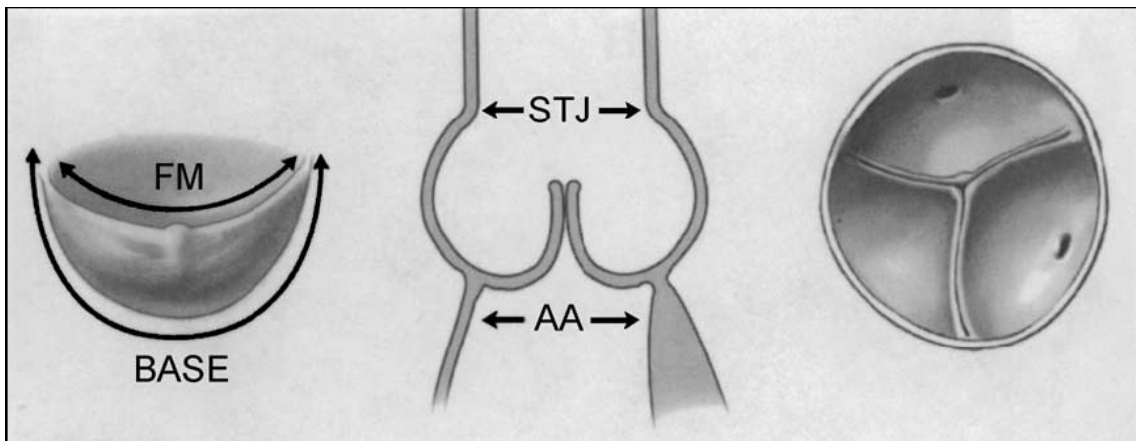


Figure 1.5: Geometric relationships of the components of the aortic root. The length of the base of the aortic leaflet is approximately 1.5 times longer than the length of free margin (FM). The diameter of the aortic annulus (AA) is approximately 15% to 20% larger than the diameter of the sinotubular junction (STJ). The free margins of the leaflets extend from commissure to commissure, and the commissures are immediately below the sinotubular junction. Therefore the diameter of the sinotubular junction cannot exceed the length of the free margin of the leaflets [5].

1.3 Biomechanical properties

The mechanical properties of the aortic valve must allow the valve to open with minimal transvalvular pressure differences and to close completely with minimal flow reversal. Although these functional requirements are simple, the mechanical properties must also provide durability. The pressure drop across the aortic valve generates large stress within the leaflets. These stresses are too great for the leaflets and must be distributed to the fibrous skeleton of the surrounding structures by the valve anatomy [7].

1.3.1 Valve anatomy influence on biomechanical properties

A valve leaflet is composed of collagen, elastin, and glycosaminoglycans [7]. These are the main components for the three principal layers of the leaflet: the *fibrosa* or *arteriosa*, the *spongiosa*, and the *ventricularis* (Figg.1.6 and 1.7). As shown in Fig.1.6, the arterial and ventricular sides of the aortic leaflet are associated with the corresponding aortic and ventricular wall. There is no boundary between the outer layers of the leaflet and the corresponding wall. The outer layers of the leaflet form a continuum with the aortic endothelium or ventricular endothelium.

The ventricular side of each aortic valve cusp contains elastin-rich fibers aligned in a radial direction, perpendicular to the leaflet free margin. Elastin is mechanically coupled to collagen. The purpose of elastin in the aortic valve leaflet is to maintain a specific collagen fiber configuration and return the fibers to their initial state, once the external forces of blood flow subside [8]. In addition, there is a collagen component lying parallel to the free margin in a circumferential direction. The aortic side contains a collagen-rich layer referred to as the corrugated fibrosa. These fibers lie in a circumferential direction and, in a relaxed state, assume a waveform pattern. The middle layer, referred to as the spongiosa, consists of mainly loose connective tissue or mucopolysaccharides.

These principal layers of the aortic leaflet provide the necessary biomechanical properties for proper valve function. On the arteriosa (fibrosa) side of the valve leaflet, endothelial cells are present. Endothelial cells normally align in the direction of stress. In an artery, endothelial cells are aligned in the direction of blood flow because flow stress is the major stress. However, endothelial cells on the aortic valve

leaflet are arranged in a circumferential pattern; i.e., they are arranged perpendicular to the blood flow. Therefore, shear stress of blood flow across the aortic valve is not the major stress. The major stress across the aortic valve is in the circumferential direction and is perpendicular to blood flow.

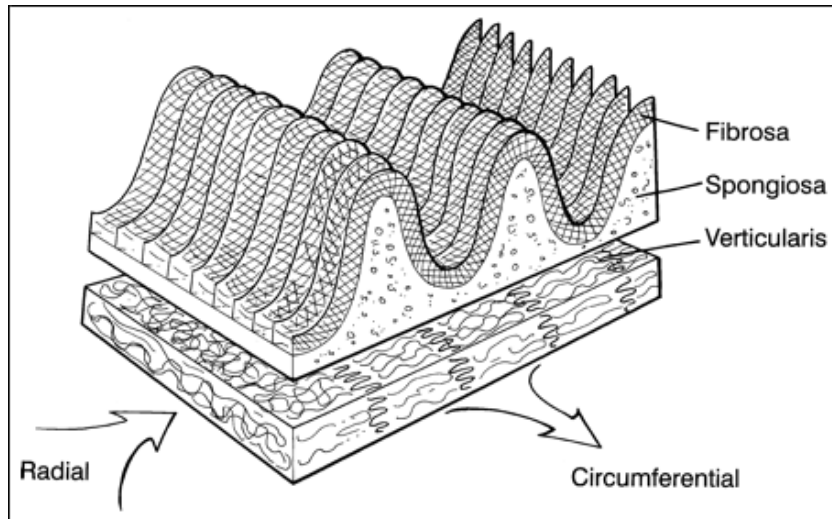


Figure 1.6: Schematic representation of the different layers of the aortic valve leaflet, showing that the fibrosa layer is corrugated, enhancing the ability to stretch in a radial direction [7].

Because of their composition, the valve leaflets demonstrate anisotropic mechanical properties¹. In fact equal leaflet strain distribution would not allow the valve to close properly during diastole. Differences in strain properties allow the cusps to stretch during closure to completely coapt along the free margins. Strain distribution is in two directions: circumferential and radial. The radial vector is perpendicular to blood flow, and the circumferential vector is in the direction of blood flow. Circumferential stiffness is increased relative to radial stiffness. The anisotropic properties allow the valve to stretch in a radial direction, whereas downward movement is relatively restricted, facilitating leaflet coaptation and sealing during diastole. As shown in Fig. 1.7, the fibrosa layer of the valve leaflet is corrugated. This property allows the fibrosa layer to stretch in a radial direction and allows each leaflet to billow toward the other leaflets. Although this layer is the principal load-bearing layer, these

¹Anisotropy is the property of being directionally dependent, as opposed to isotropy, which means homogeneity in all directions. It can be defined as a difference in a physical property (absorbance, refractive index, density, etc.) for some material when measured along different axes

properties do not prevent it from stretching. The ventricularis layer determines the stiffness in the circumferential direction.

Because the principal stresses are oriented in a radial direction, endothelial cells on the fibrosa layer of the leaflets are oriented in a radial direction. Most of the stress on the leaflets occurs at the interface between the two coapting edges of the cusp. These stresses are reduced by several factors. By mutual coaptive support, each leaflet reduces the stresses of the other. These stresses are then distributed along the leaflet edges to corners of the commissures. These mechanisms of stress reduction are important for valve durability. If stresses are unchanged due to abnormalities, such as improper coaptation of the valve leaflets or congenital anatomic abnormalities, the normal mechanism of stress reduction cannot operate. Stress reduction is important because endothelial damage on valve leaflets is directly proportional to the amount of stress. With turnover of endothelial cells and fibroblastic activity, repair of the valve incorporates calcium, which further reduces the mechanical efficiency of the valve. Inability to manage stresses efficiently explains why abnormal leaflets produce progressive deterioration of valve function.

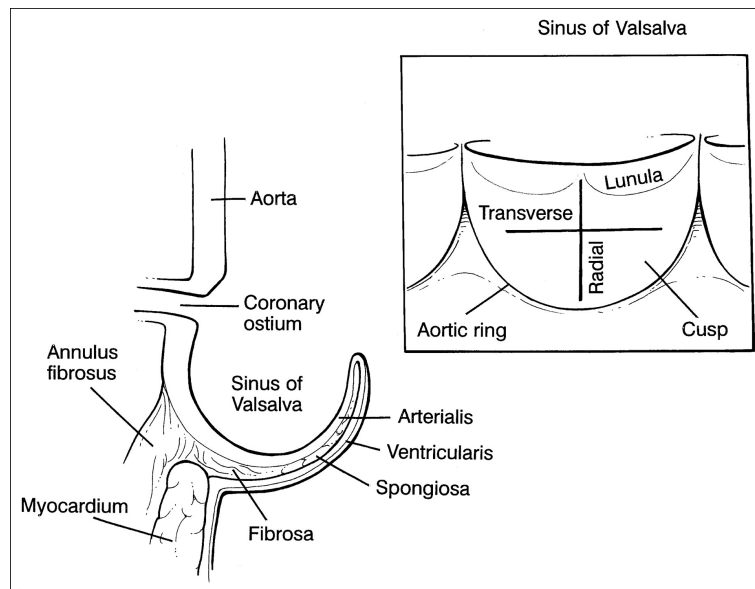


Figure 1.7: Schematic representation of a cross section through the aortic valve leaflet, showing the continuity of endocardial and endothelial components with the aortic valve. Inset illustrates the radial and transverse (circumferential) axes of the valve leaflet and the line of attachment to the aortic wall [7].

1.3.2 Mechanics of movement

The opening and closing of the aortic valve constitute a passive mechanism responding to the pressure fluctuations of the cardiac cycle and pressure differences between the ventricular chamber and the aorta (Fig. 1.8). Although pressure changes during the cardiac cycle may create some structural changes of the valve mechanism to facilitate opening or closing, the principal component is the pressure difference between the ventricle and aorta. Under normal circumstances, the valve leaflets offer little impediment to flow because the specific gravity of the leaflets is equal to that of blood. Appropriate function depends on rapid closure in response to minimal forces moving the valve leaflets.

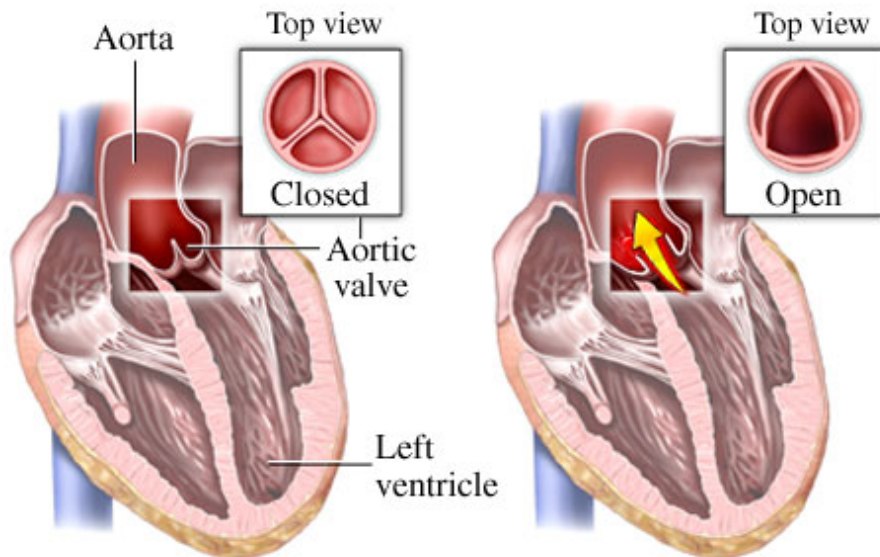


Figure 1.8: Opening and closing of the aortic valve during the cardiac cycle.

Opening of the valve

During diastole, the pressure difference between the aorta and the ventricle provides stress on the valve leaflets. This stress toward the central portion of the aortic opening constricts the base of the aortic root. In addition, the elastic properties of the aortic root contribute to this decrease in diameter. During late diastole, as the blood fills the ventricle, a 12% expansion of the aortic root occurs approximately 20 to 40 milliseconds prior to aortic valve opening [9]. Dilatation of the root alone helps in opening the leaflet to about 20%. Actually, the leaflets begin

to open even before any positive pressure is applied, due primarily to the effect of aortic root dilatation. As pressure rises in the ventricular outflow tract, tension across the leaflets reduces. As pressure continues to rise, the pressure difference across the valve leaflets is minimal, and no tension is present within the leaflet. At this point, without constriction of the aortic root at the leaflet attachments due to redistributed stress during diastole, the aortic root expands to allow the valve to open rapidly at the beginning of ejection. Ejection takes place with a brisk upward movement of straightened leaflets, and the angle at their bases becomes more acute. These mechanisms permit the valve to open quickly and to offer minimal resistance to ejection. In average opening pressure value is 80 mm/Hg (see Fig.1.9).

Closing of the valve

Closure of the aortic valve is one of the more elegant mechanisms of the valve apparatus. A principal theory involved in closure is the vortex theory. The vortex theory recognizes the importance of the sinus of Valsalva in providing a reservoir of blood for small developing vortices. These small vortices allow full expansion of the opened valve leaflets. However, by maintaining the space between the edge of the leaflet and the aortic wall, reversal of flow at the end of systole provides rapid closure. As ejection occurs, deceleration of blood at the stream edge creates small eddy currents of vortices. These small vortices along the aortic wall gradually move toward the base of the ventricular arterial junction to the edge of the leaflet and top of the sinus of Valsalva. As flow declines at end systole, the pressure difference across the opened aortic valve leaflet decreases. At the end of ejection and prior to valve closure, the vortices within the sinus of Valsalva balloon the valve leaflets toward the center of the aorta. The angle at the base of the leaflet becomes more obtuse and rounded, in contrast to the sharp angle at maximal valve opening. This point of flexure begins to move up the valve leaflet and eventually terminates at the free margin of the valve cusp. Therefore, the mechanism of valve closure begins during ejection with the development of vortices within the sinus of Valsalva that prime the leaflets for valve closure. When pressure between the ventricular outflow tract and aorta equalizes, a small reversal of flow occurs due to the deceleration of ejected blood. This small flow reversal causes the leaflets to close rapidly. In average closing pressure value is 100 mm/Hg (see Fig. 1.9).

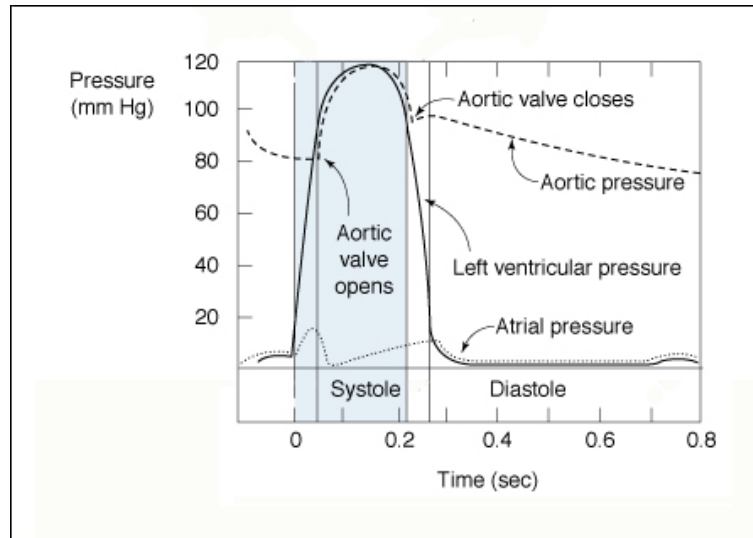


Figure 1.9: Aortic pressure trend during the cardiac cycle. The opening and closing points are indicated.

Impact of blood flow in the mechanism of Opening-Closing

Blood flow across the aortic valve is pulsatile and differs from classic laminar flow such as flow through pipe at a constant rate. Analysis of flow characteristics is difficult because structural components above and below the aortic valve differ from patient to patient. In addition, the dynamics of the valve mechanism and rate of ejection force vary considerably. However, while recognizing these limitations, certain characteristics of normal aortic flow rheology can be described.

As ventricular contraction occurs, blood pressure within the chamber increases. As the pressurized blood moves through the ventricular outflow tract, velocity increases until the blood is ejected at the aortic valve. The ventricular outflow tract acts as a funnel to increase blood flow velocity. As blood passes through the relatively fixed aortic valve ring to the slightly larger aorta, a laminar flow profile develops. The ejected blood produces a skewed peak systolic velocity profile that varies in its location along the aortic wall and during the course of ejection. This velocity profile becomes more blunt at the end of the ejection. Because the effective valve orifice is normally smaller than the aorta, the ejection flow pattern interacts with the blood column along the aortic wall that has relatively low velocity. This interaction between blood moving at varying velocities causes turbulence. Therefore, it is normal to have some turbulence; however, the degree of turbulence is directly proportional to both the velocity of ejected blood and the interface between ejected blood and

the relatively stagnant blood in the aorta.

Figure 1.10 demonstrates that as blood is ejected through the valve orifice, the position of the leaflets helps to reduce turbulence by masking the dilatation of the sinuses to produce an aortic root of nearly uniform diameter. Under these normal circumstances, the effective valve orifice is minimally smaller than the aorta. Once the flow profile reaches the aortic wall, the interaction between stagnant blood and high-velocity blood no longer occurs, and turbulence is diminished.

Abnormalities in blood rheology are present in patients with heart valve disease; plasma fibrinogen, plasma viscosity, and red cell aggregation are all elevated. These abnormalities might be related to the increased incidence of thromboembolism in patients with valvular disease.

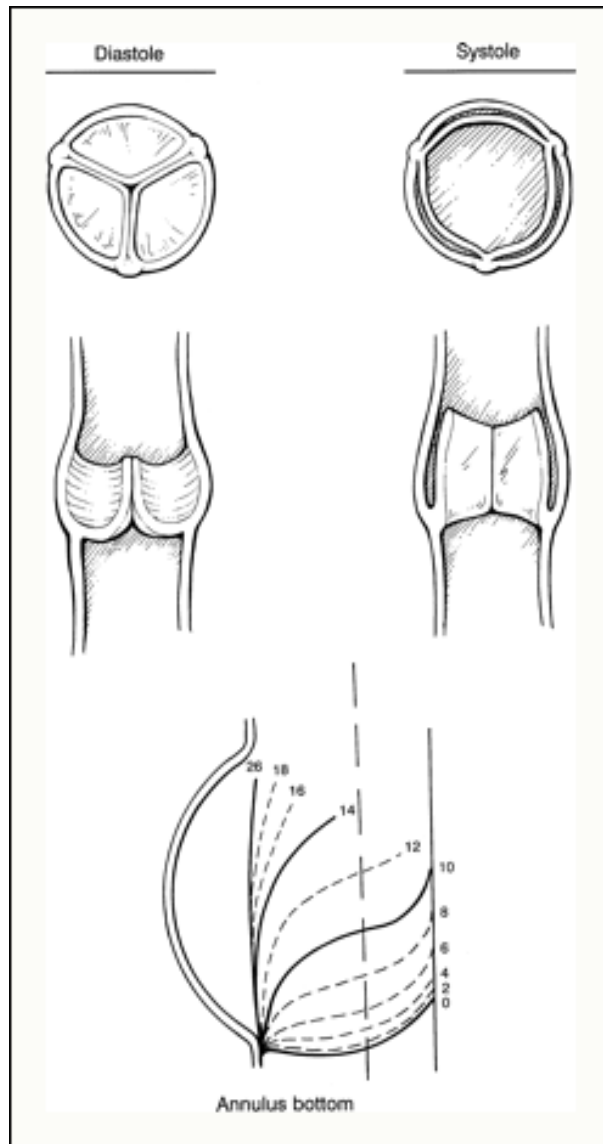


Figure 1.10: Positions of the aortic valve leaflets at end diastole and end systole and of a single leaflet in profile during ejection as the leaflet moves from the closed position (0) to full opening (26). Note how the fully opened leaflet tends to produce a uniform diameter above the ventricular-arterial junction to reduce turbulence that otherwise would be increased by the sinuses of Valsalva.

Chapter 2

Diseases of the aortic valve and aortic valve sparing operations

Diseases of the aortic valve are intimately related to abnormalities and malformations of the valve. There are several ways by which the aortic valve can become diseased; however, all diseased valves present themselves as being *stenotic*, *incompetent*, or both. After a brief description of first pathological condition (stenosis), only diseases related to the valve incompetence are detailed. These diseases are classical pathologies in which a surgery called *aortic valve sparing* operation is needed. This surgical method, described in detail in this chapter, is technically high demanding and computational tools can be used to simulate physiological behavior of aortic valve to understand which are key elements for surgery success.

2.1 Stenosis

An aortic valve is stenotic when offers significant obstruction to the forward blood flow. Generally, the obstruction results from a narrowed orifice of the valve. When the aortic valve becomes stenotic, it causes a pressure gradient between the left ventricle (LV) and the aorta [10]. The more constricted the valve, the higher the gradient between the LV and the aorta. For instance, with a mild aortic stenosis (AS), the gradient may be 20 mmHg. Consequently, at peak systole, while the LV may generate a pressure of 140 mmHg, the pressure that is transmitted to the aorta will only be 120 mmHg. So, while a blood pressure cuff may measure a normal systolic blood pressure, the actual pressure generated by the LV would be

considerably higher. In patients with aortic stenosis, the left ventricle (LV) has to generate an increased pressure in order to overcome the increased afterload¹ caused by the stenotic aortic valve and eject blood out of the LV. More severe is the aortic stenosis, higher would be the gradient between the left ventricular systolic pressures and the aortic systolic pressures. Due to the increased pressures generated by the left ventricle, the myocardium² of the LV undergoes hypertrophy (increase in muscle mass) leading to thickening of the LV walls. Concentric hypertrophy is the most common type of hypertrophy in AS and it provides an equal thickening for all LV walls.

Major causes and predisposing conditions of aortic stenosis include :

1. congenital aortic stenosis, usually resulting from failure of the valve commissures to develop fully, often resulting in unicuspid aortic valves
2. degenerative changes in a congenitally bicuspid aortic valve
3. athero-calcific disease in a trileaflet aortic valve

These conditions can be distinguished clinically by age of onset and echocardiographically by their characteristic findings. Congenital aortic stenosis usually presents in childhood, even infancy, and the echocardiographic examination will show a bicuspid or even unicuspid valve.

Bicuspid valves usually have fusion of one of the three commissures and, echocardiographically, can be distinguished by the presence of a raphe, leaflet doming, and eccentric closure.

Late life calcific aortic stenosis (traditionally characterized as 'degenerative' or 'senile-type') often affects patients with other manifestations of atherosclerotic disease (Fig. 2.1). This form of aortic stenosis progresses slowly, and patients often present it between the ages of 70 and 90 years. Echocardiographic examination typically reveals various degrees of nodular thickening and calcification of the three leaflets with restricted systolic motion. Aortic stenosis is a common disease, regarding approximately 2% of people over the age of 65, 3% of people over age 75, and 4% percent of people over age 85. Since in North America and Europe the population is aging, the prevalence of aortic stenosis is increasing. Leading to considerable morbidity and

¹In cardiac physiology, afterload defines the pressure that the chamber of the heart has to generate in order to eject blood out of the chamber.

²Myocardium is the muscular tissue of the heart.

mortality, both with large social and economic impact, consequently aortic stenosis is became a major health problem.

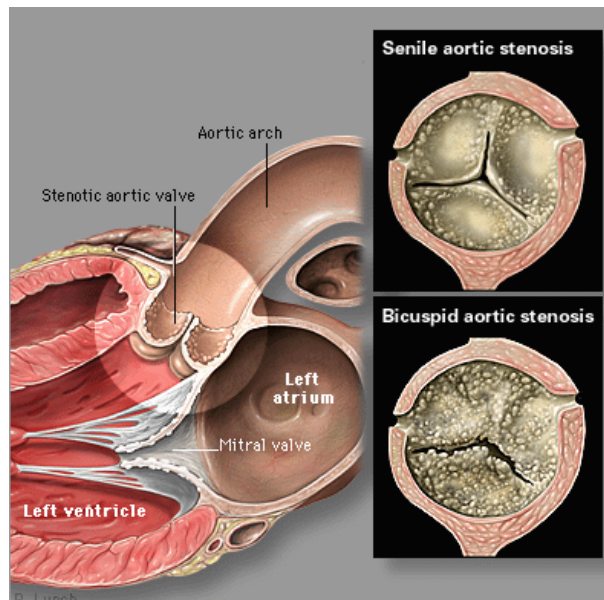


Figure 2.1: Image of senile stenosed aortic valve. It is possible to notice that a heavy calcification of the three valve leaflets causing their immobility and narrowing of valve orifice.

2.2 Insufficiency

An aortic valve is incompetent (regurgitant, insufficient or leaky) when allows blood to flow back into the left ventricle during diastole (see Fig.2.2), thereby reducing net forward flow. In aortic insufficiency, when the pressure in the left ventricle falls below the pressure in the aorta, the aortic valve is not able to completely close causing a leaking of blood from the aorta into the left ventricle [11]. The consequence of valve incompetence is that a percentage of blood (i.e. regurgitant fraction) already ejected from the heart is regurgitated back into the heart³ This regurgitant flow causes a decrease in the diastolic blood pressure in the aorta, and therefore an increase of the pulse pressure (systolic pressure - diastolic pressure). Since some of the blood that is ejected during systole regurgitates back into the left ventricle during diastole, there is decreased effective forward flow in aortic insufficiency. Aortic

³For instance, if an individual with aortic insufficiency has a stroke volume of 100 ml and during ventricular diastole 25 ml regurgitates back through the aortic valve, the regurgitant fraction is 25%.

insufficiency causes both volume overload (elevated preload⁴) and pressure overload (elevated afterload) of the heart. The pressure overload (due to elevated pulse pressure and hypertension) causes left ventricular hypertrophy⁵ (LVH). There is both concentric hypertrophy and eccentric hypertrophy in aortic insufficiency. The concentric hypertrophy is due to the hypertension associated with aortic insufficiency, while the eccentric hypertrophy is due to volume overload caused by the regurgitant fraction.

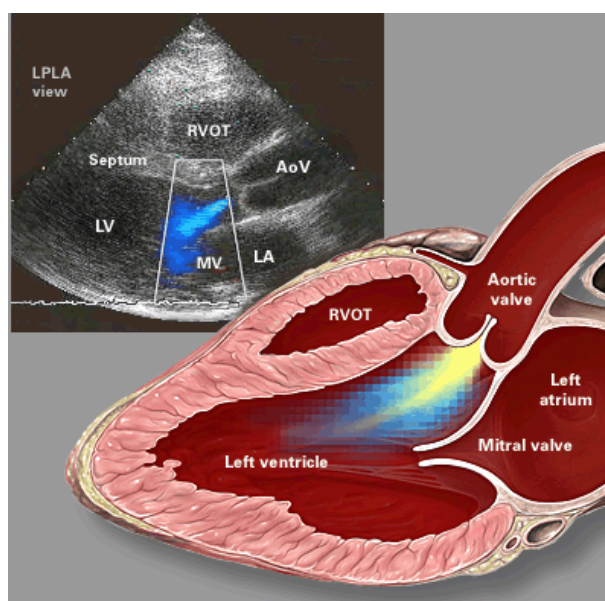


Figure 2.2: Aortic regurgitation. On the left an image of Color Doppler technique.

The diagnosis of aortic insufficiency involves auscultation of the heart in order to listen for the murmur of aortic insufficiency and the S4 heart sound⁶ which would indicate left ventricular filling against a hypertrophied LV wall. The murmur of

⁴In cardiac physiology, preload is the volume of blood present in a ventricle of the heart, after passive filling and atrial contraction.

⁵Left ventricular hypertrophy (LVH) is the thickening of the myocardium (muscle) of the left ventricle of the heart. LVH is called concentric when there is a thickening of the ventricular wall but the ventricular chamber radius not change, whereas it is called eccentric when there is a wall thickening and ventricular radius increases

⁶The heart sounds are the noises (sound) generated by the beating heart and the resultant flow of blood through it. They are four. The rare fourth heart sound S4, in an adult, is called a presystolic gallop. This gallop is a sign of a pathologic state, usually a failing left ventricle.

chronic aortic insufficiency is typically described as early diastolic and decrescendo (relating to sound intensity), which is best heard at aortic area when the patient is seated and leans forward with breath held in expiration.

Aortic regurgitation has numerous causes, which can be grouped according to the structural components of the valve affected. The valve leaflets may be distorted, thereby preventing proper valve coaptation. Calcific aortic disease, idiopathic degenerative disease, active or chronic aortic valve endocarditis, rheumatic disease, a bicuspid aortic valve, and myxomatous proliferation of aortic valve tissue all prevent the valve cusps from closing properly [7].

Aortic root diseases can cause aortic insufficiency including annuloaortic ectasia (dilatation of the proximal aortic root that occurs with aging and hypertension), Marfan syndrome, aortic dissection and ascending aortic aneurysm.

Aortic insufficiency affects approximately 5 out of every 10,000 people. It is most common in men between the ages of 30 and 60.

2.2.1 Annuloaortic ectasia and Marfan syndrome

Marfan syndrome is an autosomal dominant genetic disorder of the connective tissue characterized by disproportionately long limbs, long thin fingers, a relatively tall stature, and a predisposition to cardiovascular abnormalities, specifically those affecting the heart valves and aorta. These numerous abnormalities have been linked to a genetic defect in fibrillin [12]. Fibrillin is a component of the microfibrils making up the elastic meshwork in the aorta and other large vessels. The defect in fibrillin found in the Marfan syndrome results in disorganization and fragmentation of the elastic meshwork. Normally, elastic fibers are responsible for maintaining blood vessels at their normal dimensions by providing the ability to expand with the cyclic increase of blood pressure and then allowing complete recovery to the initial state on removal of the pressure load. In contrast, collagen fibers, which are much stiffer than elastic fibers, are responsible for preventing the aortic wall from stretching too far. Elastic fragmentation therefore reduces the ability of the aortic wall to fully recover from the cyclic distending pressure, resulting in permanent stretching and dilatation. *Annuloaortic ectasia* is a dilation of the sinuses, the sinotubular junction, as well as the annulus (Fig. 2.3), due to pathology as Marfan syndrome. Interestingly, the leaflets tend to be spared. The mechanism of aortic insufficiency in these syndrome include progressive dilatation of all components except the leaflets,

which ultimately leads to aortic dissection.[13]

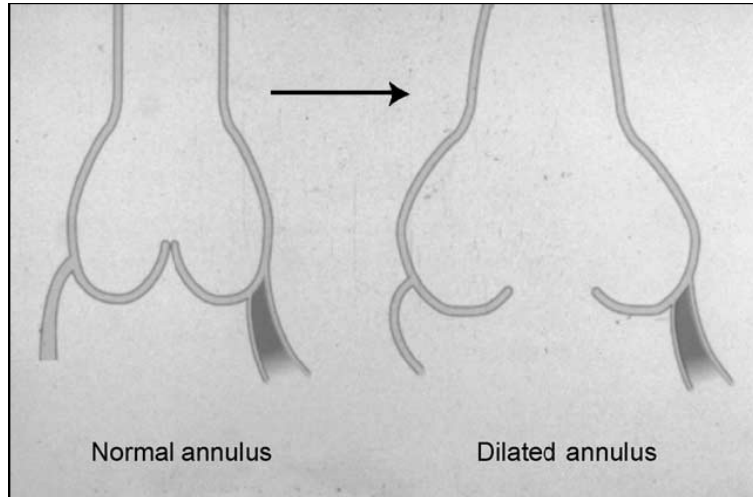


Figure 2.3: An example of annuloaortic ectasia involving aortic annulus.

2.2.2 Aortic dissection

Aortic dissection is a tear in the wall of the aorta that causes blood to flow between the layers of the wall of the aorta and force the layers apart [14]. As other arteries, the aorta is made up of three layers. The layer directly in contact with the blood flow is the tunica intima, commonly called intima. This layer is made up mainly of endothelial cells. Just deep to this layer is the tunica media, known as the media. This "middle layer" is made up of smooth muscle cells and elastic tissue. The outermost layer (furthest from the flow of blood) is known as the tunica adventitia or the adventitia. This layer is composed of connective tissue. In an aortic dissection, blood penetrates the intima and enters the media layer. The high pressure rips the tissue of the media apart, allowing more blood to enter. This can propagate along the length of the aorta for a variable distance, dissecting either towards or away from the heart or both. The initial tear is usually within 100 mm of the aortic valve. If ascending aorta is involved, aortic dissection is classified as type A (Fig. 2.4). The risk of aortic dissection is the aorta rupture, leading to massive blood loss resulting in death. In aortic dissection, there is a dilatation of the sinotubular junction with either or both acute distraction of the valve leaflets

and unhinging and prolapse of the leaflets secondary to sinus wall dissection. In absence of leaflet damage, the aortic wall and aortic root pathology can often be repaired and the valve reconstructed [13].

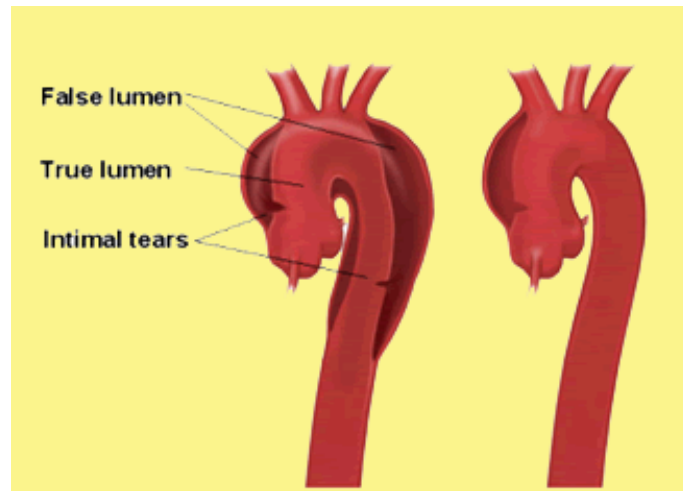


Figure 2.4: Image of ascending aortic dissection. In both cases, ascending aortic dilatation causes dilatation of the sinotubular junction.

2.2.3 Ascending aortic aneurysm

An *aortic aneurysm* is a general term for any swelling (dilatation or aneurysm) of the aorta, usually representing an underlying weakness in the wall of the aorta at certain location. Mechanism of aortic insufficiency in this disease state is a consequence of the dilatation of the sinotubular junction with distraction at the commissures of the valve leaflets. With progressive dilatation, the valve leaflets are literally pulled apart from the central coaptation point. This can be made more severe by primary or more often secondary annulus dilatation.

2.3 Aortic valve sparing operations

The traditional surgical approach for aortic root disease associated to aortic stenosis or aortic regurgitation, is replacing of diseased aorta with a synthetic valved-conduit, using either a mechanical or a biological valve prosthesis. This operation, also known as the Bentall procedure, over the years has yielded excellent results in

the hands of experienced surgeons [15]. However, the Bentall procedure also exposes the patient to the problems associated with artificial valves. Mechanical valves, while long lasting, require life-long anticoagulation. Biological valves, while not requiring anticoagulation, expose the patient to the potential need for re-operation in 10-15 years which, in the case of a redo Bentall, is a major and relatively risky operation. Since the aortic valve is abnormal in patients with aortic stenosis and aortic root disease, replacement with a composite graft and valve conduit remains the golden standard. However, in patients with aortic root disease associated to aortic regurgitation, the aortic valve may be structurally normal since the valve incompetence is the result of leaflets stretched by a dilated aortic root. Aortic root aneurysms, aortic dissection or annular aortic ectasia (see paragraph 2.2), especially in patients with Marfan's disease, represent classical situations where a diseased aorta may distract or disrupt the aortic valve commissures and lead to valve incompetence. The presence of a structurally normal valve offers the possibility of saving the valve while at the same time removing the diseased aortic root tissue. *Aortic valve sparing* surgery preserves the native aortic valve anatomy and function while at the same time removes the surrounding diseased aortic tissue. Interest in aortic valve sparing operations has increased considerably over the last decade since they have the clear advantage of avoiding all of the problems associated with artificial valves.

There are two basic types of valve sparing operations: the *remodeling operation* and the *reimplantation operation* (called also the David Type I Technique). The first technique is based on replacement of the ascending aorta and root including the sinuses of Valsalva; by effectively remodeling the aortic root and decreasing the diameter of the sinotubular junction, coaptation of the aortic leaflets is improved. Instead the second method consists in the complete root replacement, in which a Dacron graft is anchored to the aortic annulus and the aortic valve is reimplanted within the graft. In the following, after a brief description of the remodeling technique, the David method will be described in detail.

2.3.1 Screening and contraindications of Aortic Valve Sparing Operations

Before to perform the valve sparing operation, it is important to determine whether the valve is repairable. Transesophageal echocardiography is the best tool to study the aortic root and the mechanism of aortic regurgitation. The echocardiog-

rapher must understand the functional anatomy of the aortic root and the principles of aortic valve repair to obtain the necessary information to determine the possibility of aortic valve repair. Each component of the aortic root must be examined, in particular the leaflets. The number of leaflets, their thickness, the appearance of their free margins, and the excursion of each leaflet during the cardiac cycle must be carefully examined. The coaptation areas of the leaflets should also be interrogated by Doppler imaging in multiple views. Information regarding the morphologic features of the aortic sinuses, sinotubular junction, and ascending aorta is also important. The diameters of the aortic annulus, aortic sinuses, and sinotubular junction and the heights of the leaflets should be measured. The lengths of the free margins of the leaflets should be also estimated.

In some situation, the aortic valve leaflets are obviously not normal and therefore should not be considered for valve sparing surgery. Calcified valves, valves damaged by rheumatic disease, valves with large fenestrations or valves that have severely over stretched leaflets should not be spared. While repair of an isolated single valve leaflet prolapse is possible, preserving a valve with more than one prolapsed leaflet is probably not appropriate. The discovery of a pliable and well functioning bicuspid valve may also be amenable to a valve sparing operation although the surgeon should be weary of the natural history of bicuspid valves. Finally, there are circumstances in which a surgeon would be unwise to proceed with a valve sparing procedure even if the valve appears salvageable. Valve sparing operations require prolonged aortic cross clamp times and therefore should be avoided in patients with poor ventricular function. For similar reasons, valve sparing surgery should not be done when other concomitant complex procedures are necessary.

2.3.2 Aortic remodeling surgery

The remodeling technique was first described by Yacoub in 1983 and the details were published in 1993 [16]. In this technique, each of the valve commissures is sewn to a synthetic graft that is cut longitudinally to form three separate neo sinuses. These three tongues are then sewn directly to the rim of aortic tissue. This is followed by connecting the coronary buttons to the neo sinuses and then the operation is completed by sewing the distal end of the graft to the ongoing ascending aorta (Fig. 2.5). This operation, while it provides neo sinues of Valsalva, does not secure the aortic annulus. Therefore, further annular dilatation is possible unless additional

measures, such as reinforcing the fibrous portion of the annulus in the region of the non-coronary sinus, are taken.

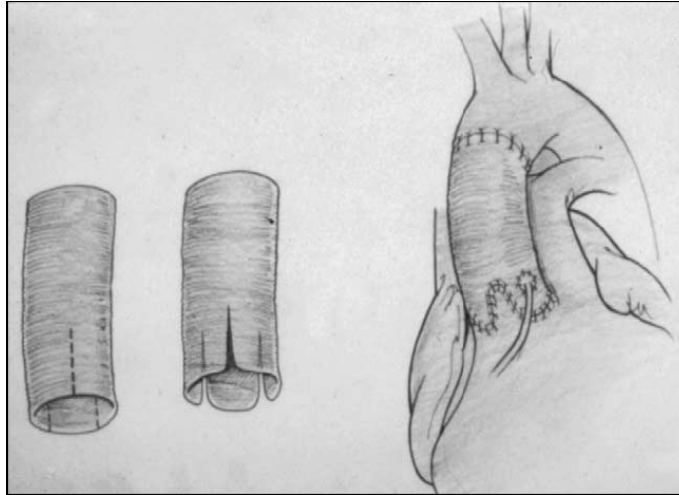


Figure 2.5: Aortic valve sparing operation: remodeling technique.

2.3.3 Aortic reimplantation surgery: procedure description

The technique of aortic valve reimplantation can be used in many cases of aortic root aneurysm whenever the aortic valve is not stenotic and/or calcified. Central mild-to-moderate regurgitation can be corrected very often, whereas eccentric regurgitation may be more difficult to treat exclusively by this technique [17]. In one hand aortic reimplantation surgery takes more time than the implantation of a valved conduit or supracoronary replacement of the ascending aorta, but, in the other hand, this operation is probably the best treatment of the dissected aortic root, because most of the diseased vessel wall may be resected and replaced by a vascular graft and at the same time, retaining the valve.

The first step during the surgery is the cannulation of the ascending aorta. Venous drainage is accomplished by a 2-stage cannula, unless there is evidence of a shunt on the atrial level, which requires for bicaval cannulation to prevent from aspiration of air into the heart-lung machine once the aorta is opened. In full extracorporeal circulation, the heart is fibrillated before the introduction of a vent catheter into the left ventricle through the right upper pulmonary vein to prevent instant left ventric-

ular over distension, maybe developing due to aortic regurgitation. In addition, the vent catheter is very helpful to clear the operative field from residual blood flowing through the pulmonary veins. Then, the distal ascending aorta is cross clamped carefully before the aorta is opened and completely transected. Because of the distal progression of aortic root dilation, the sinotubular junction may sometimes have disappeared. In this condition, the aorta should be incised 3 to 5 mm distal to the estimated level of the former sinotubular junction to prevent from injury to both the right coronary ostium and aortic valve commissure between the right and the non-coronary sinus. This is particularly important in patients with Marfan syndrome, in whom both structures may have drifted surprisingly far downstream within the aortic root.

Once the ascending aorta is transected and its distal remnant is held cephalad by a stay suture, a frontal view to the aortic root facilitates its subsequent assessment. After antegrade application of cold blood cardioplegia ⁷, the aortic valve is inspected for structural integrity with regard to the number of leaflets, calcifications, and fenestrations at the valve commissures (Fig. 2.6).

Small fenestrations ⁸ are found in many patients with aortic regurgitation and particularly in patients with Marfan syndrome. Their influence on the long-term stability of aortic valve-preserving surgery remains unclear. In case of extensive fenestrations, which are more frequently found in patients with an aortic root diameter beyond 5 cm, it may be more advisable to replace the valve.

When the decision about reimplantation of the aortic valve according to T. David, the aortic root is mobilized as far proximal as necessary to reach a mentally created virtual horizontal plane near the base of the sinuses of Valsalva. Before the sinuses carrying the coronary ostia are mobilized, both ostia are cut out of the aortic root as buttons (Fig. 2.7), just like for any other type of aortic root replacement. With the ostia carefully held away with stay sutures, the aortic root is further mobilized beyond the level of the coronary ostia and near the left/right commissure.

Mobilization of the aortic root near the pulmonary artery requires a shallow incision of the membranous septum between the 2 vessels to get down to the appropriate

⁷Cardioplegia is the intentional and temporary cessation of cardiac activity. The most common procedure for accomplishing asystole is called cold crystalloid cardioplegia. This process is considered the most successful because it protects the myocardium, or heart muscle, from damage. In most cases, the patient is first exposed to hypothermia.

⁸Fenestration is an opening, occurring naturally or created surgically, as through a membrane.

plane which is required for later anchoring of the vascular graft. When the mobilization of the aortic root is completed around its entire perimeter, a double-armed 4-0 monofilament suture is placed through the aorta from inside out right at the top of each commissure. Slightly lifting up the commissures by gently pulling on these sutures facilitates subsequent resection of the aortic sinuses, leaving a 4 to 5 mm remnant of the native aortic wall measured from the base of the aortic valve leaflets. At this stage, it is necessary to decide on the diameter of the vascular graft to be implanted. Sizing of the aortic root has been paid a lot of attention. The sutures through the commissures are again lifted up to create a virtual cylinder around a conventional prosthetic heart valve sizer. If, for example, the use of a valve sizer for a 27 mm mechanical aortic valve results in a complete line of coaptation between the leaflets, a 30 mm vascular graft is very likely to reshape the near-original dimensions of the aortic root after reimplantation. The slight 2 to 3 mm oversizing of the vascular graft compared with the appropriate size of the valve sizer pays credit to the fact the aortic valve is reimplanted into the graft. Therefore, the graft needs to be slightly wider than suggested one by the use of the sizer. This maneuver gives a good estimate of the appropriate diameter of the vascular graft that has to be implanted.

When the aortic root is completely mobilized and after the decision for a specific diameter of the vascular graft, 9 to 13 double-armed polyester sutures are placed transmurally from inside the left ventricular outflow tract out (Fig. 2.8).

The first stitch is positioned underneath the commissure between the left and the noncoronary sinus at the hinge line of the anterior mitral valve leaflet. Then, sutures are placed clockwise, keeping the horizontal subvalvular plane that was mentioned previously. Care is taken not to pass the needles accidentally through the bottoms of the remnants of the sinuses of Valsalva.

Now, the vascular graft is shortened to the estimated length of the ascending aortic segment in order to be replaced. Then, its perimeter is divided into 3 segments by marking the expected position of the commissures with a line drawn by a sterile pencil. After transferring the stay sutures at the commissures into the lumen of the graft without fixing them at this point, the sutures previously placed in the horizontal subvalvular plane are stitched out of the cardiac end of the graft perimeter at corresponding sites (Fig. 2.9). Then, the graft is anchored in the aortic root by tying the suture with the graft held in position by the assistant (Fig. 2.10). It is key not to pull too much on these sutures while tying them, because this may result

in unfavorable plication of both the graft and the annulus. Therefore, these knots should be tied like "wet toilet paper", and it should be kept in mind that this is not a hemostatic suture line.

Once the graft is anchored in the aortic root, the commissures are trimmed by placing the stay sutures at the appropriate height inside the vascular graft. It is not necessary to tie these sutures at this point. The correct position of the commissures inside the graft is identified by slightly pulling on both the commissure and the vascular graft, before stitching the sutures through the graft. At this moment, the graft should extend roughly by half of its maximum length at this segment. When the commissures are trimmed, the tissue remnants of the partially resected sinuses of Valsalva are reimplanted into the vascular graft using 4-0 monofilament running sutures starting from the depth of the left coronary sinus. The suture line then continues to the commissure between the left and the noncoronary cusp. A slight mismatch between redundant tissue of the neo sinus and the vascular graft can be easily compensated. Whether the mismatch appears too big at this point, the remnant may be shortened by another 1 or 2 mm. If this is not the reason for a mismatch, the graft is probably too narrow and should be replaced by a wider one.

After reimplantation of the neo sinuses, the respective sutures are tied at the tip of the commissures. The initial stay sutures through the commissures are tied too. The aortic valve as a whole is now reimplanted into the vascular graft prosthesis and should present with a "mercedes star" like configuration of the leaflets within the vascular graft (Fig. 2.12). The prospective valvular competence may now be estimated by assessing the lines of leaflet coaptation and/or instilling some saline solution into the aortic root. Sometimes, small tissue segments may still prolapse into the lumen near the commissures. They may be either carefully resected or plicated to the graft by additional sutures. It is important to reimplant the commissures as high as suggested by their individual anatomy, in order to prevent early postoperative valve failure.

The coronary ostia are reimplanted anatomically in the left and the right neo sinus with a 4-0 or 5-0 monofilament running suture as in any other type of aortic root replacement (Fig. 2.13). The stitches should rather pass through the rim of the ostium than through the surrounding aortic wall, to prevent later aneurysmatic dilation of the ostial implantation site. Before the prosthesis-aortic anastomosis completes the repair, both the native distal ascending aorta and the proximal vascular graft segment carrying the reimplanted valve need to be tailored in a way that allows for a

tension and torsion-free anastomosis. This may imply that the commissure between the left and noncoronary cusps is located very close to the anastomotic suture line.



Figure 2.6: The aortic valve is inspected for structural integrity .

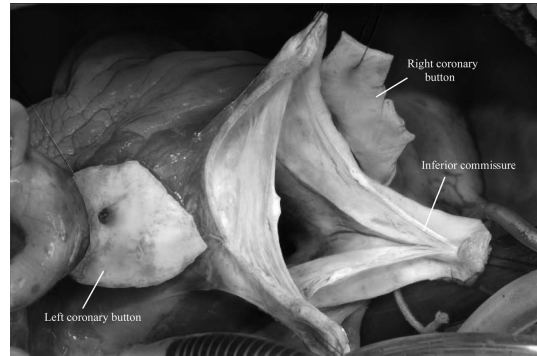


Figure 2.7: During surgery, both coronary ostia are cut out of the aortic root as buttons.

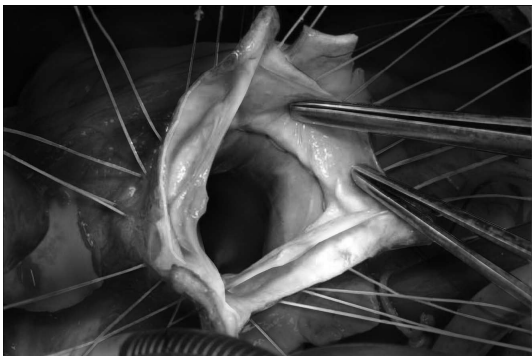


Figure 2.8: 9 to 13 double-armed polyester sutures are placed transmurally from inside the left ventricular outflow tract out. Then, sutures are placed clockwise, keeping the horizontal subvalvular plane.



Figure 2.9: Vascular graft perimeter is divided into 3 segments. Then the sutures previously placed are stitched out of the cardiac end of the graft perimeter at corresponding sites.

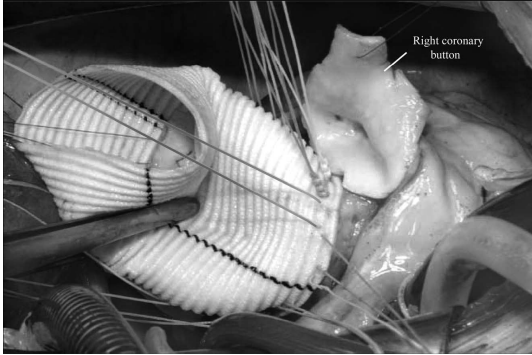


Figure 2.10: The graft is anchored in the aortic root by tying the suture with the graft held in position.

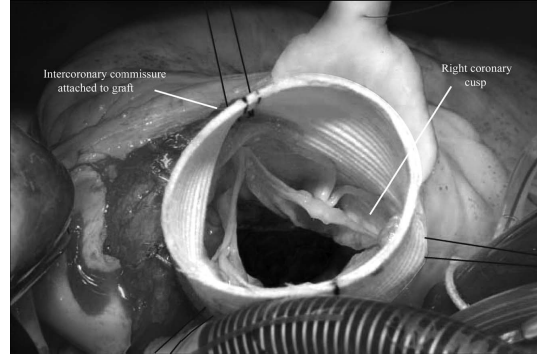


Figure 2.11: The commissures are trimmed by placing the stay sutures at the appropriate height inside the vascular graft.

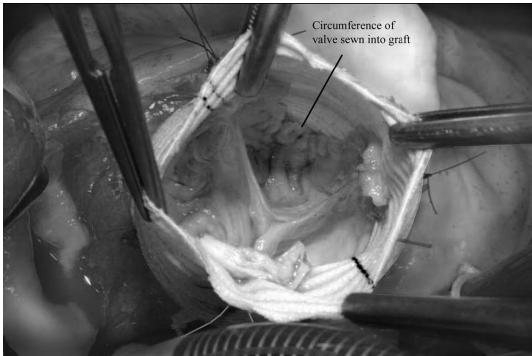


Figure 2.12: The aortic valve as a whole is now reimplanted into the vascular graft prosthesis and should present with a "mercedes star".

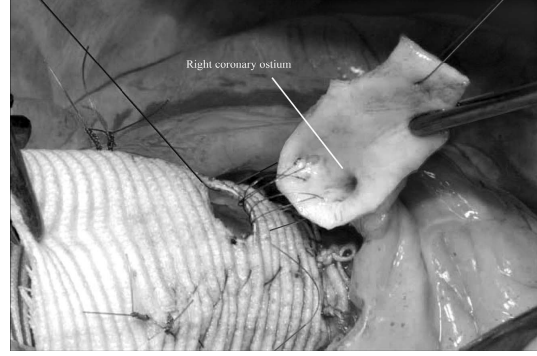


Figure 2.13: The coronary ostia are reimplanted anatomically in the left and the right neo sinus with a 4-0 or 5-0 monofilament running suture.

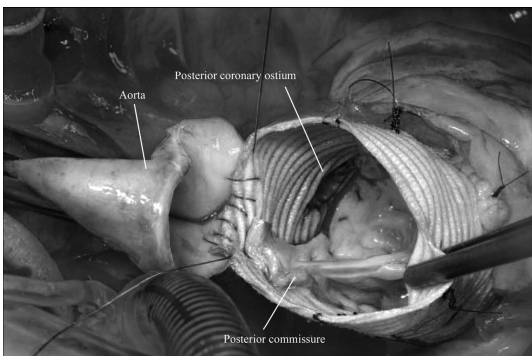


Figure 2.14: The distal ascending aorta and the proximal vascular graft segment tailored in a way that allows for a tension and torsion-free anastomosis.



Figure 2.15: Completed repair resulting in a proximal ascending aortic replacement and in a native aortic valve reimplanting: the valve sparing surgery .

2.3.4 Limitations and problems concerning the aortic reimplantation surgery

Scientific literature results demonstrate that valve-preserving aortic root surgery achieves excellent results in screened patients with low perioperative morbidity and mortality, lack of anticoagulation and perfect hemodynamics [18] . Unfortunately such technique is technically high demanding. Analysis of echocardiographic morphology after valve reimplantation in some patients demonstrated the importance of proper placement of the valve inside the prosthesis. Aggressive dissection of the aortic root and adequate height of resuspension seem to be critical technical factors for the stability of the reconstructive procedure. In fact the aortic root would have to be dissected as completely as possible down to the fibrous skeleton of the valve. This is sometimes difficult at the base of the right coronary sinus, where the muscle of the right ventricle has to be mobilized to seat the valve deep inside the prosthesis. Furthermore, the prosthesis is not stretched to resuspend the commissures, which are pulled up as high as possible, but the coaptation area of the cusps is carefully assessed to determine if they are adequate.

The coaptation area becomes the crucial parameter for durability of the surgery: if it is not perfect, there will be an aortic valve prolapse towards the left ventricle (see Fig.2.16). But this represents a new problem because cusp geometry is difficult to quantify by means of echocardiography preoperatively. Even intraoperative measurements of parameter like cusp height, length of insertion line or free margin is difficult. Most importantly, these parameters are only interdependent determinants of valve configuration and their single relevance is limited. For these reasons a new parameter, called *effective height* has been considered. Effective height is the difference between the central free margins and the lower cusp point, that sometimes coincides with the aortic insertion lines (see Fig.2.17). A

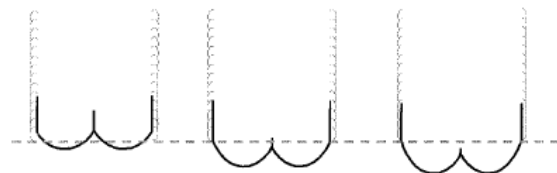


Figure 2.16: Levels of cusp coaptation. From left to right, decreasing coaptation degree is shown. Lower is the contact area among the leaflets, greater is the probability that the surgery is unsuccessful.

caliper⁹ that allows easy and reproducible measurement of this height difference has been designed [19]. This measurement allows for identification of prolapse in the native cusps and assessment of prolapse correction after valve repair.

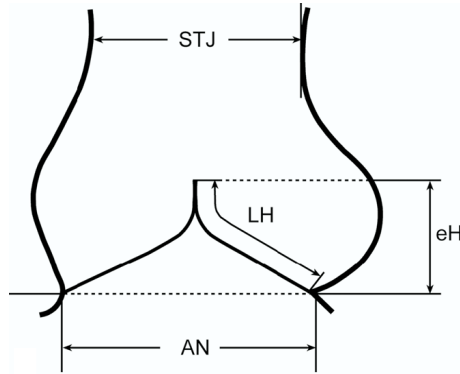


Figure 2.17: Schematic drawing of the aortic valve and root. Effective height is the height difference between the central free margins and the aortic insertion lines. This can be measured intraoperatively with a caliper. STJ, Sinotubular junction; AN, annulus or aortoventricular junction; LH, leaflet or cusp height; eH, effective height [19].

The caliper is placed in the way that the longer end rests on the lowest (i.e., central) point of the insertion line. The shorter end is pushed to the free margin, with the curve accommodating the margin (Fig.2.18). The height difference of the cusp can be measured in millimeters. In normal aortic valves effective height is into a range from 8 to 10 millimeters has been found, which correlated ± 1 mm with intraoperative transesophageal measurements [19].

Moreover it has been observed that repaired valves with low effective height (<4 mm) progressed in regurgitation and required reoperation. But, because a right judgment on the long-term durability of this surgical technique cannot be given, surgeons have still a lot of doubts about that.

Computational tools can support interventional concepts and improve clinical outcomes, simulating physiological behavior of this highly complex functional unit. For this reason the present study aims to create a 3D model of the aortic valve and

⁹A caliper is a device used to measure the distance between two symmetrically opposing sides. A caliper can be as simple as a compass with inward or outward-facing points. The tips of the caliper are adjusted to fit across the points to be measured, the caliper is then removed and the distance read by measuring between the tips with a measuring tool, such as a ruler.

investigate its mechanical behavior during cardiac cycle and then to check the importance of coaptation area.

In the next chapters some theoretical notes and the model design and its properties will be described in detail.

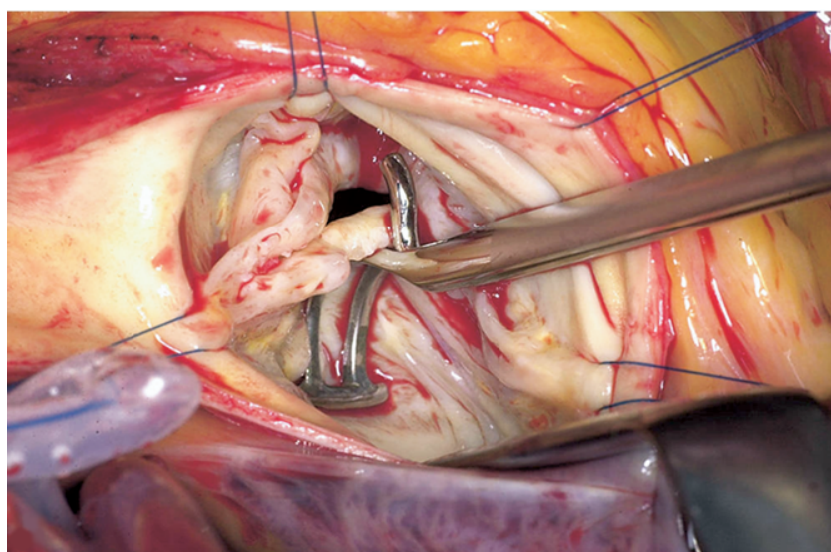


Figure 2.18: Intraoperative photograph showing measurement of the effective height of the noncoronary cusp of a bicuspid aortic valve with the caliper [19].

Chapter 3

Analysis preliminary remarks

In this chapter all necessary information will be given in order to fully understand following analysis concepts and choices. Firstly the constitutive relations of two different material properties will be shown, to understand the analysis parameter meaning. Subsequently some notes about the Finite Element Method will be described, to highlight the theoretical basis of numerical analysis. Finally we will provide a brief review of previous works in available scientific literature, analyzing the geometric models and material properties and comparing our model with the literature models .

3.1 Material property: Isotropy and orthotropy

Body strain after loading condition depends by physical-mechanical properties of the body material. These properties come from experimental tests and allow to define material behavior through *constitutive equations* [20].

Constitutive equations connect body stresses ¹ to strain ² generated after load application. Sometimes these equations represent a simplification of the real material behavior. A material can be :

- *homogeneous* if it has equal properties in every point
- *isotropic* if it has equal properties in all directions

¹ σ =normal stress applied perpendicularly to a face of a material; τ =shear stress applied parallel or tangential to a face of a material

² ε =normal strain acting perpendicularly to a face of a material.It produces dilations, however it merely stretches the body along the axis of application ; γ =shear strain acting parallel or tangential to a face of a material

- *anisotropic* if it has different properties in different directions .

3.1.1 Linear elastic behavior for isotropic material

A linear elastic isotropic material has:

- Linear relationships between the components of stress and strain
- Complete shape recovery: once the forces are no longer applied, the object returns to its original shape.

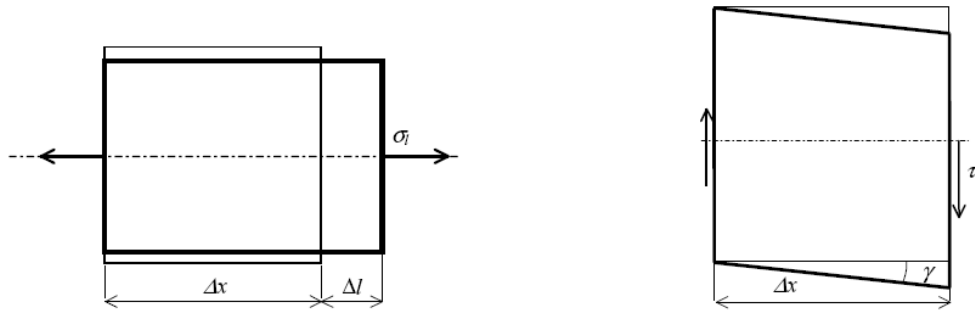


Figure 3.1: Stress and strain in elastic body.

A linear elastic material, subjected to an uniaxial load, has a longitudinal strain ε_l that is connect to stress through the following relationship:

$$\sigma_l = E\varepsilon_l \quad (3.1)$$

where E is *Young's modulus* of the material and it has stress dimensions $[N/mm^2]$. For homogeneous and isotropic material, Young's modulus is equal in all directions and its value is independent of reference system. Experimentally there is also a transversal strain; in isotropic material it is :

$$\varepsilon_t = -\nu\varepsilon_l = -\nu\frac{\sigma_l}{E} \quad (3.2)$$

where ν is *Poisson's coefficient* of the material and it is equal to:

$$\nu = -\varepsilon_t/\varepsilon_l \quad (3.3)$$

Poisson's coefficient is a nondimensional number and its value is in range 0.0 - 0.5 . For $\nu = 0.5$ we have the material incompressibility. If the material is subjected to a shear load, a shear strain is produced:

$$\gamma = \frac{\tau}{G} \quad (3.4)$$

where G is elastic *shear modulus*. For isotropic material, it is proved that:

$$G = \frac{E}{2(1 + \nu)} \quad (3.5)$$

Material constants, E , G and ν are called also *engineering constants*.

For triaxial load (general load), the constitutive equations for elastic linear homogeneous and isotropic material are:

$$\begin{aligned} \varepsilon_x &= \frac{1}{E}(\sigma_x - \nu\sigma_y - \nu\sigma_z); & \varepsilon_y &= \frac{1}{E}(\sigma_y - \nu\sigma_x - \nu\sigma_z); & \varepsilon_z &= \frac{1}{E}(\sigma_z - \nu\sigma_y - \nu\sigma_x); \\ \gamma_{xy} &= \frac{1}{G}\tau_{xy}; & \gamma_{yz} &= \frac{1}{G}\tau_{yz}; & \gamma_{zx} &= \frac{1}{G}\tau_{zx}. \end{aligned} \quad (3.6)$$

where

- σ_i is the normal stress acting on the face with normal i and directed along i axis;
- τ_{ij} is the shear stress acting on the face with normal j and directed along i axis;
- ε_i is the extension of a material fiber parallel to i axis;
- γ_{ij} is the change in angle between a material fiber parallel to i axis and one parallel to j axis.

So, we can described the mechanical behavior of the linear elastic homogeneous isotropic material through two constants only: E and ν .

Equations (3.6) can be written in matrix form:

$$\boldsymbol{\varepsilon} = \mathbf{S}\boldsymbol{\sigma} \quad (3.7)$$

where $\boldsymbol{\sigma}$ and $\boldsymbol{\varepsilon}$ are stress and strain vectors respectively and \mathbf{S} is the *compliance matrix* (see (3.8)):

$$\begin{bmatrix} \varepsilon_x \\ \varepsilon_y \\ \varepsilon_z \\ \gamma_{yz} \\ \gamma_{zx} \\ \gamma_{xy} \end{bmatrix} = \begin{bmatrix} 1/E & -\nu/E & -\nu/E & 0 & 0 & 0 \\ -\nu/E & 1/E & -\nu/E & 0 & 0 & 0 \\ -\nu/E & -\nu/E & 1/E & 0 & 0 & 0 \\ 0 & 0 & 0 & 1/G & 0 & 0 \\ 0 & 0 & 0 & 0 & 1/G & 0 \\ 0 & 0 & 0 & 0 & 0 & 1/G \end{bmatrix} \begin{bmatrix} \sigma_x \\ \sigma_y \\ \sigma_z \\ \tau_{yz} \\ \tau_{zx} \\ \tau_{xy} \end{bmatrix} \quad (3.8)$$

Matrix elements are the material elastic constants and they are function of the engineering constants.

By inversion of the compliance matrix, we obtain the material *stiffness matrix* C : it connects stresses to strains (see (3.9)).

$$\boldsymbol{\sigma} = \mathbf{S}^{-1}\boldsymbol{\varepsilon} = \mathbf{C}\boldsymbol{\varepsilon} \quad (3.9)$$

3.1.2 Linear elastic behavior for orthotropic material

Real materials are not quite isotropic and the property difference in the various direction is not negligible. For anisotropic materials, the most general form of (3.8) provides that all compliance matrix terms are different from zero and they depend of the reference system. S matrix is still symmetric and independent constants are 21.

For anisotropic materials, if we apply an uniaxial load, strains are produced along directions that are different from load direction. Moreover there is a coupling between normal stresses and shear strains and vice versa.

Orthotropic materials are particular anisotropic materials: they have symmetric deformation properties along three orthogonal planes. If we choose three parallel axes to these planes, 1,2 and 3, different from the main axes, the constitutive equations of (3.8) become :

$$\begin{bmatrix} \varepsilon_{11} \\ \varepsilon_{22} \\ \varepsilon_{33} \\ \gamma_{23} \\ \gamma_{31} \\ \gamma_{12} \end{bmatrix} = \begin{bmatrix} 1/E_1 & -\nu_{21}/E_2 & -\nu_{31}/E_3 & 0 & 0 & 0 \\ -\nu_{12}/E_1 & 1/E_2 & -\nu_{32}/E_3 & 0 & 0 & 0 \\ -\nu_{13}/E_1 & -\nu_{23}/E_2 & 1/E_3 & 0 & 0 & 0 \\ 0 & 0 & 0 & 1/G_{23} & 0 & 0 \\ 0 & 0 & 0 & 0 & 1/G_{13} & 0 \\ 0 & 0 & 0 & 0 & 0 & 1/G_{12} \end{bmatrix} \begin{bmatrix} \sigma_{11} \\ \sigma_{22} \\ \sigma_{33} \\ \tau_{23} \\ \tau_{31} \\ \tau_{12} \end{bmatrix} \quad (3.10)$$

where E_i is the Young's modulus in the i -th direction and G_{ij} is the shear modulus in ij plane. Poisson's coefficients in (3.10) are defined as:

$$\nu_{ij} = -\varepsilon_j/\varepsilon_i \quad (3.11)$$

The first index is the load direction, the second is the transversal strain direction. To respect the symmetry, the following condition must be applied:

$$\nu_{ij}/E_i = \nu_{ji}/E_j \quad (3.12)$$

So, an orthotropic material is defined by 9 independent parameters: three Young's moduli, three Poisson's coefficients and three shear moduli.

Note that, in orthotropic materials, there is no interaction between the normal stresses and the shear strains.

3.2 Finite Element Method

A Finite Element Analysis (FEA) is the investigation, by numerical tools, of the mechanics of physical system [21]. The continuum (e.g. our valve) is divided into a finite number of discrete regions, named elements, whose behavior can be described mathematically. Partitioning the continuum into elements is generally automated through a special-purpose Graphical User Interface (GUI). An approximate solution of the entire continuum is solved from the assembly of the individual elements. The mechanical behavior (displacement, strain, stress, etc.) in any point of an element is described in function of the behavior at a small number of control points (nodes) in the element. Usually, the displacements of the nodes are taken as the fundamental unknown quantities. At any other point in the element, the displacements are obtained by interpolating from the nodal displacements. The interpolation order is dependent upon the number of nodes in the element. From the displacements, the strain are evaluated by taking appropriate derivatives. The material constitutive behavior provides the necessary basis for computing stress levels from strains. Application of the principle of virtual work to an element yields the forces exerted by the element on the nodes, which are statically equivalent with the built-up stresses, and by Newton's third law the actions of the element on a particular node are easily found. Force contributions from all elements connected to a particular node are summed up, and they must be in equilibrium with any externally applied loading or force applied to the continuum.

Thus, the Finite Element Method essentially transforms continuous unknown fields into equations of discrete nodal quantities. Assuming certain basis numerical requirements and standards of practice are satisfied, the solution obtained from the FEA estimates the exact physical solution.

3.3 Previous works in literature

This section will provide an overview of works that deal with some pathological aspects of the valve or that replicate only a part of the valve or a prosthetic valve model. Each subsection briefly will summarize and highlight geometric and material properties for each model. Then we will use these information to create our model and to understand if our results are plausible.

3.3.1 Finite-Element Analysis of Aortic Valve-Sparing: Influence of Graft Shape and Stiffness

The authors, K.S. Kunzelman, K.J. Grande Allen et al. [22], dealt with aortic valve sparing operation, but they centred their study to examine the effect of graft shape and material properties on aortic valve function, using a three-dimensional finite-element model of the human aortic valve and root.

To simulate the results of an aortic valve-sparing surgical procedure, specific shapes and material properties of vascular grafts were substituted for the corresponding root shape and properties in six models. Three cylindrical graft models and three graft models in a pseudosinus shape were created and assigned the material properties of either PET (polyethylene terephthalate), ePTFE (expanded polytetrafluoroethylene), or PCU (polyurethane).

Magnetic resonance images of normal human valve/root specimens were used to establish the geometric data coordinates for the model (see Fig.3.2). The normal variations in thickness that exist in the leaflets and root wall were incorporated into the finite-element model: the root thickness values were measured directly from the magnetic resonance images of the aortic root wall, whereas the thicknesses of the unloaded valve leaflets were determined from published data.

The linearly-elastic anisotropic material properties of the leaflet and root tissues were also calculated from published stress-strain data, including a Poisson's ratio of 0.45 to represent the nearly incompressible behavior of the cardiac tissue. These anisotropic properties were applied in the root circumferential and longitudinal directions, and in the leaflet radial and circumferential directions (see Tab.3.1). Finally, to represent the pliability of the leaflets, the shell elements in the valve were constructed to have a bending stiffness that was reduced by 98.5% as compared to a traditional shell element.

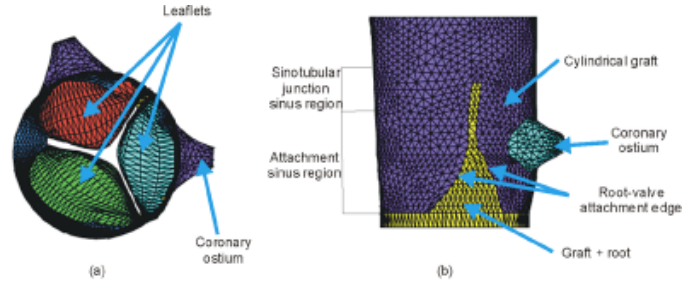


Figure 3.2: Geometry of the cylindrical graft models: (a) top view; (b) side view [22].

About the boundary conditions, first contact elements were used to allow for frictionless sliding of leaflet surfaces; second, the lowest nodal layer of the root base was constrained by assigning zero displacement out of plane; finally, a physiologic longitudinal stretch was imposed by applying tension at the distal ends of the coronary ostia and ascending aorta.

Property	Aortic valve	Aortic root
E_{circ} (kPa)	6885	334
E_{rad} (kPa)	1624	-
E_{long} (kPa)	-	350
G_{xy} (kPa)	1121	119
G_{yz} (kPa)	1121	115
G_{xz} (kPa)	560	119
ν_{xy}	0.106	0.450
ν_{yz}	0.106	0.450
ν_{xz}	0.450	0.429
thickness (mm)	0.18-2.75	0.60-2.14

Table 3.1: Material properties and element thickness for the aortic valve and normal root.

To represent early diastolic loading, simulated physiologic pressures were applied to the valve and root/graft structure.

Stresses, strains, and coaptation were recorded for the valve, root, and graft. In Fig. 3.3 the stress contours of the normal valve and root in the cylindrical graft models are shown. Regarding shape, the cylindrical graft models increased the valve stresses by up to 173%, whereas the root-shaped graft model increased valve

stresses by up to 40% as compared to normal. Regarding material properties, the polyurethane models demonstrated valve stress, strain, and coaptation values closest to normal, for either root shape. Graft shape had a greater effect on the simulated valve function than did the material property of the graft. Optimizing the shape and material design of the graft may result in improved longevity of the spared valve if a normal environment is restored.

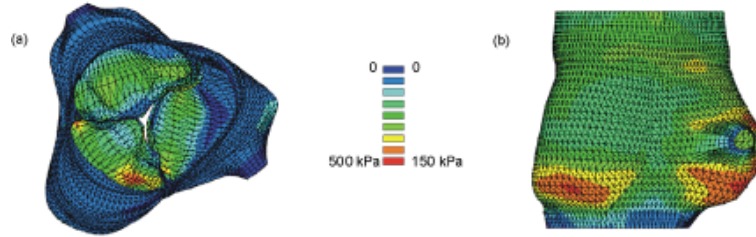


Figure 3.3: Stress contours of the valve and root in the cylindrical graft models: (a) normal root model, top view; (b) normal root model, side view [22].

This model is our main element of comparison because it is very complete: it takes in account the leaflet asymmetry, the ostium presence, material anisotropy, the leaflet contact, etc. Moreover it reproduces exactly the physiological valve condition after a valve sparing surgery.

3.3.2 Functional analysis of bioprosthetic heart valves

In this study the authors, G. Arcidiacono, A. Corvi and T. Severi [23], analysed the effect of orthotropy on tricuspid bioprosthetic aortic valve, using a three-dimensional finite element model, during the entire cardiac cycle. The subject of the analysis was the PericarbonTM aortic tricuspid valve, manufactured by Sorin Biomedica S.p.A. (see Fig.3.4).

Multiaxial tensile tests were also performed to determine the anisotropy of pericardium. Specifically, as many other biological soft tissues, pericardium can be represented as an orthotropic material. In this study, linear orthotropy has been considered as representative of the pericardium's behavior because, in vivo, the device usually works in the range of to $\sim 0.02\text{MPa}$, in which mechanical properties can be considered linear. Two different linear isotropic models were studied: in the first one the three leaflets have the same Young's modulus ($E_1 = E_2 = E_3 = 5\text{MPa}$), while

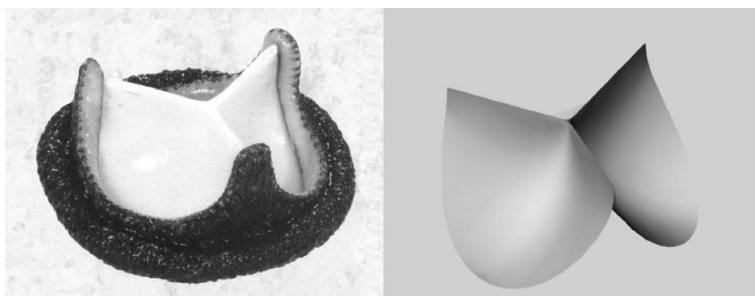


Figure 3.4: The PericarbonTM Sorin S.p.A. aortic valve and the geometric model in closed configuration.

in the second one the leaflets have three different Young's modulus ($E_1 = 5\text{MPa}$; $E_2 = 3\text{MPa}$; $E_3 = 8\text{MPa}$). This approach was used for the purpose of emphasizing any differences in cinematic behaviour due to different mechanical properties among the leaflets. The models has showed unacceptable mechanical behaviour, consisting of asynchronous leaflet movements. Then two different orthotropic models A and B were considered; they have the following mechanical values, respectively: $E_r=3.4\text{MPa}$, $E_c=4.3\text{MPa}$ for model A; $E_r= 4.3\text{MPa}$, $E_c=3.4\text{MPa}$ for model B.

As boundary condition, all the nodes at the stentattached edges were constrained in both displacement and rotation and contact was taken in account. The load curve corresponded to the difference between the ventricular and aortic pressures.

The results showed that even a small difference between values along the two axes of orthotropy can negatively influence leaflets performance as regard both displacement and stress distribution (see Tab.3.2 and Fig.3.5).

Model	Parameter (MPa)	
A	UTS along x	7.7
$E_r=3.4\text{MPa}$	UTS along y	15.1
$E_c=4.3\text{MPa}$	σ_x max	2.6×10^{-1}
	σ_y max	1.2
B	UTS along x	15.1
$E_r=4.3\text{MPa}$	UTS along y	7.7
$E_c=3.4\text{MPa}$	σ_x max	4.2×10^{-1}
	σ_y max	7.5×10^{-1}

Table 3.2: Maximum stresses values along x and y directions for models A and B.

This study demonstrates that taking into consideration the orthotropy of pericardium during the bioprosthesis manufacturing process makes it possible to optimise the valve's dynamic response in terms of better displacement and lower stress. This finding could significantly influence the construction, durability and functionality of pericardial bioprosthetic valves.

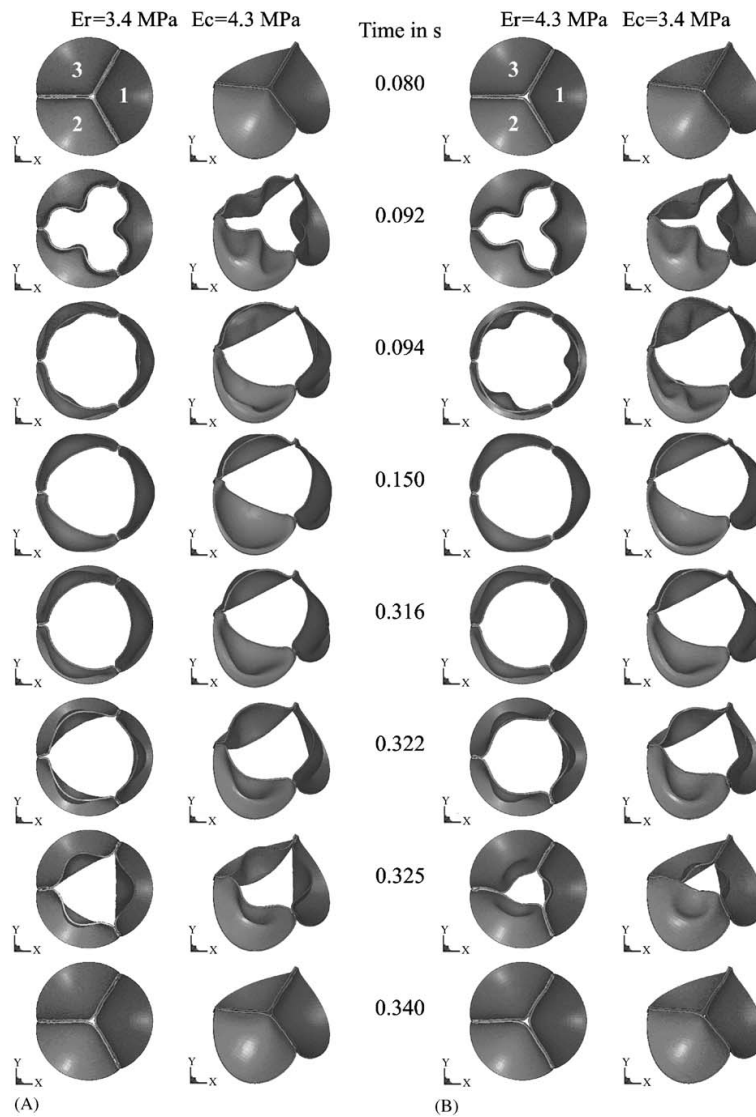


Figure 3.5: Sequences of displacement plots during the whole cycle for the models A (left) and B (right).

3.3.3 Geometric modeling of functional trileaflet aortic valves: Development and clinical applications

The authors, M. Labrosse, M. Thubrikar et al. [6], want to establish a method to determine by how much the dimensions of the aortic valve components can vary while still maintaining proper function.

Measurements were made on silicone rubber casts of human aortic valves to document the range of dimensional variability encountered in normal adult valves. It is very important to consider that the dimensions of the valve components do not change significantly enough during the cardiac cycle and that their variation should be accounted for in a first-order analysis. Analytical equations were written to describe a fully three-dimensional geometric model of a trileaflet valve in both the open and closed positions (see Fig.3.6). The design parameters are: X_s , the coaptation height in the center of the valve, α (resp. β), the angle of the closed (resp. open) leaflet, H_s , the height of the commissures, and Ω , the angle of the free edge in open position.

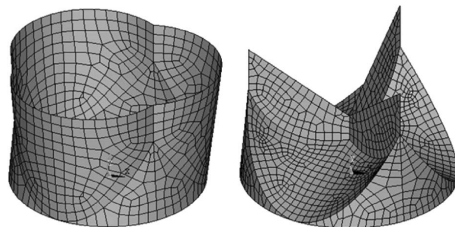


Figure 3.6: 3D model of a trileaflet valve in the open and closed positions.

A complete set of analytical, numerical and graphical tools was developed to explore a range of component dimensions within functional aortic valves. A list of geometric guidelines was established to ensure safe operation of the valve during the cardiac cycle, with practical safety margins. The geometry-based model presented here allows determining quickly if a certain set of valve component dimensions results in a functional valve. This is of great interest to designers of new prosthetic heart valve models, as well as to surgeons involved in valve-sparing surgery.

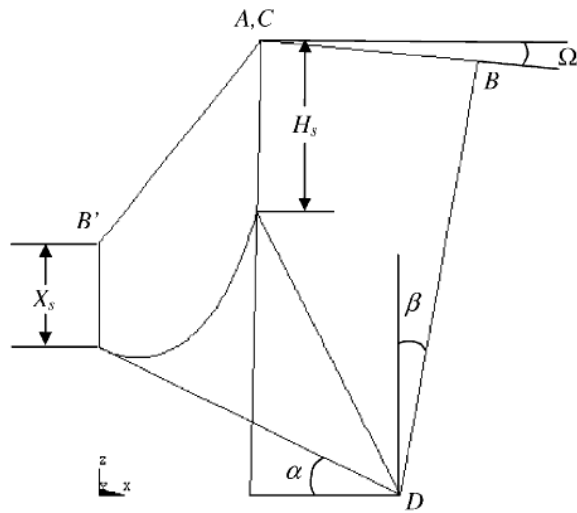


Figure 3.7: Schematic showing the side view of one leaflet in both the open and closed positions. X_s , the coaptation height in the center of the valve, α (resp. β), the angle of the closed (resp. open) leaflet, H_s , the height of the commissures, and Ω , the angle of the free edge in open position.

Chapter 4

Study of aortic valve mechanical behavior through Finite Element Analysis

4.1 Introduction

The aim of present work is to investigate the aortic valve behavior during cardiac cycle, to provide useful information supporting valve sparing operations. Our study has been developed in collaboration with Dr. Stefanos Demertzis, chief service of the heart surgery department of Cardiocentro Ticino¹ and with Samtech Italia², producer of software used for our simulations, Samcef Field V 6.1 .

First some different geometrical models (see Appendix A) have been created before arriving to the definitive one. This has been useful to better understand which were the solving difficulties related to geometry and which were the crucial aortic valve elements that couldn't be left out. Then we have generated our model, introducing some working hypothesis. It is very important to underline that obtained results will be rigorous by methodic point of view , but approximate by quantitative point of view for two reasons: first because passage from physical to simulated reality requires the introduction of simplifications (the so-called working hypothesis);

¹Cardiocentro Ticino is one of the most important swiss heart centre.

²SAMTECH s.a. is the European leading provider of simulation software for Finite Element Analysis and Optimization.

then results will be influenced by type and number elements choice.

We have performed our analysis under large displacement hypothesis and through an implicit nonlinear solver. Two loading conditions (i.e. systole and diastole) were defined applying pressure in the valve leaflets in order to simulate respectively valve opening and closing. The soft tissue material was assumed firstly linear elastic isotropic and subsequently linear elastic orthotropic. Simulations have been performed about both physiological and pathological model. The pathological model has same material properties, boundary conditions, loading conditions, but it has a different geometry. In fact its coaptation area is smaller than normal valve one. The goal of such model would be to demonstrate the importance of coaptation area for the valve sufficiency.

4.2 Geometric model design and construction

Design and definition of a geometrical model able to reproduce aortic valve is very difficult. Aortic valve is a complex biological structure by both anatomical and physiological point of view. So, it is necessary to introduce some simplifications about valve geometry, materials and loading conditions. In this section, we will describe in detail only work hypothesis concerning model design.

Only a third of the aortic valve was considered for FEA (Finite Element Analysis) assuming that three leaflets are identical in size and properties, lying at 120° from each other in the circumferential direction. The real anatomy shows that the three leaflets are not exactly equal to each other, but this small asymmetry don't influence our results in significant way. Then aortic annulus diameter is considered equal to sinotubular junction diameter and consequently equal to aorta diameter. This simplification, in our opinion, is more strong than previous one, because in this way the size of sinuses of Valsalva is reduced and some fluid dynamic aspects are strongly influenced (see vortex theory in paragraph 1.3.2). But we can consider our assumption acceptable because we have performed only structural analysis, ignoring fluid dynamics point of view. Besides we are interested in reimplantation operation effects and during the surgery, in practice, sinuses of Valsalva are removed, because the three leaflets are included into synthetic graft, that is a cylindrical tube.

The geometrical properties of the model are chosen according to the literature [6].

To create our aortic valve model, we have used the *Modeler* module of Samcef

Field. The model, shown in Fig. 4.1, is composed by:

1. an external structure
2. a cusp
3. two caoptation faces.

Now, we will describe the sequence of necessary operations for model generation. For leaflet creation, we have considered a hollow sphere (Fig.4.2-a) with a radius of 7.5 mm. We have cut the sphere by a parallel plane to xy plane, in order to consider only the resulting semi-sphere (Fig.4.2-b).

Subsequently other two cutting operations have been performed by two inclined planes, in order to achieve the desired geometry (see Fig.4.2-c and Fig.4.2-d).

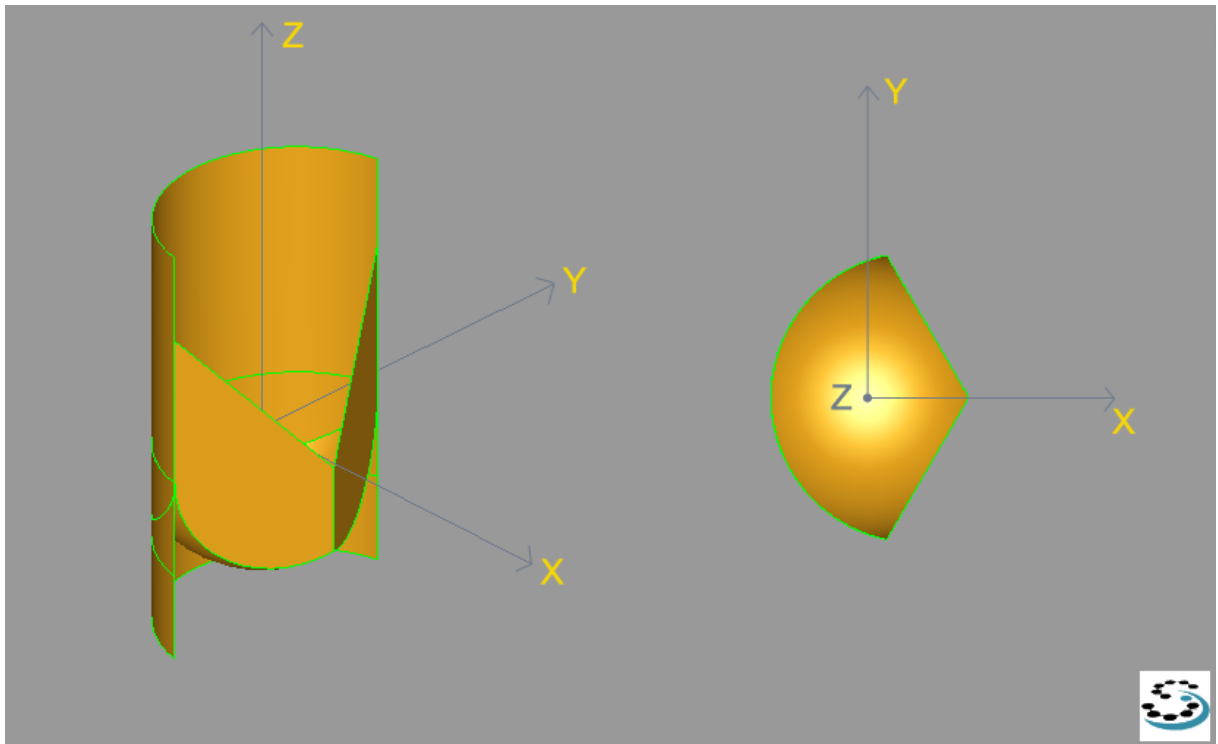


Figure 4.1: Aortic valve model. On the left a three dimensional view and on the right a top view of the third of valve.

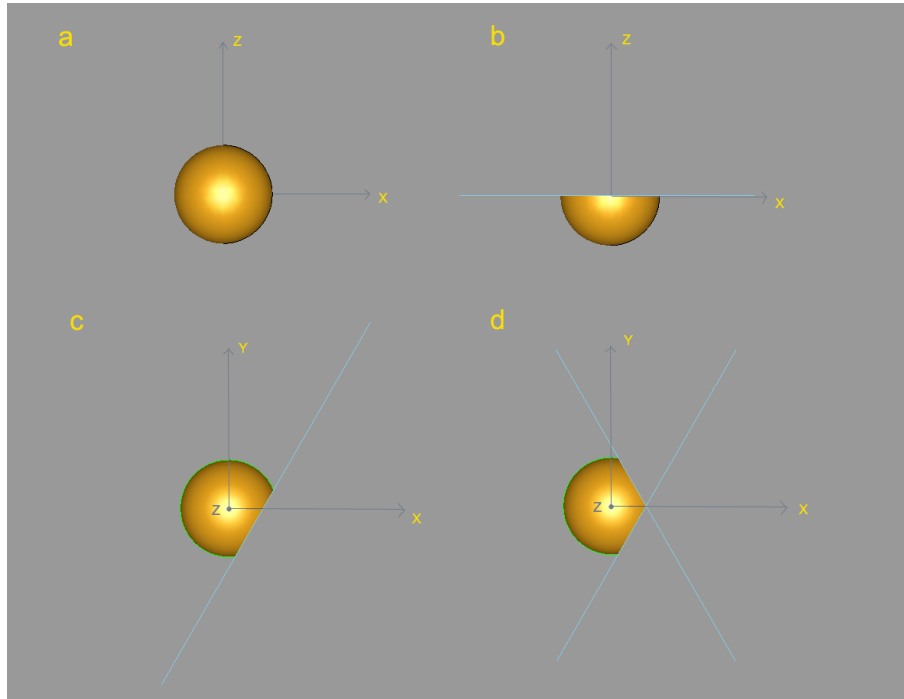


Figure 4.2: Steps for leaflet model generation. a) Whole hollow sphere from side view. b) The sphere is cut with a parallel plane to xy plane. c) The remaining sphere is cut with the first inclined plane. d) The sphere is cut with the second inclined plane.

Such procedure is important to generate a central angle of 120° defined by symmetry hypothesis previously discussed.

To assess the exact point in which the sphere has to be cut, we have considered two lengths, r and h , defining two sides of triangle as shown in Fig.4.3. Their value is respectively 5.33 mm and 9.232 mm. In order to better understand these two sides we have observe the leaflet from the top. In particular r is the distance between the central point of the sphere and the coaptation point, and h is the distance between the central point of the sphere and the point of the space that give us a triangle with angles 30° - 60° - 90° .

The next step is to cut the obtained cusp with a cylinder of radius of 7.586 mm and

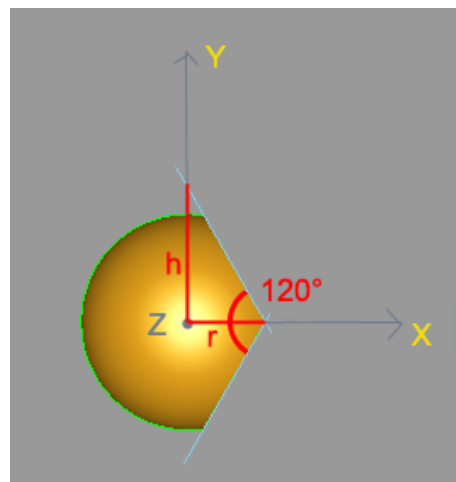


Figure 4.3: The lengths r and h are shown. To respect our symmetry hypothesis we must have a central angle of 120° from a top view.

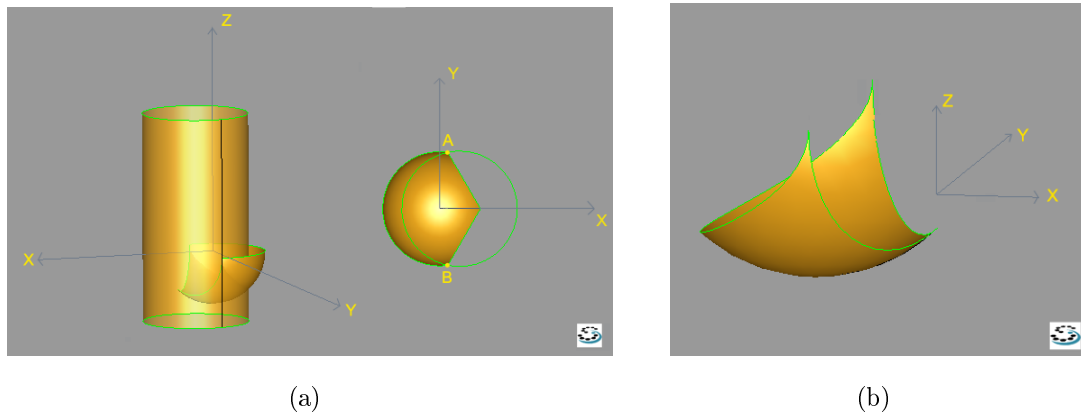


Figure 4.4: a) Tridimensional and top view of the cylinder and the leaflet. b) Final shape of the leaflet.

passing for A and B points (see Fig.4.4-a).

In this way we prepare the leaflet to be placed inside the external structure. The final cusp is shown in Fig.4.4-b.

For external part of the model, an other cylinder has been considered. This derives from our second hypothesis, regarding the diameters of ascending aorta, sinotubular junction and aortic annulus. The radius of cylinder is 7.586 mm and its total height is 24.174 mm. This cylinder is cut in the same way in which we have cut the leaflet previously by the two inclined planes. Then the cylinder and the leaflet have been joined forming a single structure. A and B are the insertion points: they are at 10.587 mm from the bottom of the cylinder. Further information about dimensions are shown in Fig.4.7 .

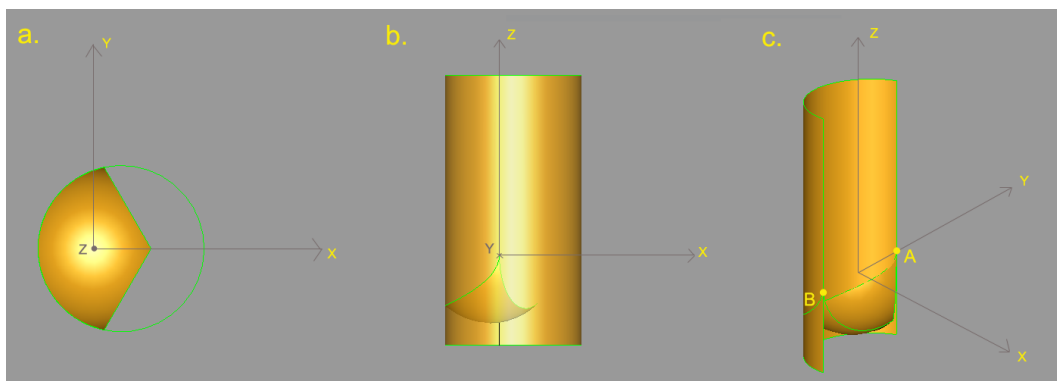


Figure 4.5: Steps for external structure model generation. (a)The cylinder and the leaflet seen from top. (b)The cylinder and the leaflet seen from side. (c) Tridimensional view of the external structure joined the leaflet.

The last step of the procedure is to create the coaptation faces (those in contact with the other two leaflets and that permit valve closing). We have considered points C and D that are both far from A and B 8.587 mm. From coaptation point we have drawn a 5 mm long right line and joined the C and D points with the top of this segment (E point) . So we have generate the face shown in Fig.4.6. The other coaptation face is a mirrored image of the first face.

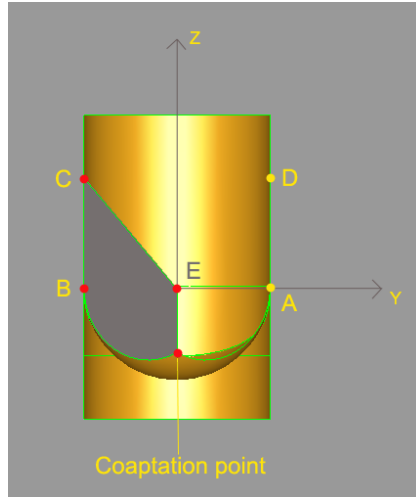
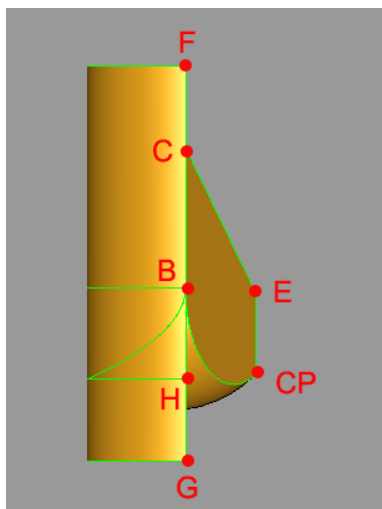


Figure 4.6: Coaptation face is shown in grey. We have obtained it joining the red points.

The final model is given by merging all components up to now described. The model dimensions are shown in detail in the Fig. 4.7.



Segment	Distance [mm]
FC	5
BC	8.587
BG	10.587
GH	5
BF	13.587
ECp	5

Figure 4.7: On the left some reference points of the model, and on the right a related table to distance among these points.

For this model the effective height is 6.9 mm. All cut operations have been performed using *Limit* function, whereas assembly operations have been performed with *Append* and *Sew* function.

4.3 Mesh generation

After geometric model creation, we have generated 2933 nodes and 2902 elements. Mesh is composed by linear quadrangular elements for 97.14 % and by linear triangular elements for 2.86 %. An *Average Length* of 0.516 mm has been used as Mesh Constrains. The obtained mesh is shown in Fig.4.8

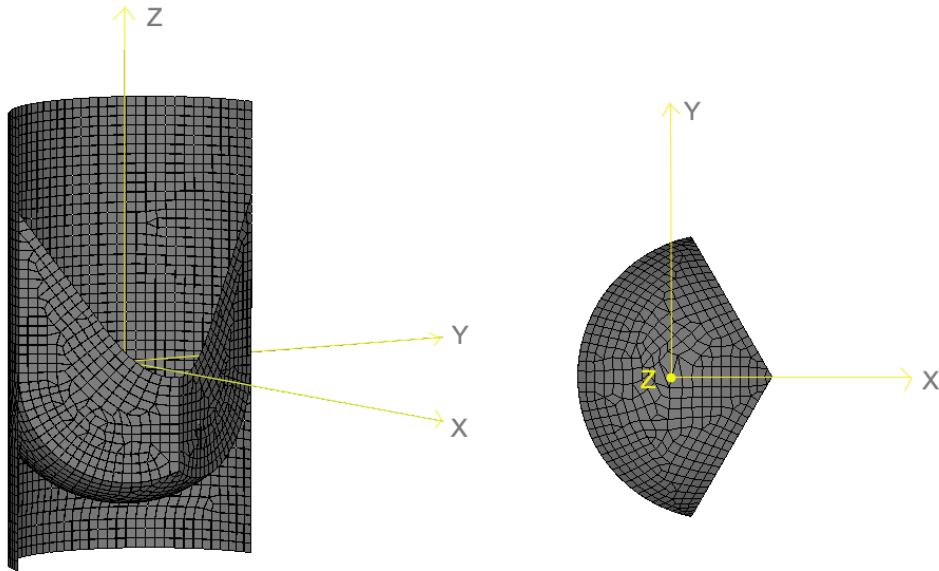


Figure 4.8: A tridimensional and top view of mesh model.

As element we used shell element. A shell is a three-dimensional elastic body occupying a thin neighborhood of a two-dimensional submanifold of \mathbb{R}^3 . 3D shell elements can carry forces and moments lying in their plane as well as forces and moments transverse to their plane. These elements can be used for spatial structures, whose extension in one direction is much smaller than in the other two. Compared to the modeling with solid elements, using shell elements is more comfortable and exact. In fact meshing thin models with solid elements results in generating a large number of elements since you have to use a small element size. Using a larger

element size can deteriorate the quality of the mesh and lead to inaccurate results. Although you can use mesh controls to reduce the number of elements, shell meshing is the natural choice for thin parts. Six degrees of freedom per each node (three translations and three rotations) are considered within structural analysis. In shell elements, a constant thickness is assumed throughout the element. Integration rules (Fig.4.9) in the surface are the following:

- for quadrangular elements, 4 integration points.
- for triangular elements, 3 integration points.

With linear materials, the integration along the thickness is analytical; with nonlinear materials the integration is numerical.

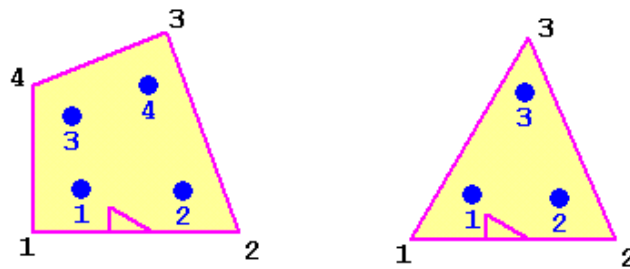


Figure 4.9: Integration point in the surface.

The results of shell elements are reliable only if the following concepts are taken in account:

- the local numbering of the element nodes starts at a corner node and is counterclockwise
- quadrilateral elements are more reliable than triangular elements
- using second order elements produces better results than first order elements or for equal accuracy, the mesh density with linear elements must be larger than with quadratic elements
- the aspect ratio of elements should be near to one (not less than 1:2 to 1.3)
- the edge length should be much greater than the thickness (not less than 5:1)

After type element choosing, we have assigned different thickness to model parts. The external structure has a thickness of 0.8 mm, the leaflet and coaptation faces have a thickness of 0.2 mm and sinuses of Valsalva have a thickness of 0.5 mm. The thickness assignment is shown in Fig.4.10.

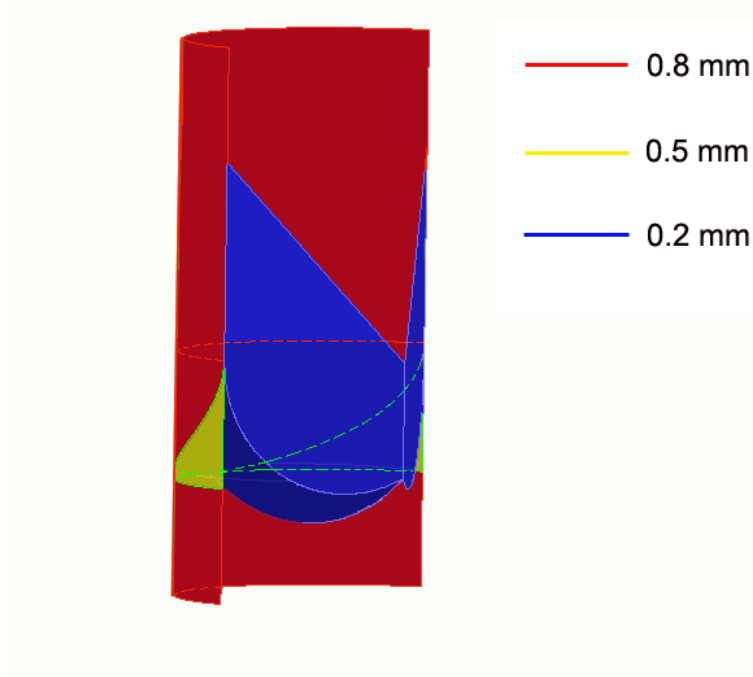


Figure 4.10: Thickness assignment to aortic valve model parts.

4.4 Constraints and Loading conditions

In this section, we will describe the constraints and loading conditions applied to the model. We adopted the same boundary and loading conditions in all simulations.

4.4.1 Definition of constraints

Cause symmetry hypothesis, we have to choose some appropriate constraints to mimic the remaining structure behavior.

The first constraint is contact condition of the faces due to the coaptation area, reproducing the presence of the two other leaflets. Contact has been defined between a rigid structure (not meshed rigid plane) and a flexible part, represented by the coaptation face. This face is pushed against the rigid plane when the load is applied. A contact constraint prevents the coaptation face movement beyond other leaflet

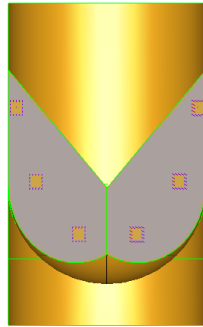


Figure 4.11: Contact condition on the two coaptation faces.

face. The two rigid plane are placed in the same way of the inclined planes used for cutting the sphere previously. In Fig.4.11 it is shown the contact symbol on the two coaptation faces. The same type of constraint has been applied to the lateral ends; consequently the points belonging to these ends can't move in the normal direction to the edges (Fig.4.12). This is important because the two lateral ends coincide respectively with the left end of one leaflet and with the right end of the other leaflet. Penetration among several parts of the model has to be avoided, so

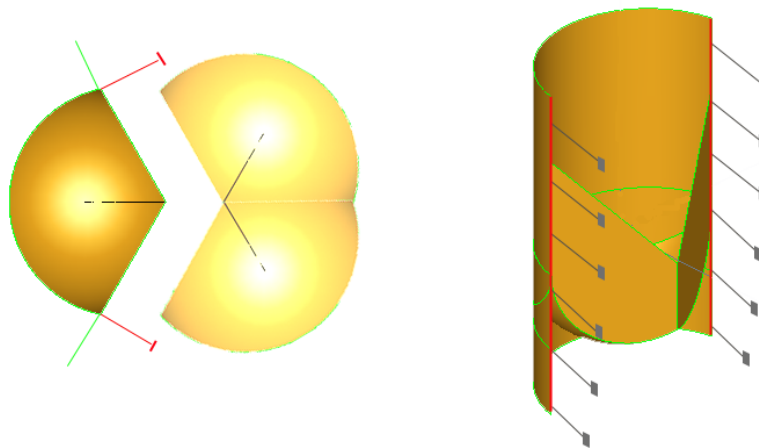


Figure 4.12: Constraints applied to lateral ends of the model. On the left a top view of the valve, with a presence of two other leaflets: in red the forbidden direction. On the right a tridimensional view of the valve: in red the lateral ends subject to constraint.

we have defined also contact conditions among various surfaces. Because contact conditions are discrete, contact is written between node and face or between node and surface and not between face and face. Nodes are defined as "slave nodes"

and faces are defined as "master faces". We have chosen in diastole the external structure as master face and the leaflet as slave nodes, while in systole the external structure and leaflet as master faces and the coaptation faces as slave nodes. An additional constraint has been applied to lower end of the model. Its displacement along Z axis have been locked, allowing only the displacement moving only on the plane that contains the lower end and perpendicular to it (see Fig.4.13). The upper end is free to move, allowing the following of aorta movement.

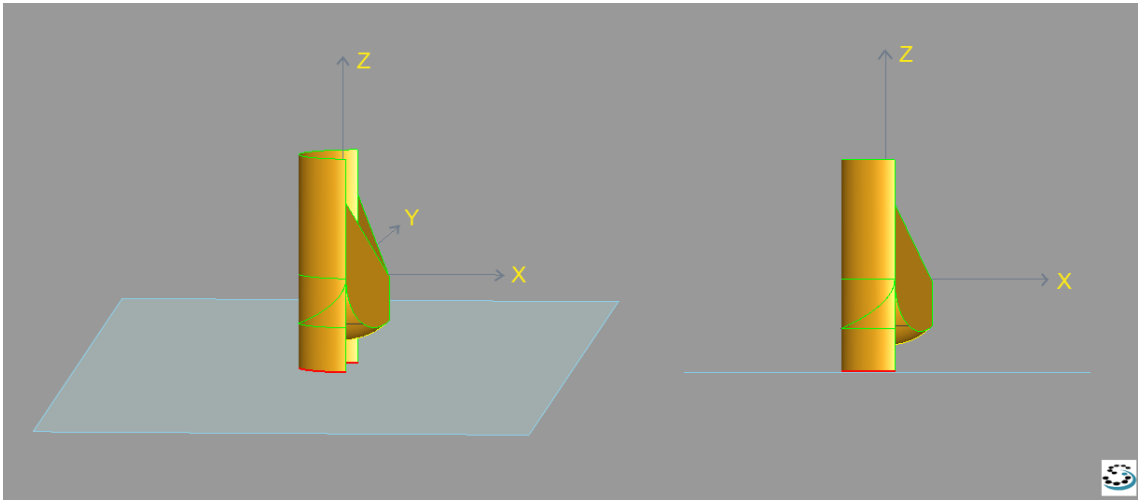


Figure 4.13: Lower end (in red) can move only on a parallel plane to xy plane. Z displacement are locked.

4.4.2 Loading phases: *diastole* and *systole*.

In the first chapter, we have described mechanics of the aortic valve movement, defining two important phases: valve closing (occurring during diastole) and valve opening (occurring during systole). These behavior derived from a pressure difference between the ventricular chamber and the aorta. Blood flow across the aortic valve is pulsatile. It is characterized by high velocity and turbulence presence especially near sinuses of Valsalva that optimize the leaflets closing and opening.

In this study, the fluid dynamics aspects are not taken in account, but we have analyzed aortic valve behavior only through static structural analysis. For this reason we have replaced blood flow with pressure values. Consequently we have defined

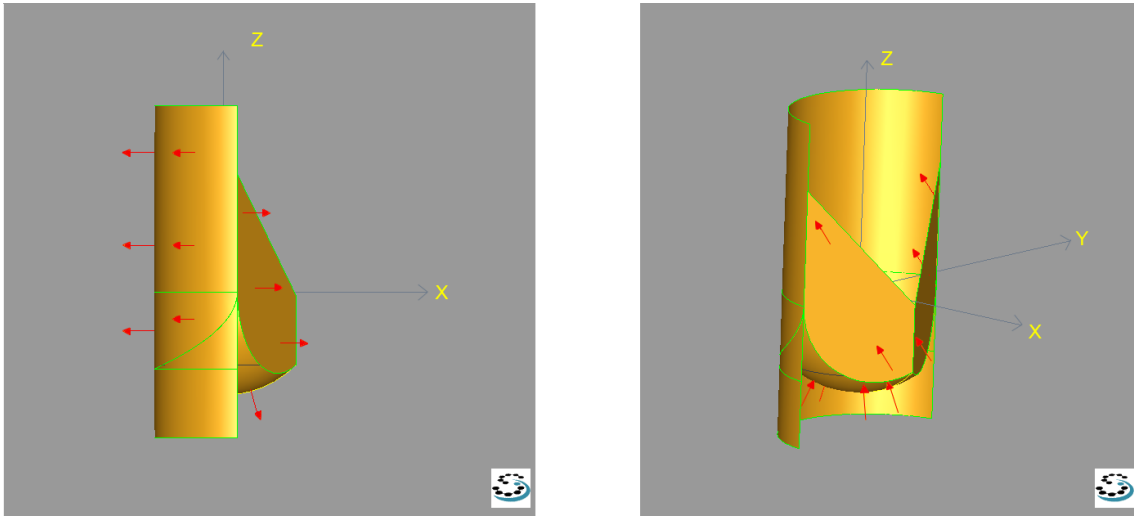


Figure 4.14: Diastole loading condition (left). Systole loading condition (right).

two loading conditions, called *diastole* and *systole*. Pressure values for both phases have been taken from literature (see Chapter 1).

For *diastole* we have chosen a pressure value of 100 mm/Hg reached into 1 second with linear growing. So we have applied an internal pressure to leaflet, coaptation faces and the upper external structure (see Fig.4.14-a).

For *systole* we have chosen a pressure value of 80 mm/Hg, always reached into 1 second with linear growing. In this phase (see Fig.4.14-b), we have applied :

- an external surface force directed along Z to upper part of the leaflet
- an external pressure to the leaflet
- an external surface force directed to 45° to coaptation faces.

The choice of the direction forces during systole is not quite physiological, as in diastole. But, because of the complexity of this movement, we had to find some force types that reproduce the aortic valve opening configuration at the final time. If we had applied an external pressure on the leaflet and on the coaptation faces, omitting fluid dynamics aspects, we would have had a coaptation faces crushing against the external structure before that the leaflet was up, and so a not valve opening.

4.5 Material properties and Analysis

The analysis have been performed under large displacement hypothesis and through an implicit nonlinear solver. As we said previously, we have considered two different material laws: linear elastic isotropic and linear elastic orthotropic. Obviously, we know that valve material behavior is high nonlinear and not quite elastic. In fact aortic valve leaflet has a mechanical behavior more represented by an hyperelastic constitutive law³. But our goal is starting from a model as simple as possible, to arrive to a model that contains all valve property, from geometric to material point of view.

4.5.1 Material isotropic analysis and Results

Assuming isotropic material, we have supposed that the leaflet main tissue component is elastin. This is partially true, because as discussed in chapter 1, the leaflet is made up both elastin and collagen. First component returns the fibers to their initial state, once the external forces of blood flow subside, whereas second has a restrain role. But we think as first approximation it can be reasonable. Two parameters define an elastic linear isotropic material: ν , Poisson's ratio, and E , Young's modulus . We have chosen Poisson's ratio of 0.45 to represent the nearly incompressible behavior of the cardiac tissue [12]. Young's modulus values are the following:

1. 0.6 MPa for leaflet and coaptation faces (it is elastin Young's modulus)
2. 6 Mpa for external structure (it is more rigid than leaflet)
3. 3 MPa for sinuses of Valsalva.

In Fig.4.15 and Fig.4.16 stress-strain diagram for the three material and their assignment to model parts are shown.

³A hyperelastic or Green elastic material is an ideally elastic material for which the stress-strain relationship derives from a strain energy density function. The hyperelastic material is a special case of a Cauchy elastic material. The behavior of unfilled, vulcanized elastomers often conforms closely to the hyperelastic ideal. Filled elastomers and biological tissues are also often modeled via the hyperelastic idealization.

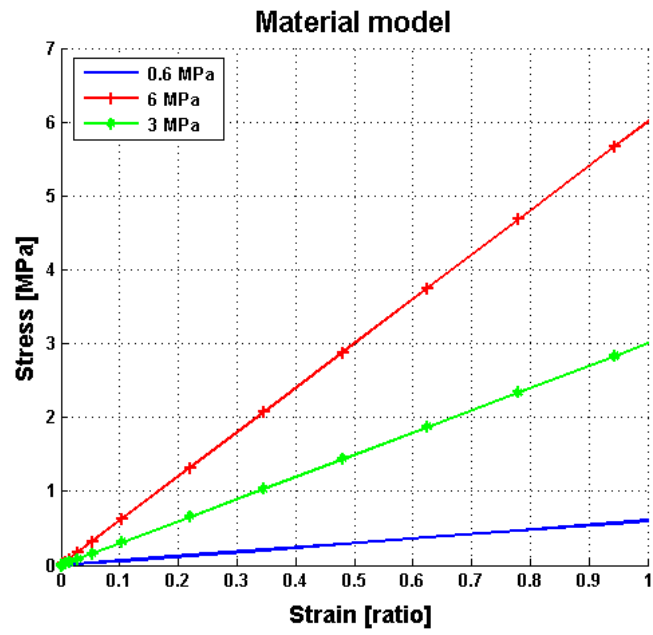


Figure 4.15: Stress-Strain diagram of isotropic materials.

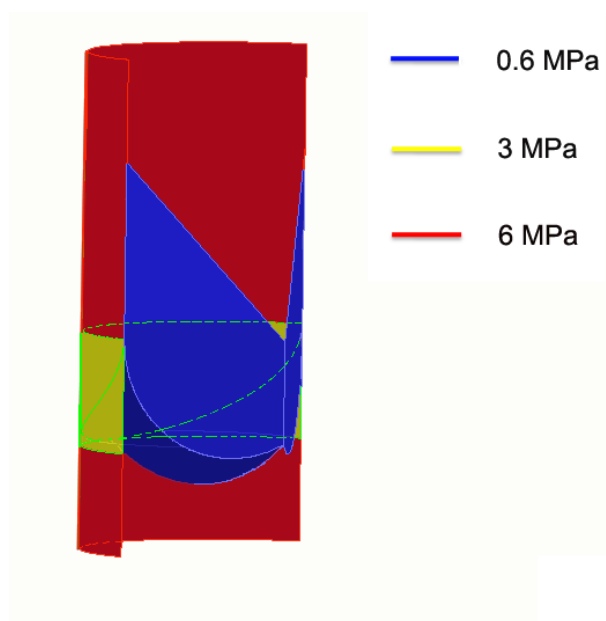


Figure 4.16: Material assignment to model parts.

Even if we have performed static analysis, we have taken in account the mass density values. They are 1000 Kg/m^3 for leaflets, coaptation faces and sinuses of Valsalva and 2000 Kg/m^3 for external structure. In the following, we will describe obtained results about the two loading conditions (diastole e systole).

Diastole

We have performed the first analysis applying all constraints and diastole loading condition described previously. We have observed the difficulty of solver to converge and to find a final solution. Analyzing nodal stress and strain values of the deformed we have noted a concentration of high stress and strain values by Nodule of Arantius (see Fig.4.17). This is due to an high slope of the edges that join in this point.

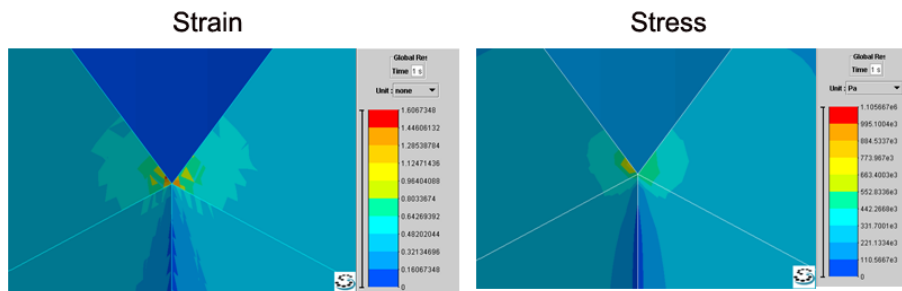


Figure 4.17: Strain and stress values in Nodule of Arantius during diastole.

So, we have made this slope milder, building a U-connection in the critical point (see Fig.4.18).

Performing the analysis with the new model, we have achieved a good improvement.

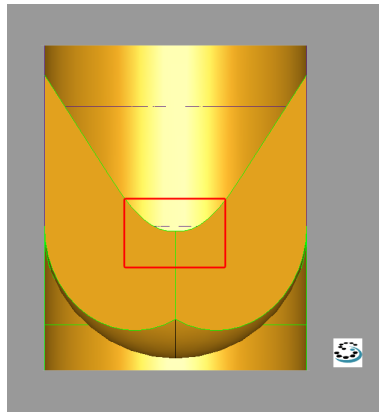


Figure 4.18: In the red rectangle the new U-connection.

In fact, in the Nodule of Arantius stresses are decreased by 50% and strains are passed from 170% to 60% (Fig.4.19). Moreover the new U-connection reproduces better an anatomical aortic valve property .

All next simulation will be performed on the new model.

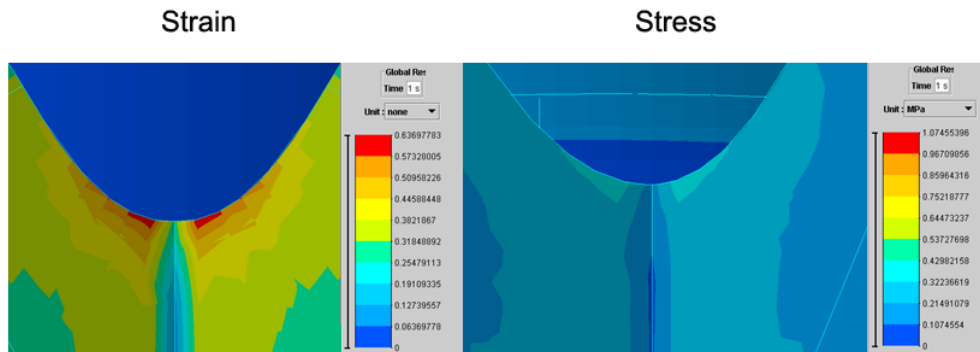


Figure 4.19: Strain and stress in Nodule of Arantius with the new U-connection during diastole.

Therefore we have launched again diastole simulation, getting the results shown in Fig.4.20.

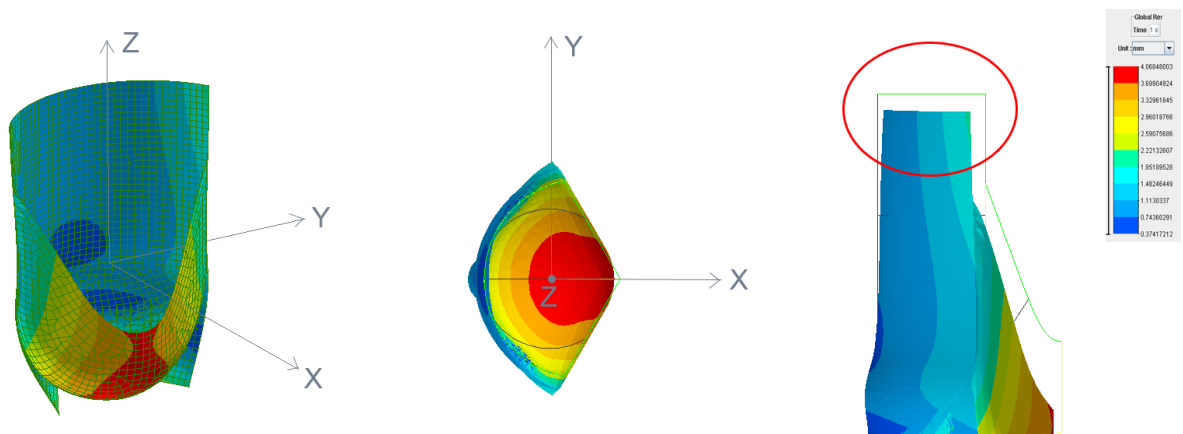


Figure 4.20: Nodal displacements after diastole load condition with U-connection. In order a tridimensional, top and side view. In red circle the external structure lowering.

As we can note, there is a clear leaflet expansion downward due to applied load (an internal pressure). In real aortic valve, this expansion is not so large; leaflet expansion is inferior to millimeter while in our case the leaflet displacement reach about 4 mm. The achieved numerical results can be evaluated keeping in mind the hypothesis about the components of leaflet. In fact in our model the leaflet is

made only of elastin. Consequently it is reasonable to state that the cusp is able to deform so much. Then we can observe the external structure lowering. This behavior happens because upper end is free to move and , as blood vessel, it dilates causing a tissue shortening. Finally there is the coaptation faces crashing against rigid planes.

Checking displacement values, we have noticed that after pressure had reached its maximum value of 100 mm/Hg, at the end of simulation, there was a no complete valve closure. This failed closing is due to a negative displacement along X axis of some nodes belonging to coaptation segment. As reference points, we consider the two end of this segment: the node 324 (top) and the node 323 (bottom) (see Fig.4.21). The maximum displacement along x-axis is 0.461 mm for node 324 and 1.393 mm for node 323.

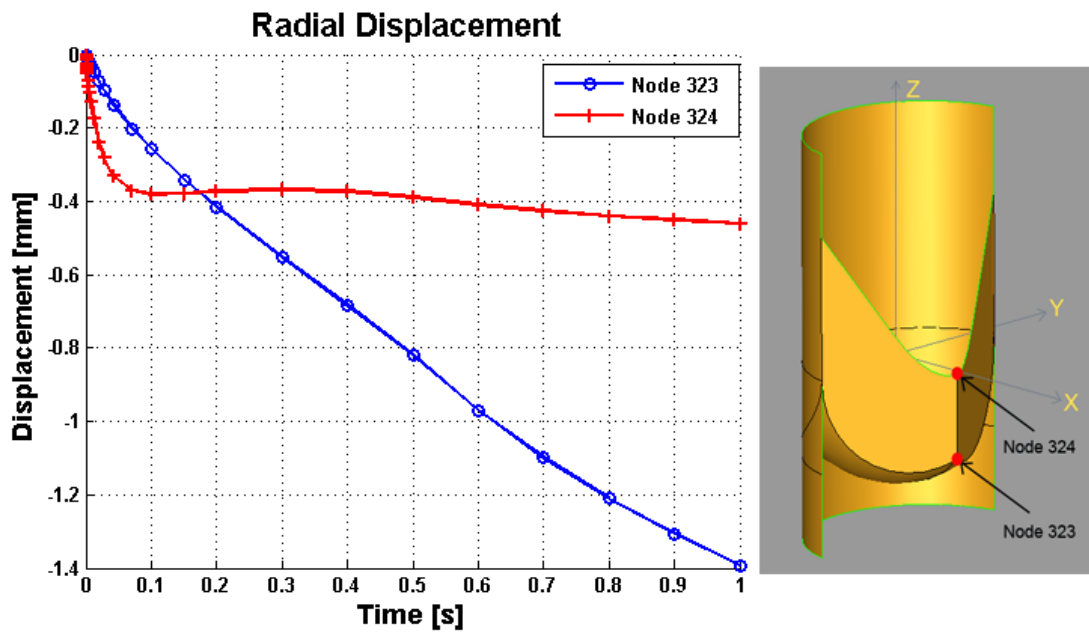


Figure 4.21: Time-Radial displacements graphic of nodes 323 and 324 in isotropic normal valve case.

The "non-perfect" valve closure is caused by the hypothesis of the model, in particular:

- Nodule of Arantius absence: it is like a little ball that seals the valve when the three leaflet meet in the center.

- Uniform thickness of the leaflet and of the coaptation faces: they have an uniform thickness except in the upper end of the coaptation faces where thickness increases, like if there was a string.
- Absence of fluid dynamic aspects (turbulence).
- Material and geometric hypothesis.

For these reason we could retain this *non-perfect* closure value unimportant. On the other hand, we can use it as a comparison tool among the different models (isotropic, orthotropic and pathological). In fact we can retain the best model that has a lower non-perfect closure value.

In isotropic case, we choose as comparison term the lower value, that belongs to node 324. Even if node 323 has a greater displacement along x-axis (radial direction), the lower displacement of node 324 guarantees the valve "closing".

In Fig. 4.22 are shown the valve stresses after load phase. Highest stresses are localized on the top of the valve, on the part of the coaptation faces in contact with rigid planes, on junction area between the leaflet and the external structure and on the leaflet. The stress values are in accord with literature [22]. They have the same order of magnitude (E5 Pa) even if our maximum value is lower than literature one (370E3 Pa against 500E3 Pa).

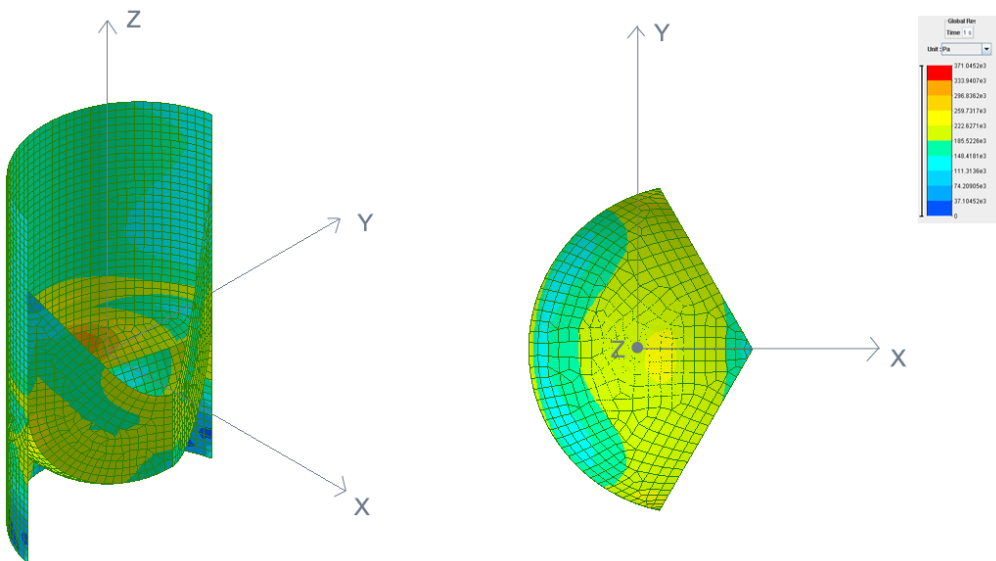


Figure 4.22: Equivalent stresses of isotropic valve during diastole.

Systole

Systole has represented a very complicated simulation type. The high problem non-linearity (contact,geometric non-linearity, large deformations,etc.) made difficult to reach convergence in solution computation. To help the solver to converge we have modified the thresholds of some convergence parameters, increasing them. This involves in a less reliable results than for diastole (in which convergence parameters haven't been modified). But this is not very important, because for aortic valve sparing operations diastole phase is that more significant.

Applying same constraints and systole loading condition described previously, we have obtained the results shown in Fig. 4.23. In this case the leaflet springs up progressively to press itself against the external structure. A little expansion of this occurs (~ 1 mm). The valve model behavior seems to reproduce the real one.

Regarding stresses, we can see their distribution in Fig.4.24. Highest stresses are localized near connection leaflet points to external cylinder. In fact when the leaflet springs up, it tends to stretch with itself the structure to which it is joined. These connection leaflet points are very stressed, because they represent the limit between the free edge and bonded edge. The maximum stress value has still the same order of magnitude of diastole, but it is double ($663\text{E}3$ Pa against $370\text{E}3$ Pa).

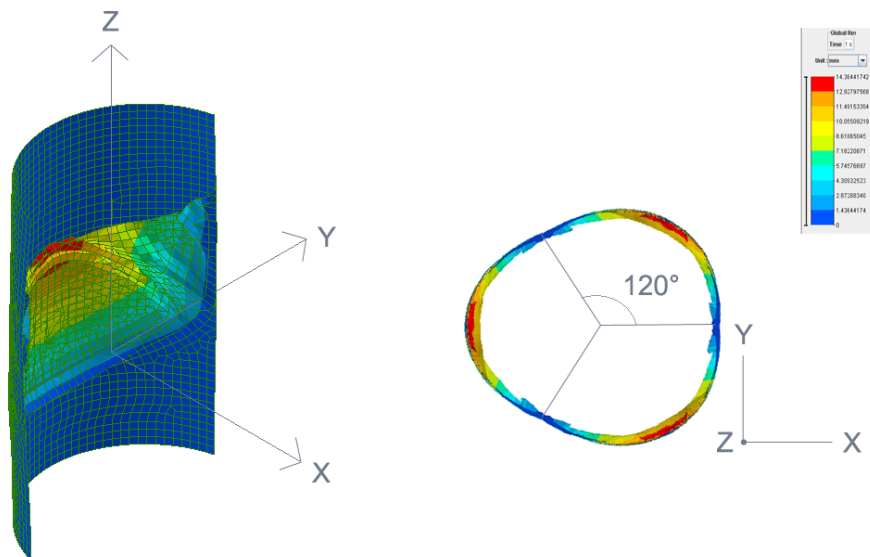


Figure 4.23: Displacement of the valve during systole: on the left a tridimensional view of the deformed and on the right a top view of the whole valve .

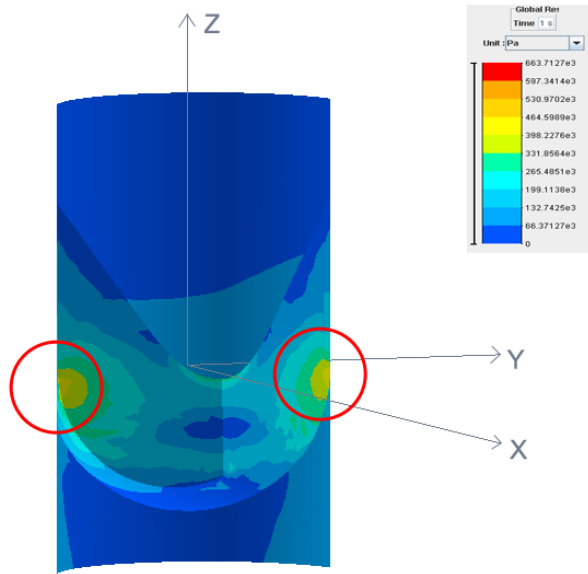


Figure 4.24: Equivalent stresses of isotropic valve during systole. In the red circle the connection leaflet points are highlighted.

4.5.2 Material orthotropic analysis and Results

The second material property hypothesis considered has been orthotropy. As told in previous chapter, this linear elastic material property allows us to assign, along three orthogonal directions, various material parameter values. In this way, we can improve problems related to material property uniform distribution (isotropy), defining on the model three orthogonal directions that allow us to describe aortic valve mechanical behavior in a more realistic way. The leaflet is made up both elastin and collagen, and their fiber alignment depends on the layer to which they belong. Fibrosa is rich in collagen fibers arranged in circumferential direction, whereas ventricularis is rich in elastin fibers arranged in radial direction. So, the leaflet is able to control own expansion in circumferential direction, being more rigid, and to dilate in radial direction. The different behavior along the two directions is shown in Fig.4.25. Constitutive curve progress is not linear, but it has a sigmoidal trend [25]. In our analysis we consider the σ - ε relation linear. We have defined three orthogonal directions, circumferential, radial and longitudinal, as shown in Fig.4.26. For the leaflet and for external cylinder are classical direction of spherical and cylindrical reference system. For coaptation face, radial direction is normal one to face, circumferential direction is aligned fibers direction on the face, the longitudinal direction

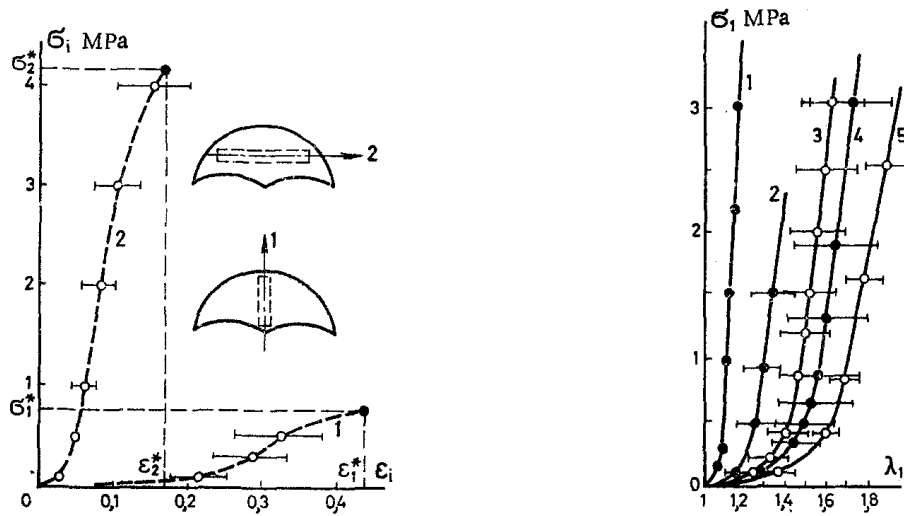


Figure 4.25: On the left: Dependence of σ and ε for human aortic valve leaflets and the scheme for sectioning of the samples in the radial (1) and circumferential (2) directions. On the right: Dependence of σ and λ for individual elements of the human aortic valve: 1) aortic annulus, 2) commissure, 3) sinus wall, 4) arched ring 5) ascending aorta; the unfilled circles indicate the circumferential direction [25].

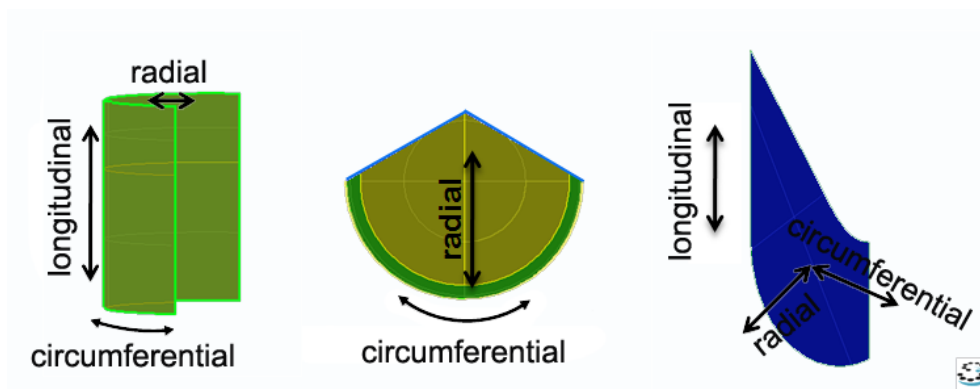


Figure 4.26: Radial, circumferential and longitudinal direction for leaflet, external structure and coaptation face.

is parallel one to Z axis. For aortic annulus (lower cylinder) we have chosen to leave isotropy hypothesis, because there is no study attesting the tissue preferential direction existence.

For material characterization we have used the nine orthotropic independent elastic coefficients: three Young's moduli E_1, E_2, E_3 , three shear moduli G_{12}, G_{13}, G_{23} and three Poisson's ratio $\nu_{12}, \nu_{13}, \nu_{23}$. As for isotropy, we have chosen Poisson's ratio $\nu = \nu_{12} = \nu_{13} = \nu_{23} = 0.45$ to represent the nearly incompressible behavior of the cardiac tissue. Material parameter values are shown in Tab. 4.1 and their assignment to model parts is shown in Fig.4.27.

Young's modulus of aortic annulus is equal to 15 MPa. In Fig.4.25 we can see as aortic annulus is the most rigid structure of the whole valve and we have chosen that value because it represents the slope of the segment that joins the two curve ends. The leaflet orthotropic Young's and Shear moduli are taken from literature [12]. These values take in account both of elastin and collagen concentration. In fact the higher value (6.885 MPa) is allocated to circumferential direction in which collagen fibers are aligned giving more stiffness to the valve. If we consider that Young's modulus of pure collagen is 10 MPa, we understand that its value is diminished by elastin presence. In the same way, if analyze the lower value (1.624 MPa), allocated to radial direction, we note that it is a little more high than elastin Young's modulus, that is 0.6 MPa (used by us for isotropic simulations), because it includes collagen presence.

Property	Leaflet	External structure	Coaptation face
E_1	6885	20	1624
E_2	1624	6	6885
E_3	1624	6	1624
G_{12}	1121	10	560
G_{13}	560	3	1121
G_{23}	560	3	560
ν	0.45	0.45	0.45

Table 4.1: Material properties for aortic valve. Young's and Shear modulus measure are in KPa.

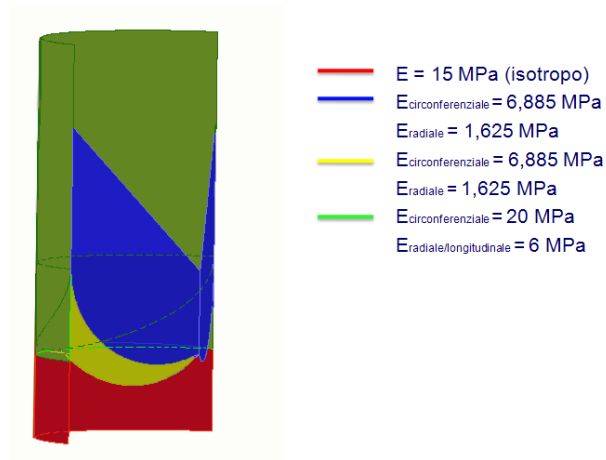


Figure 4.27: Material parameter assignment to model parts.

We consider again a mass density values of 1000 Kg/m^3 for leaflets, coaptation faces and sinuses of Valsalva and of 2000 Kg/m^3 for external structure. Now, we will describe the obtained results during diastole and systole.

Diastole

Applying all constraints and diastole loading condition described previously, for the orthotropic model we have obtained the results shown in Fig.4.28.

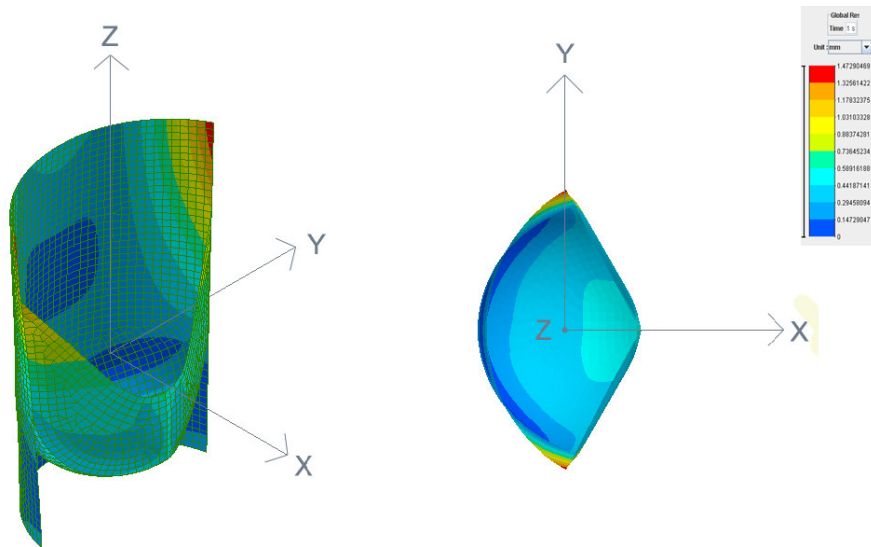


Figure 4.28: Nodal displacements after diastole load condition. In order a tridimensional and top view of the orthotropic model.

First of all we note that displacement peaks are decreased of 70%, passing from a top value of 4.068 mm to 1.48 mm. Moreover these peaks don't concern any more the leaflet, but upper ends of the external structure. This behavior replicates the real valve one. The leaflet is not able to expand oneself like in the isotropic case because of a greater stiffness in circumferential direction. Therefore it is present a restrain effect due to collagen. The upper part of the external cylinder is subject to the bigger displacements: when we apply an internal pressure, the sinotubular junction dilates to follow aorta expansion. But only junction points among the leaflets, previously called lateral ends, distend. They are the most dilatable part of model during diastole.

Analyzing the *non-perfect* closure level defined in the previous paragraph, we have noted that the negative displacements along x-axis are diminished. In particular, the maximum displacement value is 0.58 mm for node 324 and 0.40 for node 323.

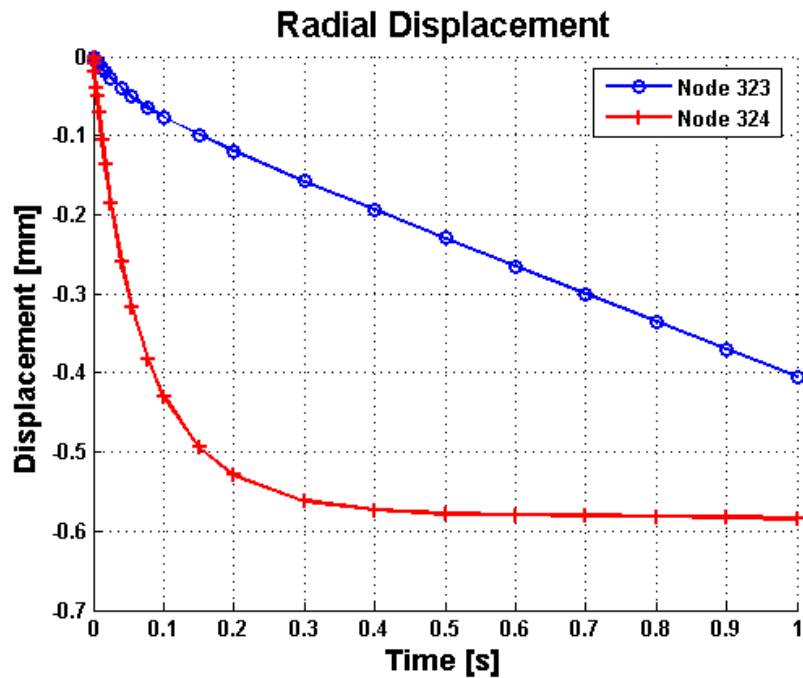


Figure 4.29: Time-Radial displacements graphic of nodes 323 and 324 in orthotropic normal valve case.

We observe that, in this case, the node 323 has a lower displacement than the node 324. This is due to the different way in which the valve warps. While in isotropic case the node 324 moved forward and the node 323 went back, now, the node 323 moves forward and the node 324 goes back. So, for orthotropic case we

choose as comparison value the displacement of node 323.

In Fig.4.30 are shown the valve stresses after load phase. Most high stresses are localized on the part of the coaptation faces in contact con rigid planes (Fig.4.31), on junction area between the leaflet and the external structure and on the leaflet. In this case they don't correspond to the parts with greater displacements, but they are the regions that have to support the greater tensions. Stress values are about three times little if compared with isotropic model one, but they have the same order of magnitude.



Figure 4.30: Equivalent stresses of the valve after diastole load condition. In order a frontal, tridimensional and top view.

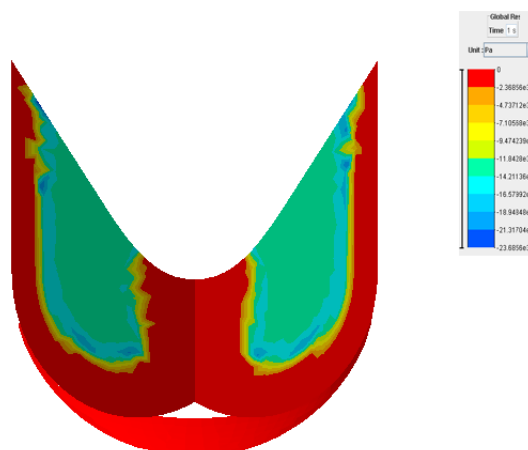


Figure 4.31: Contact pressure on the orthotropic coaptation faces after diastole.

Systole

Systole has represented a very complicated simulation type also in the orthotropic case. To problems already described, a greater material stiffness has complicated matters further. In Fig.4.32 we can see that, at the end of systole simulation, the leaflet has not been able to press oneself against the external structure totally. This simulation has come to the end without any error or warning, but obviously solver has difficulties to calculate the correct solution. Observing final deformed, we see that it is as if coaptation faces ensconce themselves on the leaflet, after an initial raising. We obtain a valve opening, but it is not just the correct physiologic one. Moreover valvular lumen is reduced compared with isotropic lumen after systole. After these considerations, we must highlight again that the results about systolic load condition are important but not fundamental to give support to the valve sparing operations. They are useful for understanding the aortic valve behavior better, but what interests us is the accuracy of the diastolic case.

About stresses, we can see their distribution in Fig.4.33. For orthotropic case higher stresses are localized near connection leaflet points to external cylinder and on the leaflet center. Stress values are one order more of magnitude compared with isotropic model stress values.

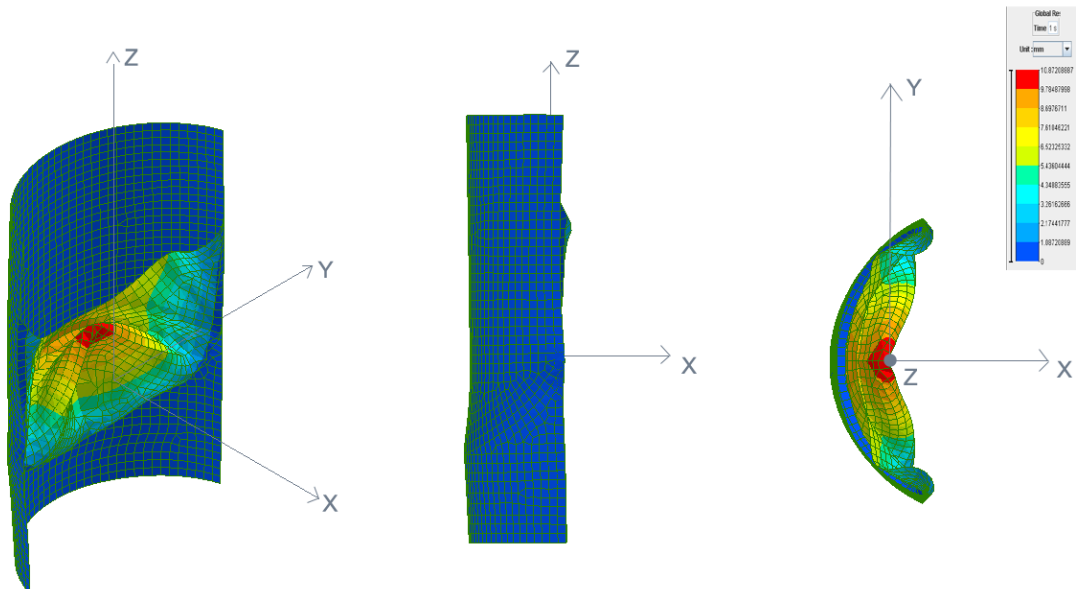


Figure 4.32: Displacement of the orthotropic valve during systole. In order a tridimensional, side and top view of the deformed.

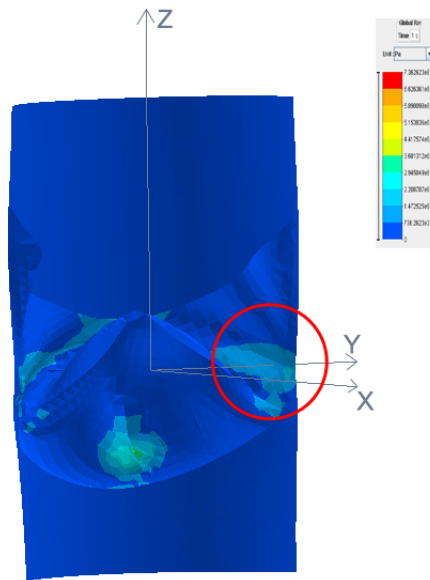


Figure 4.33: Equivalent stresses of isotropic valve during systole. In the red circle the connection leaflet point is highlighted.

4.6 Pathological model Analysis

The idea to design and construct a pathological model serves to understand if the size of coaptation area is important for the valve competence. Really, this model doesn't represent a true pathological valve, because this has the dilated sinotubular junction that doesn't allow the valve to close perfectly. But in this case we have called the model like pathological because, in some sense, a lower coaptation could make the valve as incompetent. So, our pathological valve is the native valve that has been reimplemented into a graft with a lower coaptation.

Now, in this paragraph we will describe the model construction, the performed analysis with respective results and the comparison with the normal valve model.

4.6.1 Model design and construction

For the pathological model design we have considered the same simplifications adopted for the normal model: diameter of the sinotubular junction equal to aortic annulus diameter, leaflet symmetry and lack of the sinuses of Valsalva.

Also the pathological model has composed of three principal parts: a leaflet, two coaptation faces and an external structure. We still have considered an hollow sphere and we cut it like in the Paragraph 4.2 obtaining the leaflet shown in Fig 4.34. In

this case the sphere radius is still 7.5 mm but the lengths r and h are respectively 4.33 mm and 7.49 mm.

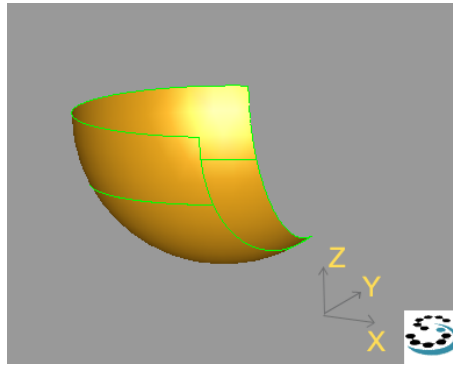


Figure 4.34: Pathological leaflet.

Then we have created a cylinder of radius 11.849 and 24 mm tall. We have cut also the cylinder with the same planes used for the sphere and we have joined the two elements as shown in Fig. 4.35. The joining between the two parts has been made along a leaflet edge.

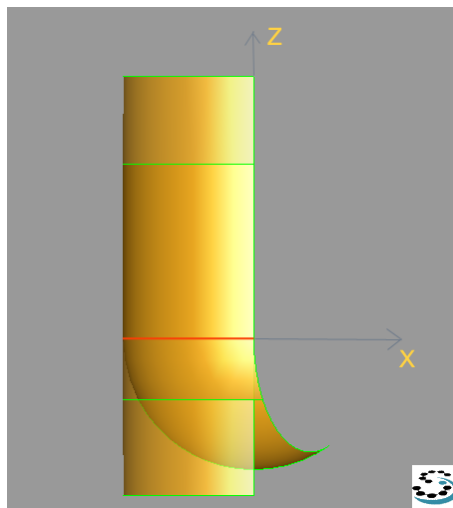


Figure 4.35: The cylinder and the leaflet, joined along the leaflet edge shown in red.

Finally we have created the two coaptation faces in the same way of the normal model. The complete pathological model is shown in Fig. 4.36.

The model has been so designed and constructed because we want reproduce a particular situation in which the effective height (see paragraph 2.3.4) is less than

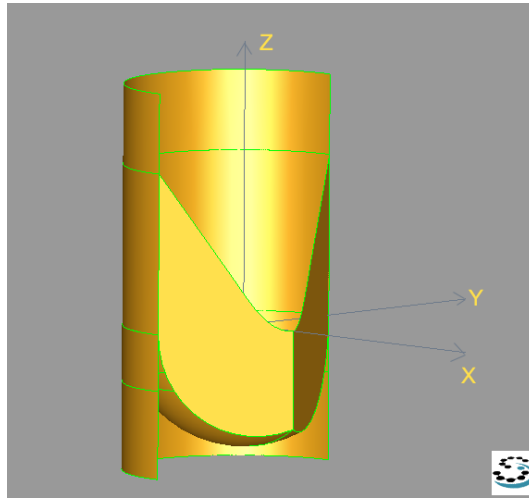


Figure 4.36: A three-dimensional view of the pathological model.

4 mm . This is the condition for which the lower coaptation doesn't guarantee the success of the aortic valve sparing surgery. The effective height is the distance between the points 3 (the highest point of the coaptation) and the lowest point of the leaflet (see Fig. 4.37). For the normal model it is 6.9 mm while for the pathological is 4.2 mm. Sometimes the lowest point of the leaflet coincides with the point 1 (the leaflet insertion point). Moreover a typical characteristic of a "pathological" valve is that the point 2 and 3 are lower or equal than the point 1. This means in a leaflet relaxation downwards and in a possible valve opening.

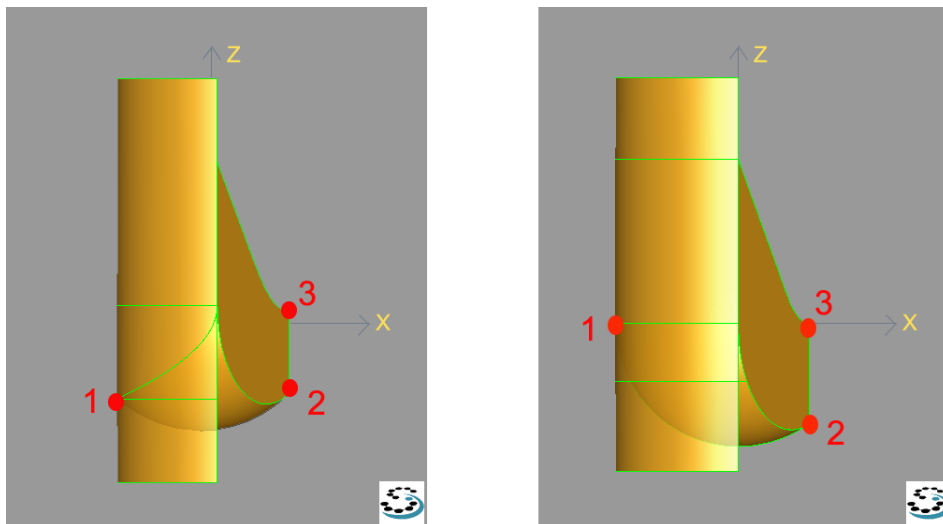


Figure 4.37: The normal (left) and the pathological model (right). The typical points to evaluate the valve coaptation are highlighted.

4.6.2 Analysis and results

The analysis for pathological model have been performed under the same normal model hypothesis (large displacement, static analysis, implicit nonlinear solver). We have applied the same thicknesses, the same constraints, the same materials and the same loads described previously. Here, we will analyze only the results obtained after diastole because it's the physiological condition in which a lower coaptation could cause the valve incompetence.

The results of the pathological model with isotropic material are shown in Fig.4.38.

Like the normal model, there is a great leaflet expansion. The nodal displacements

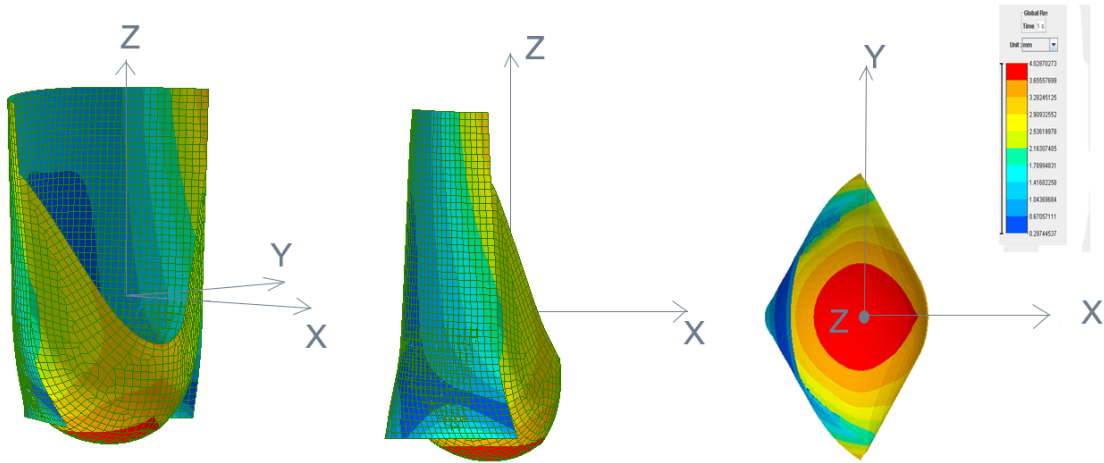


Figure 4.38: Displacement of the isotropic pathological valve after diastole. In order a tridimensional, side and top view of the deformed.

are comparable and they are arranged in the same way. The maximum displacement value is 4.028 mm. But if we look to the displacement along the x-axis of the two ends of the coaptation segment, the node 174 (top) and the node 138 (bottom), we can note that their value is almost double than the normal model. They are 0.88 mm for the node 174 and 2.11 mm for the node 138. This means that the geometry change has influenced the displacement of those important nodes for a greater valve closing. Like comparison value we choose the lower, that belongs to node 174. In Fig.4.39 the graphic time-radial displacement of node 174 (belonging to pathological model) and of node 324 (belonging to the normal model) is shown. Both are upper ends.

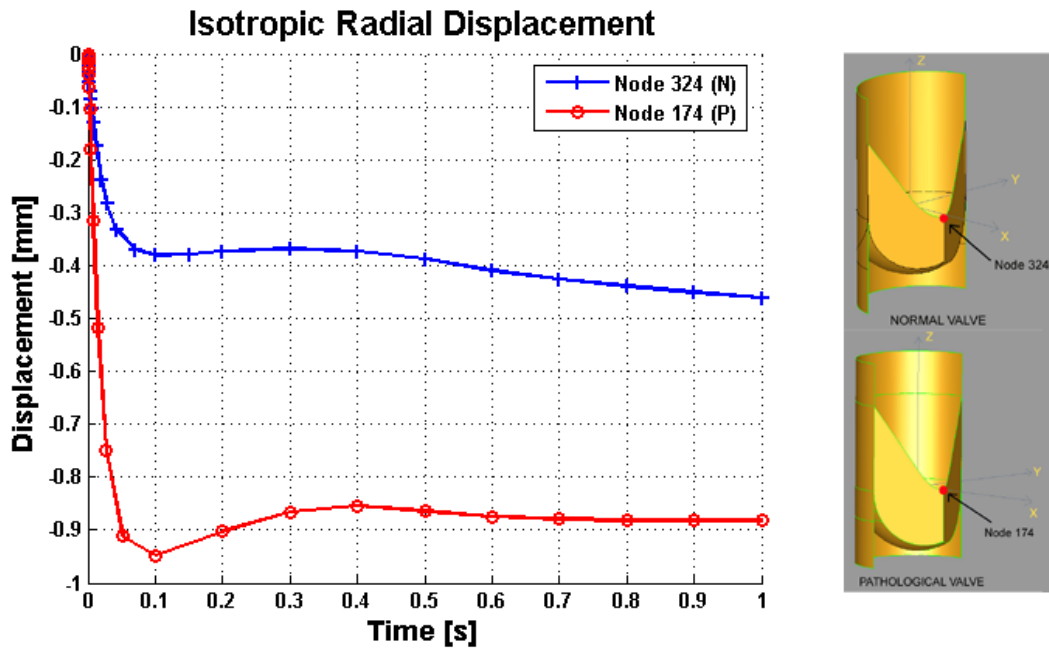


Figure 4.39: Time-Radial displacements graphic of nodes 174 and 324 in isotropic case. The node 174 and the node 324 are respectively the upper ends of the coaptation segment of the pathological and normal model.

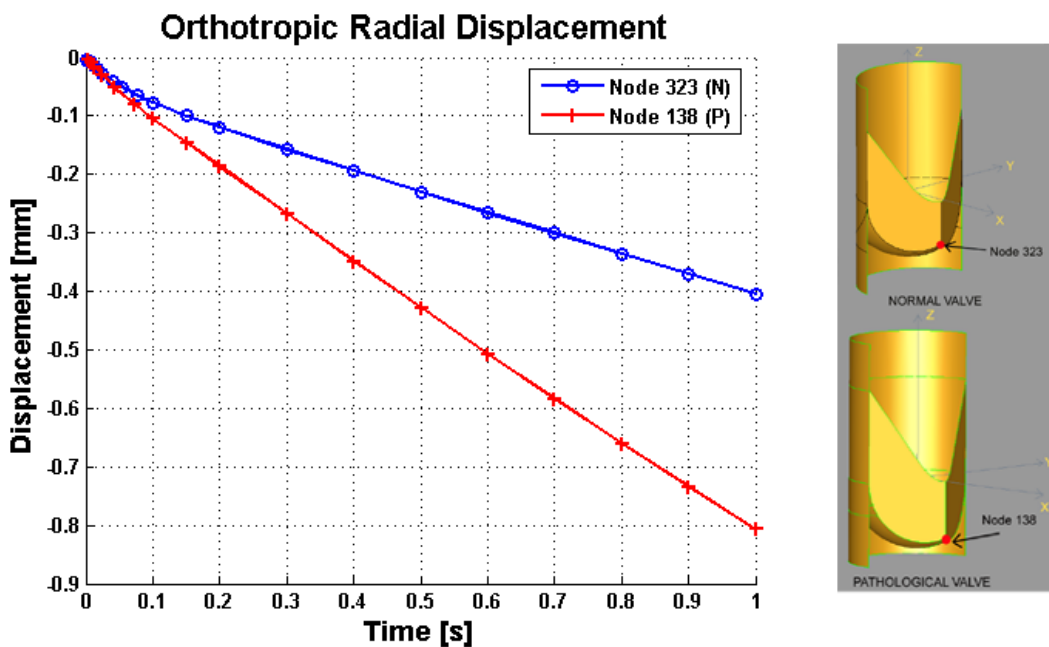


Figure 4.40: Time-Radial displacements graphic of nodes 138 and 323 in orthotropic case. The node 138 and the node 323 are respectively the lower ends of the coaptation segment of the pathological and normal model.

For the pathological model with orthotropic material we have obtained the results shown in Fig. 4.41. Also in this case the behavior of the orthotropic pathological

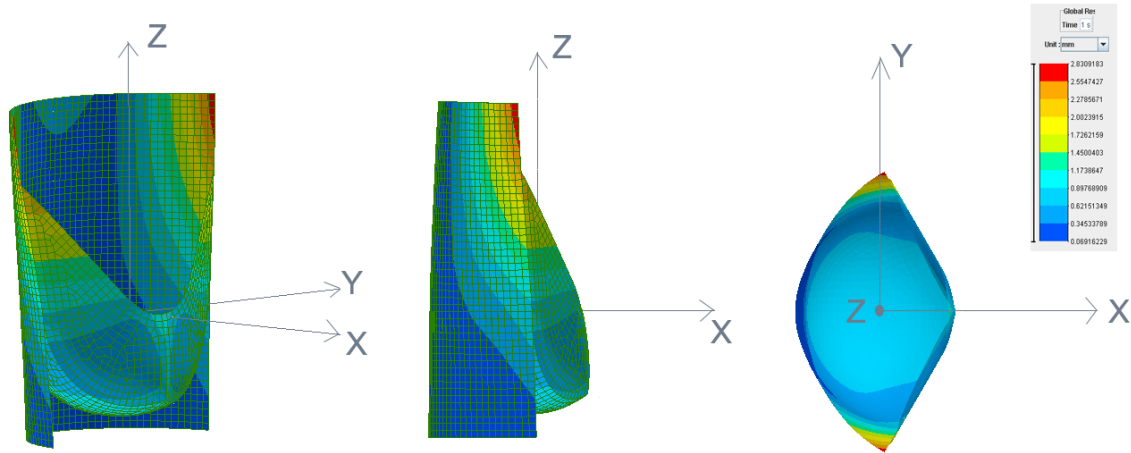


Figure 4.41: Displacement of the orthotropic pathological valve after diastole. In order a tridimensional, side and top view of the deformed.

model is comparable with the normal one. There is a great reduction of the displacement value(the maximum pass from 3.96 mm to 2.83 mm) and the peaks don't concern any more the leaflet, but upper ends of the external structure. Even if the displacements are diminished, they are greater than the normal model. In particular if we analyze again the displacements along the x-axis of the nodes 174 and 138, also in this case, we can note that they are double than the radial displacements of the orthotropic normal model. The two node reach a displacement value respectively of 1.18 mm and 0.80 mm. Like in the normal case, the node 138 has a lower displacement than the node 174. This means that the node 138 moves forward and the node 174 goes back (see Fig. 4.41). For these reasons we choose as comparison value the displacement of node 138. In Fig.4.40 the graphic time-radial displacement of node 138 (belonging to pathological model) and of node 323 (belonging to the normal model) is shown. Both are lower ends.

In conclusion, Table 4.2 summarize the obtained results. We have performed the same analysis, with isotropic and orthotropic material during diastole, on two different models, the pathological and the normal. We have choose as reference points the ends of the coaptation segment, with aim to prove that a lower coaptation doesn't allow to valve to close fully. We have considered the negative radial displacement of these ends to evaluate the "opening" degree. Both the isotropic and

the orthotropic analysis have shown that the radial displacements of the pathological model are greater than the normal one and that the opening degree is always greater in the pathological model. For these reasons we can say that the coaptation level influenced the valve competence.

		Normal valve	Pathological valve
Isotropy	Top	0.46	0.88
	Bottom	1.393	2.11
Orthotropy	Top	0.58	1.18
	Bottom	0.40	0.80

Table 4.2: Maximum radial displacement of up (324 and 174) and down (323 and 138) nodes of the normal and pathological model, in isotropic and orthotropic case.

In the next chapter, we will described briefly an alternative way to generate a pathological model. It is still a developing approach, but it allows to performed a parametrical analysis without, every time, creating a new model (like in this case).

Chapter 5

The parametric aortic valve model: an alternative approach

In this chapter we will describe an alternative approach used to generate a new aortic valve model. This was made with contributions of Davide Vailati for the geometry and Laura Pozzi and Michele Conti for the analysis. The new approach is based on necessity to have a model in which can change parameter sizes without generating another model. We have created directly the mesh model through Pyformex program and then we have performed some analysis with hyperelastic behavior, to check the geometric model validity. It is still a developing approach.

5.1 Pyformex

PyFormex [26] is an innovative and creative platform based on Python. It is a tool for generating, manipulating and operating on large geometrical models of 3D structures by sequences of mathematical transformations and it is currently under development at Ghent University. PyFormex is especially suited for the automated design of spatial frame structures, but it can also be used for other tasks, like finite element preprocessing, or just for creating some nice pictures. By writing a simple script, a large and complex geometry can be created by copying, translating, rotating, or otherwise transforming geometrical entities. pyFormex will interpret the script and draw what you have created. pyFormex also offers interesting possibilities for executing specialized operations on surface meshes, usually STL type triangulated meshes originating from CT or MRI images.

In Fig. 5.1 are shown some pictures generated by PyFormex.

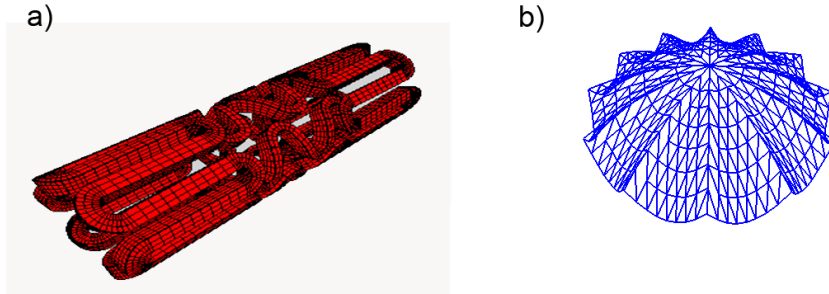


Figure 5.1: Some pictures generated with PyFormex: an expanding stent (a) and a scallop dome (b).

5.2 Parametric model generation

The parametric model generation comes from the limitation of the code used for generate our model in changing the parameters value without modify the valve geometry. As the parametric analysis is an important step of our study, we thought proper to find a simpler way to do these analysis. In fact, by Pyformex, once defined the parameters, it is possible to modify directly their value through a graphical interface. The parameters that can be modified (see Fig. 5.2) are :

- Aortic radius (R_a)
- Aortic connection height (L_a)
- Bending of the sinus of Valsalva
- Leaflet height (C_{max})
- Coaptation height (H_c)
- Centre angle (α)
- Leaflet mesh (thickening)
- Aortic root mesh (thickening)

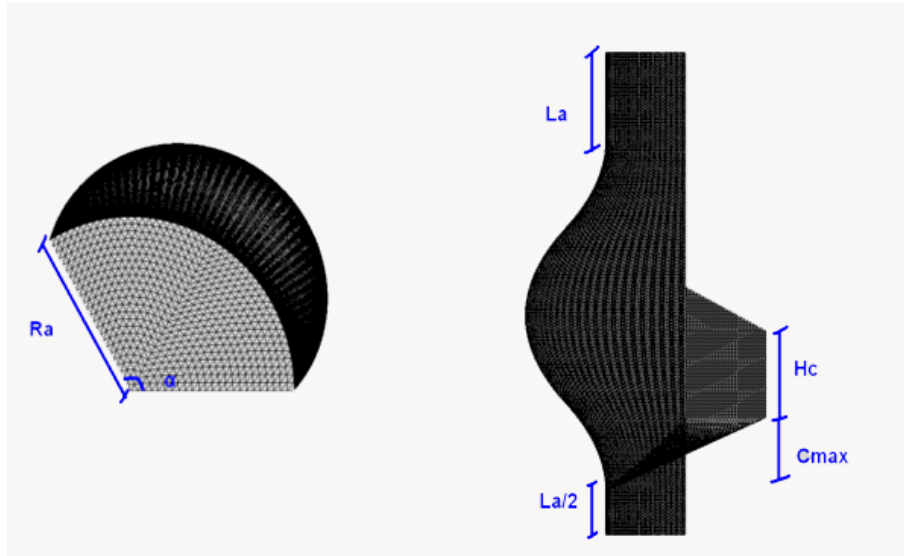


Figure 5.2: Model parameters that can be modified: R_a (aortic radius), L_a (aortic connection height), C_{max} (leaflet height), H_c (coaptation height), α (centre angle) .

The parametric model is made of three principal parts:

1. a cylinder that replaces the external structure of the first model
2. a leaflet
3. a coaptation faces

To generate each part, Pyformex starts from creating of simple triangles (see Fig.5.3): they are replicated according to some mathematical functions and their number establishes the mesh thickening. In this model, the sinuses of Valsalva are included:

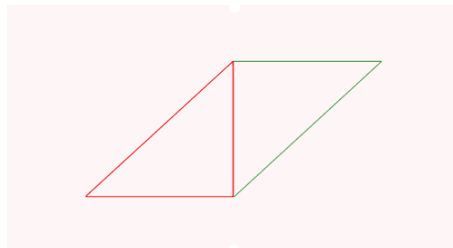


Figure 5.3: Core triangles for geometry generation by Pyformex .

they are represented by the bending of the cylinder to outside.

The leaflet has been created taking account of its real roundness. In Fig.5.4 are shown each model component, like these elements have been joined to generate the

third of the valve and the whole valve.

The default values for model generation are:

- Aortic radius (R_a)= 12 mm
- Aortic connection height (L_a)= 6 mm
- Bending of the sinus of Valsalva = 4
- Leaflet height (C_{max})= 5 mm
- Coaptation height (H_c) = 6 mm
- Centre angle (α) = 120°
- Leaflet mesh (thickening)=12
- Aortic root mesh (thickening) = 24

The aortic root mesh is more thick than leaflet one, because it is very important to have correct strains in this region: it is geometrically more complex than the leaflet. The model, so obtained, has 4250 nodes and 8064 elements. These values refer to one third of the valve.

If we modify the default values, we can obtain different degrees of valve pathology, and check the coaptation influence in the valve competence. So, we have generated also a pathological model (see Fig.5.5) with a lower coaptation area ($H_c = 3$ mm) and a lower leaflet height ($C_{max} = -1$ mm). The aortic root dilatation is not included.

In this model there are still some geometric limitations, like the acute angle in the coaptation point, the sinotubular junction diameter equal to aortic annulus one, the leaflet depth, etc. Obviously this is not a definitive model, but it represent a start point can reproduce the real behavior of the aortic valve.

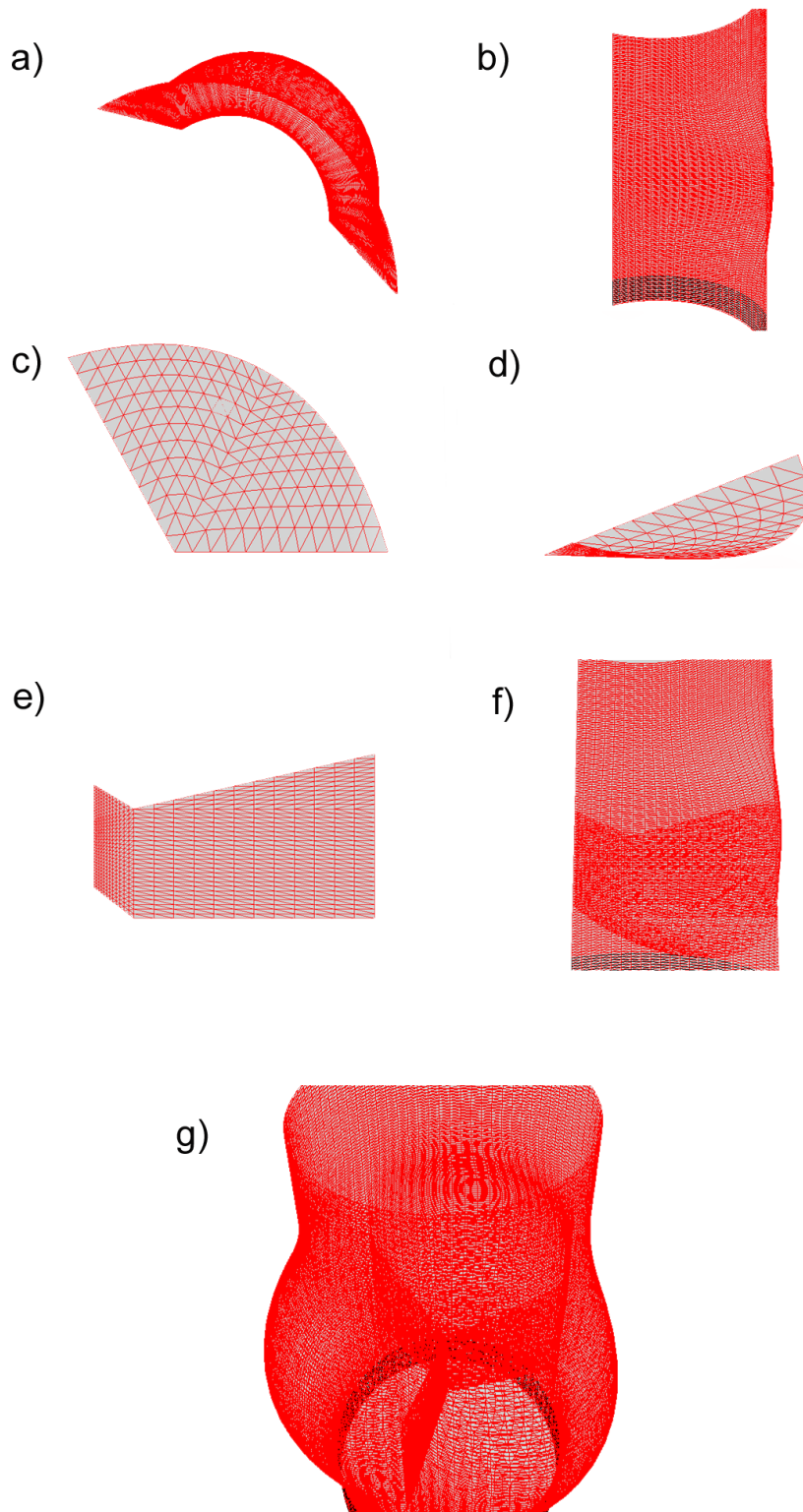


Figure 5.4: Components of parametric model. Top (a) and side (b) view of the cylinder with sinuses of Valsalva. Top (c) and side (d) view of the leaflet. Coaptation face (e). One third of the valve (f). The whole valve (g).

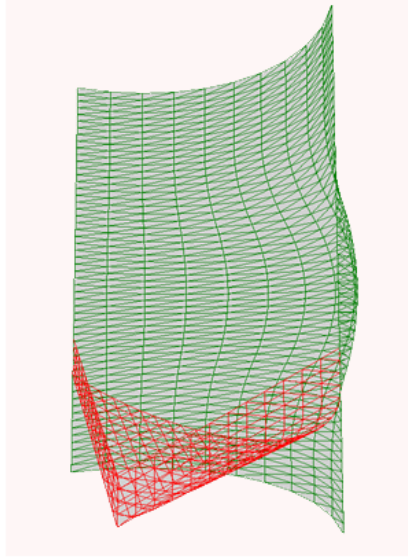


Figure 5.5: Pathological valve model.

5.3 Study of parametric model through F.E.A.

After geometry generation, we have imported the model in ANSYS, another F.E.A. code, to evaluate the mechanical behavior of the parametric valve.

This time, we have performed dynamic analysis, to begin introducing of some more real elements. Time simulation is 1 second, that is, more or less, the time of cardiac cycle. The density value is 1000 Kg/m^3 and it is the same for the whole structure. Also for the parametric model different thickness values have been assigned: the cylinder and the sinuses of Valsalva have a thickness of 1.5 mm, whereas the leaflet and the coaptation faces have a thickness of 0.5 mm.

We have performed only diastole simulation, because, as explained previously (Chapter 4), it is the load condition that, during valve sparing operation, assures the surgery success. So, an uniform internal pressure of 0.1 MPa has been applied.

The constraint conditions are still the same of the first model, but, in this case they are applied according to cylindrical coordinates.

To make the parametric model more real, we have applied a hyperelastic constitutive law. It is the Mooney Rivlin model described by following strain energy function:

$$W = C_{10}(I_1 - 3) + C_{01}(I_2 - 3) + \frac{1}{d}(I_3 - 1)^2 \quad (5.1)$$

where C_{10} and C_{01} are the two independent material constants characterizing the deviatoric deformation of the material, d is the material incompressibility parameter,

and I_1, I_2, I_3 are the invariants of the Cauchy deformation tensor. In our case we have chosen $C_{10} = 0.5516$ MPa, $C_{01} = 0.1379$ MPa and $d = 0.0145$. These values are taken from literature [27].

We have performed our analysis on the normal valve model and on the pathologic one. The results of the normal valve model are shown in Fig. 5.6.

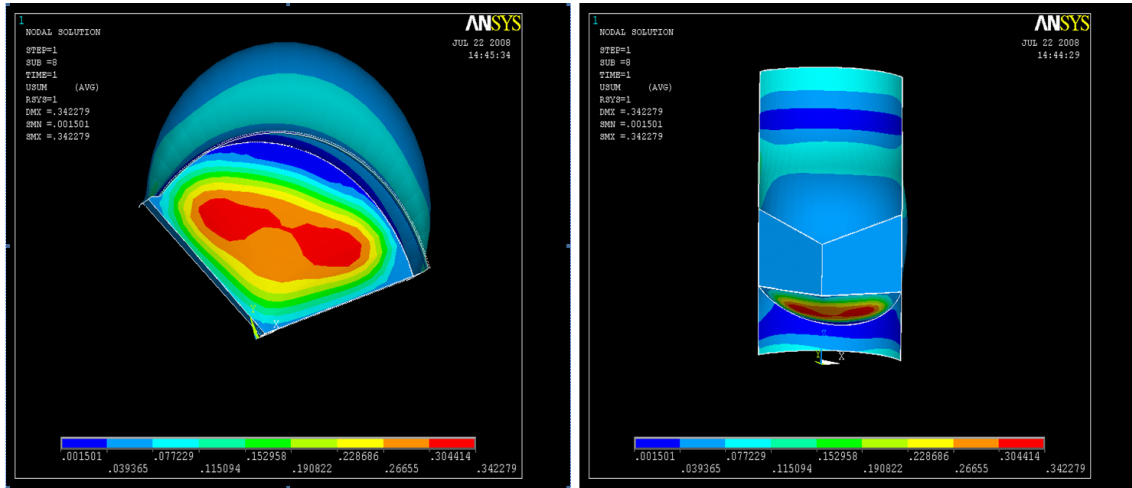


Figure 5.6: A top (left) and a three-dimensional (right) view of the displacements of the "normal" parametric model.

We can observe that the greater displacements are confined to the leaflet, and the maximum value is 0.342279 mm. The coaptation faces have a small displacement about between 0.04 and 0.077, while the cylinder has displacements about between 0.001 and 0.1.

If we compare the parametric model with the first model, we can observe that there is a considerable displacement reduction. This highlights that the new model with the new material is more rigid than the first.

The leaflet displacements are comparable (they are almost equal), but the coaptation faces and the cylinder (included sinuses of Valsalva) have displacements of one order of magnitude short. Because of greater stiffness of the coaptation faces, the radial displacements of the two ends of the coaptation segment will be lower. In fact, if we see the graphic in Fig. 5.7 we can note that the maximum value reached is 0.0038 mm.

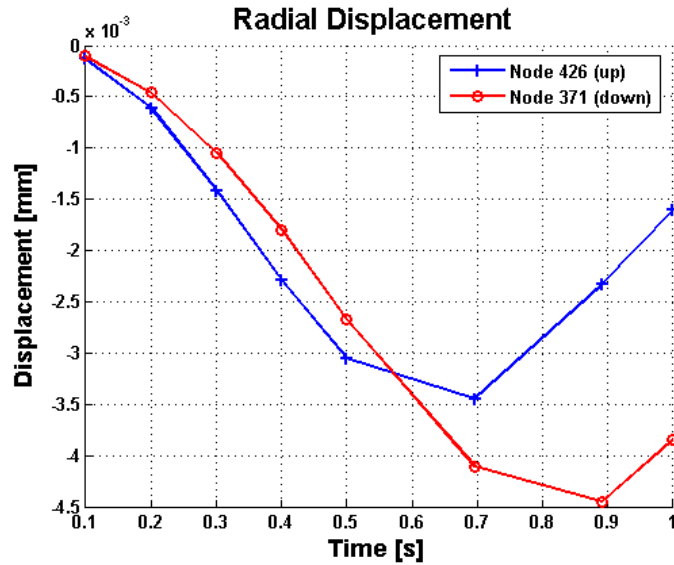


Figure 5.7: Radial displacements of the two ends of the coaptation segment.

The results of the pathologic valve model are shown in Fig. 5.8.

In this case we observe an increase of the displacements in each component (one order of magnitude). There is a greater dilatation of the sinuses of Valsalva; this involves that the maximum displacement doesn't concern the leaflet, but the side extremities, those to contact with the other two leaflets. The coaptation faces move more than the normal case, but not like we expect. In fact, as a consequence of reduced coaptation, we would like that their movement caused the valve opening, making it incompetent. Instead, the two faces go down, not opening the valve, but causing a moving forward of the bottom end of the coaptation segment (see Fig. 5.8). This behavior comes from the geometric simplification that we have introduced into the model. First of all the acute angle that the two coaptation faces make between them: in the real valve it is more beveled. Then the face thickness that in reality is not uniform; the material hypothesis; the not dilatation of the aortic root, etc.

In conclusion we can say that this parametric model is certainly a good start point to reproduce the behavior of the real aortic valve and to understand the role of coaptation for the valve competence. In fact, the possibility to shift from the normal model to the pathological one, simply changing the parameter values is a very easy way to obtain good results soon. Obviously, to get valid results we will have improve some geometric details; we will have introduce more real constitutive law; we will have introduce some nonlinear parameters, etc. But having to do with a complex biological structure, nothing is ever perfect!!!!

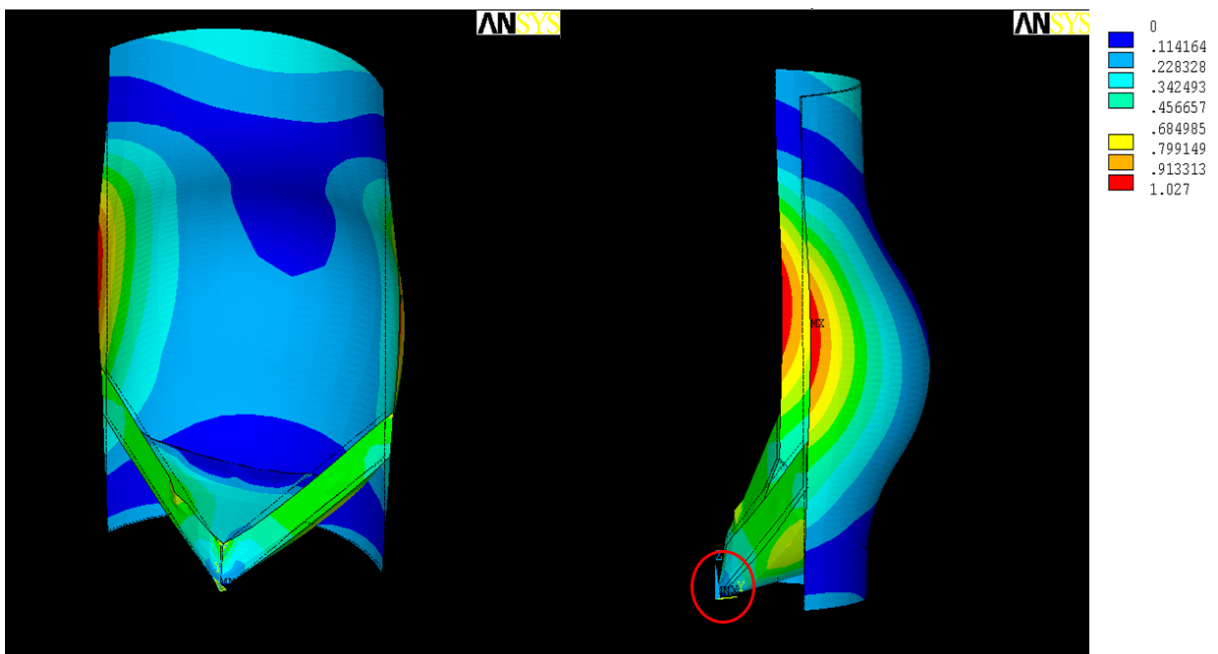


Figure 5.8: A three-dimensional (left) and a side (right) view of the displacements of the pathologic parametric model. Moving forward of the bottom end of the coaptation segment in the red circle

Conclusions

In this work we presented the investigation of the mechanical behavior of the aortic valve by Finite Element Analysis. In particular, we wanted to understand which was the role of the coaptation area in the aortic valve sparing operation. First of all, we created a model of a healthy aortic valve and we analyzed its displacements and stress after diastole and systole loading condition. We considered two different material laws: linear elastic isotropic and linear elastic orthotropic.

For the isotropic case we performed the two load conditions. After diastole, we noted a greater leaflet expansion downward. In real aortic valve, this expansion is not so large, but we have to keep in mind the hypothesis about the components of leaflet that is made only of elastin. Consequently it is reasonable to state that the cusp is able to deform so much. The stress values have the same order of magnitude of literature. After systole, the leaflet springs up little by little to press oneself against the external structure, reproducing the real valve behavior.

For the orthotropic case (a more real material law), after diastole, we noted a displacement decrease of 70%. The greater displacements don't concern any more the leaflet (more rigid in circumferential direction due to collagen), but upper ends of the external structure. The orthotropic behavior is very similar to real one. Also orthotropic stresses have the same order of magnitude of literature. After systole, we observed that it is as if coaptation faces ensconce themselves on the leaflet, after an initial raising. We obtained a valve opening, but it is not just the correct physiologic one: valvular lumen is reduced compared with isotropic lumen after systole.

Then we created a model of a pathological aortic valve, with a lower coaptation, and we analyzed its displacements after diastole loading condition and with isotropic and orthotropic material. To compare the two models, we chose as reference points the ends of the coaptation segment, with the aim to prove that a lower coaptation doesn't allow to valve to close fully. We considered the negative radial displacement of these ends to evaluate the "non-perfect" closure degree. Both the isotropic and

the orthotropic analysis have shown that the radial displacements of the pathological model are greater than the normal one and that the opening degree is always greater in the pathological model. For these reasons we can conclude that the coaptation level influenced the valve competence.

Finally, we created a parametric model that allow us to pass from the normal model to the pathological simply modifying some parameter values. We performed only diastole simulation with hyperelastic material model. The results shew that there is a considerable displacement reduction: the new model with the new material is more rigid than the first. The leaflet displacement are comparable (they are almost equal), but the coaptation faces and the cylinder (included sinuses of Valsalva) have displacements of one order of magnitude short. For the pathological model, the maximum displacement doesn't concern the leaflet, but the side extremities, those to contact with the other two leaflets. The coaptation faces move more than the normal case, but not like we expect:the two faces go down, not opening the valve, but causing a moving forward of the bottom end of the coaptation segment. It is still a developing approach, so for this model we cannot reach a conclusion. We can say that it a good start point to reproduce the behavior of the real aortic valve: the possibility to shift from the normal model to the pathological one, simply changing the parameter values is a very easy way to obtain good results soon.

Appendix A

Early geometrical models

We have created other geometric models, before arriving to definitive one. This has been useful to understand better which were the solving difficulties related to geometry and which were the crucial aortic valve elements that couldn't be left out. So, in this appendix, we will describe briefly the main geometric properties of the early models, highlighting advantages and disadvantages of each. In every model the same hypothesis made for the definitive one are valid (symmetry, central angle of 120° , etc.).

A.1 First model

The first model was made in the same way of the definitive model: we have generated a sphere, then we have cut it by two inclined planes to respect the symmetry condition. But in this case the hypothesis on equality between aortic annulus diameter and sinotubular junction diameter is not valid. In fact we have generated a surface connection that reduces the sinotubular junction diameter (see Fig.A.1). This model doesn't include the aortic annulus, but it represents only the leaflets, the sinuses and the sinotubular junction.

Advantages: It is a very realistic model, representing the aortic valve elements in a very complete and accurate way.

Disadvantages: The structural complexity involves a computational complexity. Not linearity increase doesn't enable the solver to reach a convergence threshold.

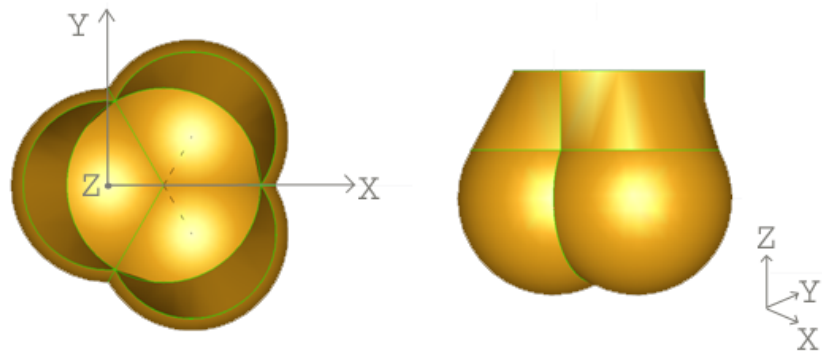


Figure A.1: First aortic valve model. On the left a top view and on the right a three-dimensional view of the whole valve.

A.2 Second model

The second model has a circular shape and it is composed of three leaflets. Every cusp was generated by the rotation of the contour shown in Fig.A.2 around an axis passing through the valve centre. To respect symmetry condition, this rotation is obviously of 120° . The obtained whole model is shown in Fig.A.3. This aortic valve model represents the leaflets and the first part of sinuses of Valsalva. The aortic annulus and the sinotubular junction are absent.

Advantages: It is a very simple model. This involves a reduction of computational costs and a more easy convergence problem resolution.

Disadvantages: Too much simplicity doesn't reproduce very well the real valve behavior.

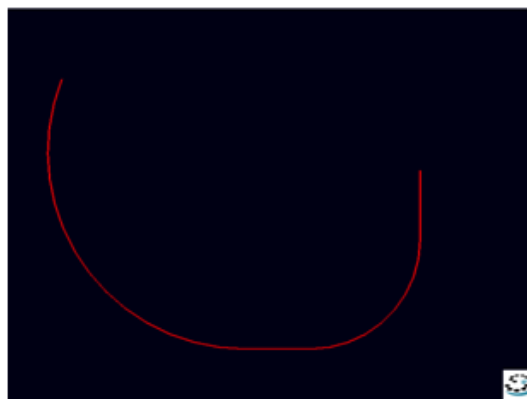


Figure A.2: Second aortic valve model: contour created for leaflet generation.

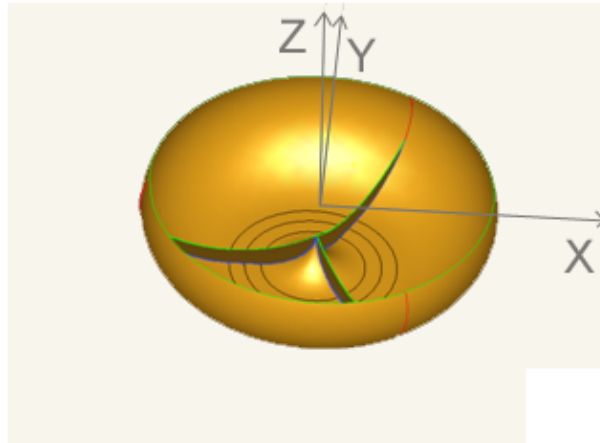


Figure A.3: A three-dimensional view of the second aortic valve model.

A.3 Third model

The third model has a circular shape. It was made considering as valve the bottom of a sphere. Then, the new "valve" was divided into three parts. The commissures start from the valve centre and arrive to the valve upper edge. This assures a full valve opening. So, this aortic valve model represents only the leaflets with their commissures, without sinuses of Valsalva, aortic annulus and sinotubular junction (see Fig.A.4).

Advantages: It is still a very simple model. It allows a full valve opening

Disadvantages: Too much simple. The main aortic root elements are absent.

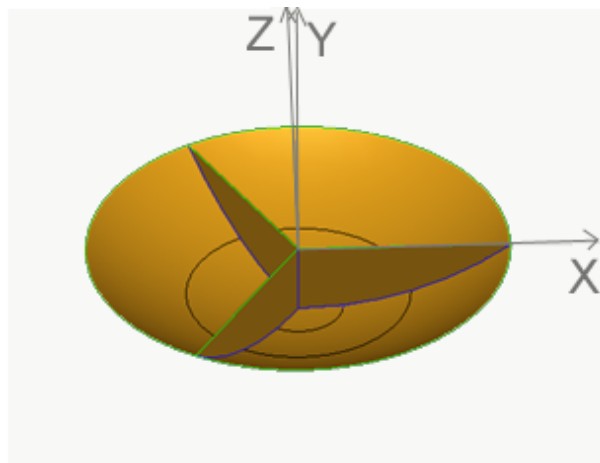


Figure A.4: A three-dimensional view of the third aortic valve model.

Appendix B

Definition of orthotropic properties for aortic valve elements

In this appendix we want briefly explain like to assign orthotropic properties to different parts of the valve by Samsef Field. We will described the steps to follow to create a orthotropic material for a sphere and for a cylinder, defining the needed parameters to do it.

B.1 Orthotropy for a cylinder

The most important steps to define an orthotropic material properties for a cylinder are two:

1. choice of the plane on which to project the cylinder
2. local reference system representation of the cylinder element respect to the main reference system.

The first step allows to identify the material fiber direction. To do it, we have to imagine to cut the cylinder along the longitudinal direction and to open it on the chosen plane (see Fig.B.1). The cylinder elements will have all the same local reference system or not according to this choice. If the chosen plane is ZX or YZ (that in our case contain the material fiber directions), all elements will have the same local reference system (rotated and moved according to the specific element position), otherwise not (XY plane case).

To understand better this concept, we analyse the following examples. We consider

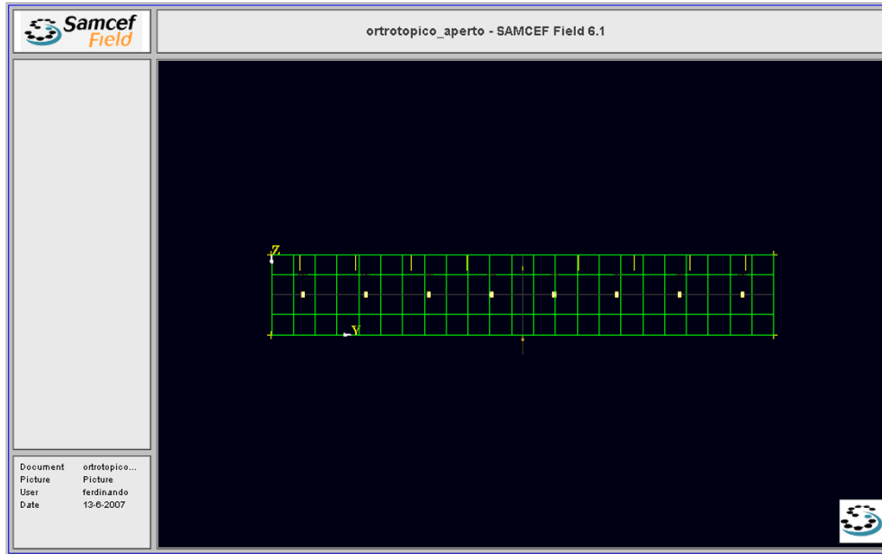


Figure B.1: Cylinder projection on the YZ plane. It contains the material fiber direction.

the three projection cases: ZX plane, YZ plane and XY plane. For each case, we observe the local reference system orientation of generic cylinder element respect to the main reference system.

ZX Plane As our cylinder was made, ZX plane contains the material fiber direction. We consider two generic cylinder elements: element n. 61 (parallel to XZ plane) and element n. 37 (parallel to YZ plane). By Fig. B.2 it is possible to see like the elements have their own local reference system orientated in the same way. In both v_1 represents the longitudinal direction, v_2 the circumferential direction and v_3 the radial direction. Obviously, local reference system of each element is oriented in different way respect to the main reference system.

YZ Plane Also YZ plane contains the material fiber direction. So ,also in this case, the same remarks made for ZX plane are valid. We consider still the same elements (n.61 and n. 37), but in this case they will have the local reference system rotated respect to the ZX case. Now, v_1 represents the circumferential direction, v_2 the longitudinal direction and v_3 the radial direction (see Fig. B.3).

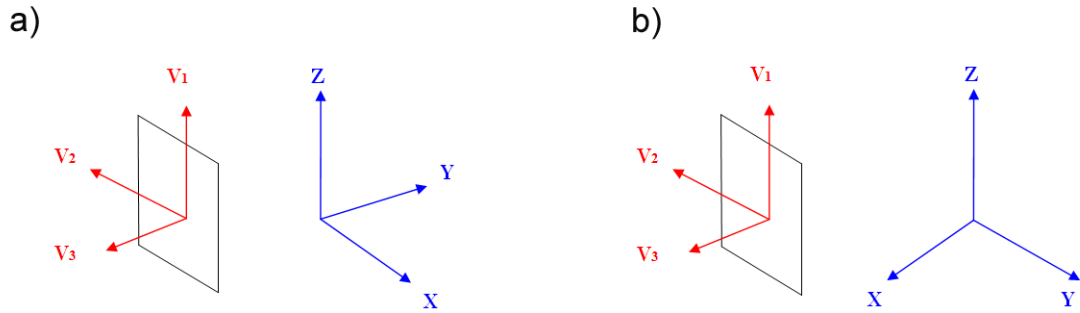


Figure B.2: Local reference system orientation (in red) respect to main reference system (in blue) of element n. 61 (a) and element n. 37 (b) in ZX case projection. In both v_1 represents the longitudinal direction, v_2 the circumferential direction and v_3 the radial direction.

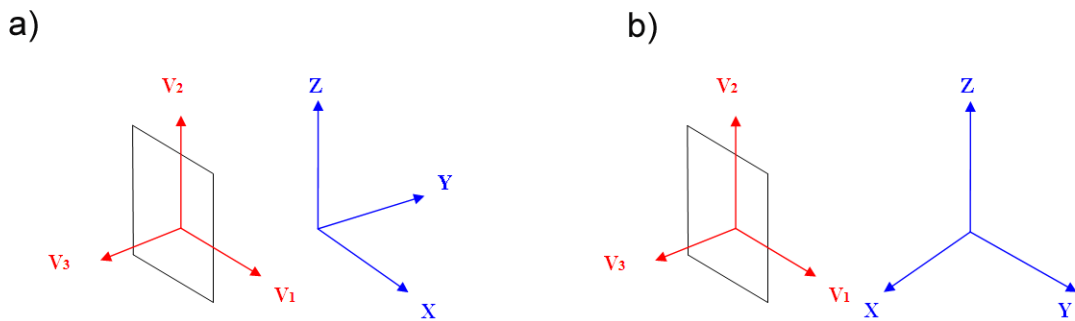


Figure B.3: Local reference system orientation (in red) respect to main reference system (in blue) of element n. 61 (a) and element n. 37 (b) in YZ case projection. In both v_1 represents the circumferential direction, v_2 the longitudinal direction and v_3 the radial direction.

XY Plane The cylinder projection on this plane doesn't contain the material fiber direction (the projection is a circle, not a rectangle). We consider three generic cylinder elements: element n. 61 (parallel to XZ plane), element n. 37 (parallel to YZ plane) and element n. 53 (parallel to YZ plane). We can observe like the local reference system orientation changes according to the chosen element (see Fig. B.4). In this case there is no regularity in the local

reference system, but it is different for each element. For these reasons, the orthotropic properties assignment is very difficult and also inaccurate.

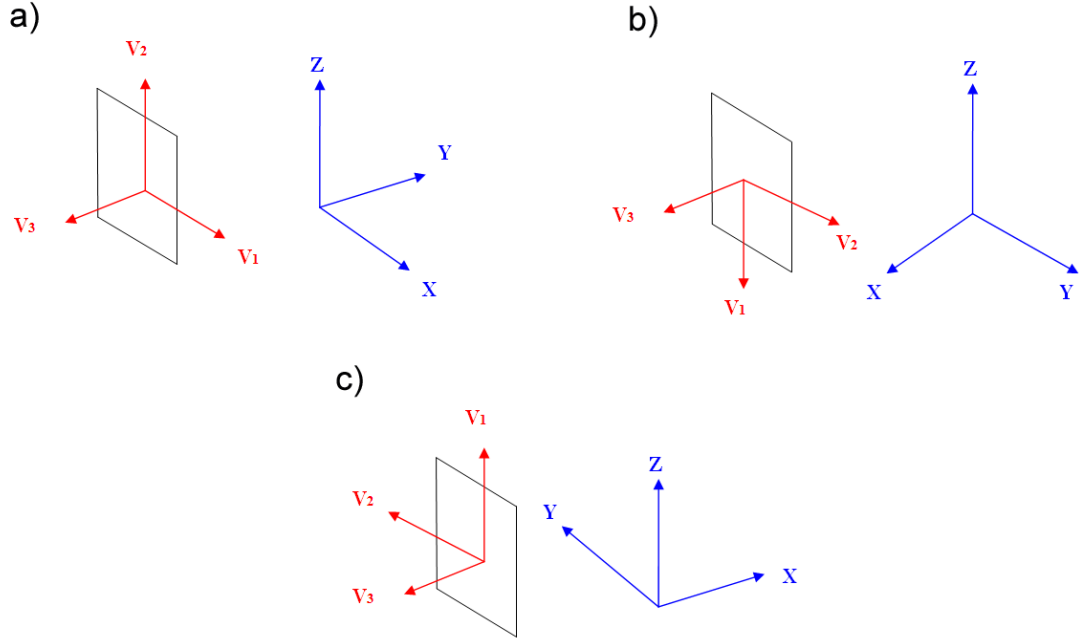


Figure B.4: Local reference system orientation (in red) respect to main reference system (in blue) of element n. 61 (a), element n. 37 (b), and element n. 53 (c) in XY case projection. For every element the local reference system is different.

Once the local versor directions have been detected, on the graphical interface, to v_1 axis is assigned the Young's modulus of the first column, to v_2 axis is assigned the Young's modulus of the second column and to v_3 axis is assigned the Young's modulus of the third column.

We have checked this on the following example. We have created a cylinder, applying on it an internal pressure. Then we have chosen to project the cylinder on YZ plane and we have considered three cases:

1. $E_{v1} = 100\text{KPa}$ $E_{v2} = 10\text{KPa}$ $E_{v3} = 10\text{KPa}$
2. $E_{v1} = 10\text{KPa}$ $E_{v2} = 100\text{KPa}$ $E_{v3} = 10\text{KPa}$
3. $E_{v1} = 10\text{KPa}$ $E_{v2} = 10\text{KPa}$ $E_{v3} = 100\text{KPa}$

In the first case we expect reduced circumferential displacements, because of a greater Young's modulus in the first column. In the second case we expect reduced longitudinal displacements for the same reason explained above. In the third case we expect reduced radial displacements.

The results are shown in Fig.B.5 , Fig. B.6 and Fig. B.7. They confirm our thesis.

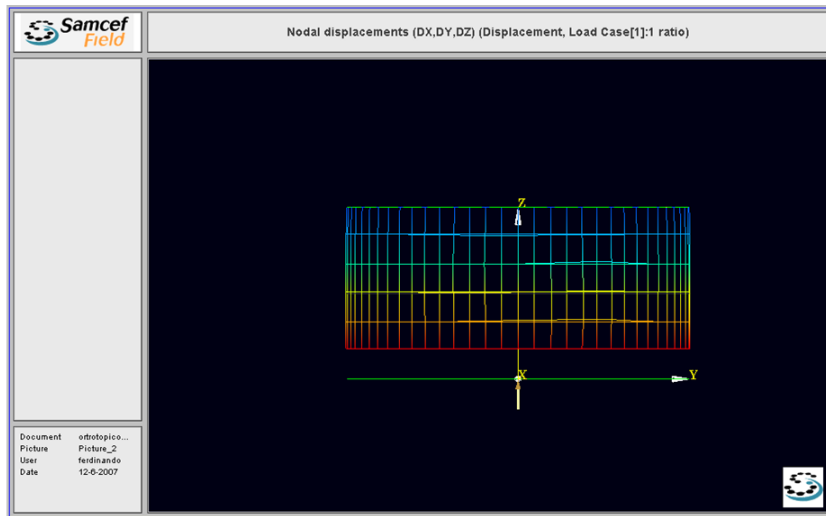


Figure B.5: Nodal displacements of the first case ($E_{v1} = 100\text{KPa}$ $E_{v2} = 10\text{KPa}$ $E_{v3} = 10\text{KPa}$).

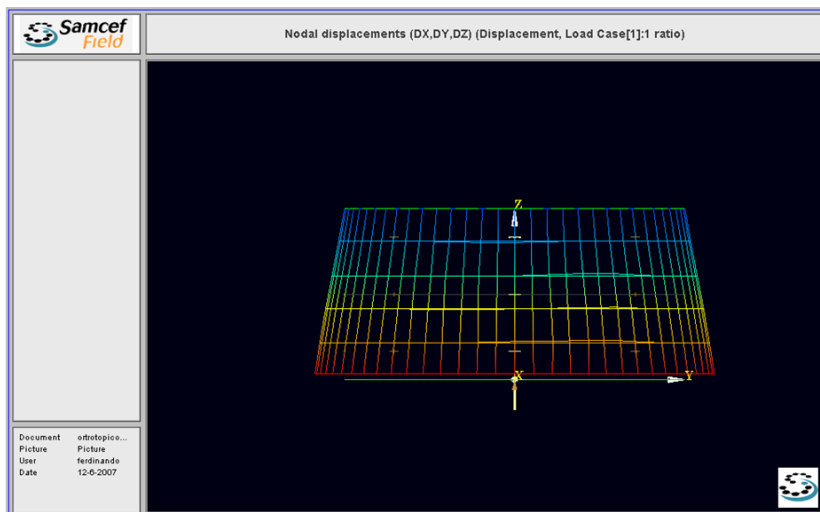


Figure B.6: Nodal displacements of the second case ($E_{v1} = 10\text{KPa}$ $E_{v2} = 100\text{KPa}$ $E_{v3} = 10\text{KPa}$).

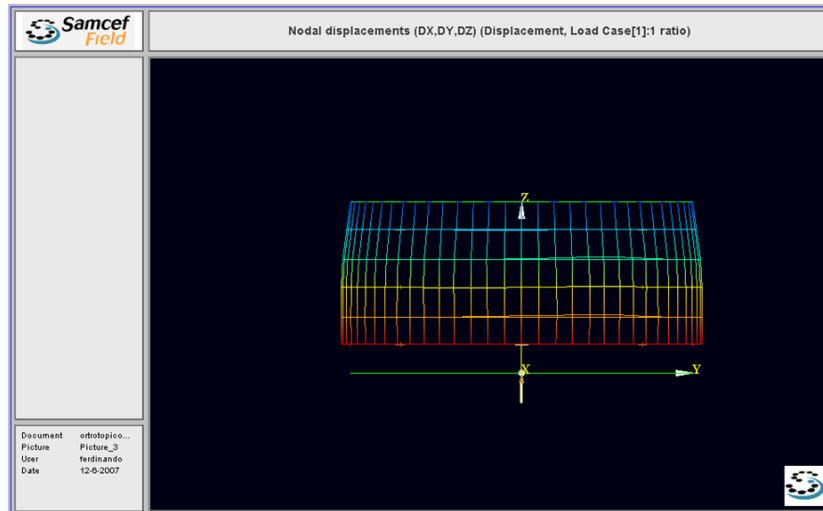


Figure B.7: Nodal displacements of the third case ($E_{v1} = 10\text{KPa}$ $E_{v2} = 10\text{KPa}$ $E_{v3} = 100\text{KPa}$).

B.2 Orthotropy for a sphere

If we have a sphere and we want assign it different mechanical properties along the radial and the circumferential directions, we cannot use the traditional graphical interface of Samcef Field to do it. By default the first axis is along the first edge of the element. E_1 , E_2 and E_3 are defined using the orientation of the element. E_1 is along the first edge, E_2 along the second one and E_3 is normal to the shell. In Samcef Field you will not be able to apply properties according to the circumferential and radial direction. If you defined an orthotropic material in Samcef Field you will have to define a direction for laminate but this direction won't respect the circumferential and radial direction. In your case the only solution is to use *Epilogue* present in the *Solver* Modulus.

The main steps are:

1. You define an orthotropic material in the Epilogue
2. You define a frame type spherical at the origin (0,0,0) with v_1 along x and v_2 along y.

The instructions to define an orthotropic material in Samcef Field are:

```
.MATERIAL
I 1
BEHAVIOR "Elastic"
YT 1624 6885 6885
```

```
NT 0.45 0.45 0.45
```

```
G 560 1121 1121
```

```
M 1e-06
```

```
A 0 0 0
```

The instructions to define a frame type spherical at the origin (0,0,0) with v_1 along x and v_2 along y in Samcef Field are:

```
.FRAME I 300 type spherical
```

```
origine 0 0 0
```

```
v1 1 0 0
```

```
v2 0 1 0
```

After doing it, there is a problem : the axe 1 for a spherical frame must be the radial one. The solution is using the *Renum* parameter of the `.FRAME` command :

```
Renum 3 1 2 -2.
```

With this syntax the axe 3 of the frame is the axe 1 of the shell , the axe 2 of the frame is the axe 2 of the shell. As we need a dextorsum system we have use the sign "-". In this case with have the axe 1 = circumferential East - West ; axe 2 circumferential North - South ; axe 3 = radial.

Bibliography

- [1] Mano J. Thubrikar. The aortic valve.(1990)
- [2] <http://www.lpch.org/DiseaseHealthInfo/HealthLibrary/cardiac/as.html>
- [3] Tirone David TE. Surgery of the aortic valve. *Current Problem in Surgery*,36, 425-501 (1999).
- [4] <http://heartlab.robarts.ca/dissect/dissection2.html>
- [5] Kunzelman KS, Grande J, David TE, et al. Aortic root and valve relationships: impact on surgical repair. *Journal Thorac Cardiovasc Surg*,70, 107-162 (1994).
- [6] Michel R. Labrosse, Carsten J. Beller, Francis Robicsek, Mano J. Thubrikar. Geometric modeling of functional trileaflet aortic valves:Development and clinical applications. *Journal of Biomechanics*, 39, 2665-2672 (2006).
- [7] Mihaljevic T, Paul S, Cohn LH, Wechsler A. Pathophysiology of Aortic Valve Disease. *Cardiac Surgery in the adult*,30,791-829 (2003)
- [8] Vesely I The role of elastin in aortic valve mechanics. *Journal of Biomechanics*, 31-115 (1998).
- [9] Deck JD, Thubrikar MJ, Schneider PJ, Nolan SP Structure, stress, and tissue repair in aortic valve leaflets. *Cardiovasc Res*, 22, 7-16 (1988).
- [10] http://en.wikipedia.org/wiki/Aortic_valve_stenosis
- [11] http://en.wikipedia.org/wiki/Aortic_insufficiency
- [12] K. Jane Grande-Allen, Richard P. Cochran, Per G. Reinhall, Karyn S. Kunzelman. Mechanisms of aortic valve incompetence: Finite-element modeling of Marfan syndrome. *The Journal of Thoracic and Cardiovascular Surgery*,122 , 946-954 (2001).

- [13] Richard A. Hopkins. Aortic valve leaflet sparing and salvage surgery: evolution of techniques for aortic root reconstruction. *European Journal of Cardiothoracic Surgery*,24 , 886-897 (2003).
- [14] http://en.wikipedia.org/wiki/Aortic_dissection
- [15] Bentall HH, de Bono A. A technique for complete replacement of the ascending aorta. *Thorax*,9 , 23-338 (1968).
- [16] Sarsam Mai, Yacoub M. Remodelling of the aortic valve annulus. *The Journal of Thoracic and Cardiovascular Surgery*,8 ,105-435 (1993).
- [17] Matthias Karck, Axel Haverich. Aortic Valve Reimplantation According to the David Type I Technique. *Operative Techniques in Thoracic and Cardiovascular Surgery* ,10 ,246-258 (2005).
- [18] Wolfgang Harringer, Klaus Pethig, Christian Hagl, Gerd P. Meyer, Axel Haverich. Ascending Aortic Replacement With Aortic Valve Reimplantation. *Circulation* ,100 ,II24-II28 (1999).
- [19] Hans-Joachim Schäfers, Benjamin Bierbach,Diana Aicher. A new approach to the assessment of aortic cusp geometry. *The Journal of Thoracic and Cardiovascular Surgery* ,132 ,436-438 (1999).
- [20] G. Petrucci. Dispense "Lezioni di costruzioni di macchine" (2008).
- [21] Matthieu De Beule. Finite Element Stent Design. (2008)
- [22] K. Jane Grande-Allen, Richard P. Cochran, Per G. Reinhall, Karyn S. Kunzelman. Finite-Element Analysis of Aortic Valve-Sparing: Influence of Graft Shape and Stiffness. *IEEE Transaction on Biomedical Engineering*,48 , 647-659 (2001).
- [23] G. Arcidiacono, A. Corvi, T. Severi. Functional analysis of bioprosthetic heart valves. *Journal of Biomechanics*,38 , 1483-1490 (2005).
- [24] Ralf A. Boerboom, Niels J.B. Driessen, Carlijn V.C. Bouten, Jacques M. Huyghe, Frank P.T. Baaijens. Finite Element Model of mechanically induced collagen fiber synthesis and degradation in the aortic valve. *Annals of Biomedical Engineering*,31 , 1040-1053 (2003).

- [25] V. A. Kas'yanov, B. A. Purinya, and V. P. Ose. Structure and mechanical properties of the human aortic valve. *Mechanics of Composite Materials* ,20 ,637-647 (1985).
- [26] <http://pyformex.berlios.de/>
- [27] A. Ranga, R. Mongrain, Y. Biadilah, R. Cartier. A compliant dynamic FEA model of the aortic valve. *12th IFToMM World Congress* ,1-6 (2007).

Ringraziamenti

Finalmente sono arrivata a scrivere la parte piú importante di questo lavoro. Spero di non dimenticare nessuno, ma se dovessi farlo non me ne vogliate.

Credo che debba ringraziare per primo il Prof. Auricchio, innanzi tutto per avermi riaccolta dopo la prima laurea, e soprattutto per la grande pazienza e disponibilitá mostratami nel periodo della tesi. Grazie, in particolar modo per la fiducia che ha avuto nei miei confronti.

Vorrei poi ringraziare il Dr. Demertzis per aver sempre mostrato entusiasmo per le mie presentazioni e per il valido aiuto che ha fornito per il lavoro svolto.

Un ringraziamento particolare va a Davide Fugazza, per la pazienza che ha avuto con me e per le ore passate al telefono per cercare di trovare una soluzione ai miei problemi. Grazie di cuore.

Grazie anche a Michele per avermi aiutato a "pubblicizzare" il mio lavoro e per avermi sostenuto moralmente in questi mesi, e ad Alessandro per essere una figura sempre presente per chiunque abbia bisogno.

Passiamo adesso agli affetti personali.

Ringrazio mamma e papá per avermi permesso, con il loro sostegno, sia psicologico che economico, di raggiungere anche questo traguardo. Vi ringrazio per non avermi mai messo fretta, per avermi assecondato in ogni mia scelta e per la totale fiducia che avete sempre riposto in me. GRAZIE.

Un grazie a :

Roberta, Valeria, Mimmo e Marco per essermi sempre stati vicini anche a mille chilometri di distanza, e per avermi fatto sempre sentire una persona importante nella loro vita;

Ai miei nonni: a nonna Rosa per essere stata sempre presente, a nonna Rosaria e nonno Ciro per avermi chiamato ogni sabato, e a nonno Domenico per avermi sempre protetta da lassú;

Ad Annamaria, Franco e Gabriella per avermi accolto nella loro famiglia come se ne avessi sempre fatto parte e per avermi trattato sempre come una figlia;

A tutti i miei parenti, in particolar modo a chi mi é vicino in questo giorno importante.

Ora é il turno degli amici.

Ringrazio gli amici del Sud, quelli che conosco ormai da una vita e che, nonostante gli anni e la lontananza , sono rimasti sempre le persone semplici , genuine e affettuose che ho conosciuto: Ciro, Dario, Francesca, Marino, Luisa e Angelo.

Un grazie particolare a Mimmo e Peppe per avermi sempre trattato con rispetto e per non avermi fatto sentire solo la ragazza del loro migliore amico.

Ringrazio gli amici del Nord, che , anche se piú recenti, hanno sempre dimostrato di volermi bene come ad un'amica di vecchia data: Simone, Daniela, Paola, Market e Pistone. Un grazie a Roberto e Sara, per essere stati dei buoni amici nonostante la conoscenza recente.

Un ringraziamento speciale a Chiara, che in questi anni, é sempre stata nel mio cuore, anche se lontana fisicamente.

Un grazie ad Angela per essere stata la mia unica vera amica "settentrionale" e ad Angelo per avermi sempre spronato ad arrivare alla fine.

Grazie a tutti i miei compagni di corso, in particolare a quelli che sono diventati miei amici.

Un ringraziamento particolare va alla mia piccola Trudi, che, con i suoi disastri e le sue coccole, ha fatto in modo di rendere la mia vita ancora piú bella.

Adesso, l'ultimo ringraziamento, forse il piú importante. Vorrei ringraziare la persona che in questi ultimi nove anni ha fatto in modo che la mia vita fosse felice, mi ha fatto sentire, ogni giorno trascorso insieme, una persona importante, e ha fatto in modo che ognuno di questi giorni fosse migliore del precedente. Alla persona migliore che io abbia conosciuto in vita mia. A Giuseppe. Grazie amore mio.